REPUBLIC OF TÜRKİYE
ALTINBAŞ UNIVERSITY
Institute of Graduate Studies
Electrical and Computer Engineering

RECONFIGURABLE INTELLIGENT META-SURFACE FOR 5G COMMUNICATION SYSTEM

Saba Talib Hamada AL-HADEETHI

Doctor of Philosophy

Supervisor
Asst. Prof. Dr. Abdullahi Abdu IBRAHIM

İstanbul, 2024

RECONFIGURABLE INTELLIGENT META-SURFACE FOR 5G COMMUNICATION SYSTEM

Saba Talib Hamdad AL-HADEETHI

Electrical and Computer Engineer

Doctor of Philosophy

ALTINBAŞ UNIVERSITY

2024

The dissertation titled RECONFIGURABLE INTELLIGENT META-SURFACE FOR 5G COMMUNICATION SYSTEM prepared by SABA TALIB HAMADA AL-HADEETHI and submitted on / /2023 has been **accepted unanimously** for the degree of PhD in Electrical and Computer Engineering.

Asst. Prof. Dr. Abdullahi Abdu IBRAHIM

the Supervisor

Thesis Defense Committee Members:

Academic Title - First/Last Name	Department, University	___________________
Academic Title - First/Last Name	Department, University	___________________
Academic Title - First/Last Name	Department, University	___________________
Academic Title - First/Last Name	Department, University	___________________
Academic Title - First/Last Name	Department, University	___________________

I hereby declare that this thesis/dissertation meets all format and submission requirements of a …………………………… (Master's/PhD) thesis/dissertation.

Submission date of the thesis to Institute of Graduate Studies: ___/___/___

I hereby declare that all information presented in this graduation project has been obtained in full accordance with academic rules and ethical conduct. I also declare all unoriginal materials and conclusions have been cited in the text and all references mentioned in the Reference List have been cited in the text, and vice versa as required by the abovementioned rules and conduct.

Saba Talib Hamada AL-HADEETHI

Signature

DEDICATION

First and foremost, I want to thank Allah for enabling me to overcome every challenge. In order to help me throughout my PhD studies, I would like to acknowledge and extend my sincere gratitude to my supervisor, Asst. Prof. Dr. Abdullahi A. Ibrahim. His direction and encouragement saw me through the entire project writing process. I express my gratitude to my committee members for making my defense a delightful experience and for their insightful remarks and recommendations.

I would like to sincerely thank all of the members of the Altinbas University Department of Electrical and Computer Engineering for their assistance.
I want to express my sincere gratitude and admiration to my co-advisor, Prof. Dr. Taha A. Elwi, who helped me every step of the way while I completed my research by providing guidance and assistance.

I can never express how grateful I am to my family, especially my husband and my best parents. I would like to dedicate my triumph to my father's soul, who has always been my biggest supporter. I would especially like to thank my mother for providing me all the support I required during this process. I want to express my gratitude to my spouse in particular for his help, understanding, and support while I was writing my project and studying.

Sincere gratitude to my beautiful "son and daughter" (Mascara and Muhammad).

Finally, thank you to my friends and everyone who prayed for my success and completion of PhD in shaa Allah.

ABSTRACT

RECONFIGURABLE INTELLIGENT META-SURFACE FOR 5G COMMUNICATION SYSTEM

AL-HADEETHI, Saba Talib Hamada

PhD, Electrical and Computer Engineering, Altınbaş University,

Supervisor: Asst. Prof. Dr. Abdullahi Abdu IBRAHIM

Date: 01 /2024

Pages: 96

For 5G mobile communication networks, a novel antenna array is built using a printed monopole based on a metamaterial (MTM). For 5G communication networks, the architecture and functionalities of a Multiple-Input Multiple-Output (MIMO) antenna array are anticipated. Four components make up the MIMO antennae array, which is stacked in an octagon 3D array arrangement consecutively. The components are arranged to create a particular pattern. The array is constructed on a 25 x 25 x 30 mm^3 FR4 substrate. Because of its RF characteristics, this substrate option is frequently used in antenna designs. A split ring resonator (SRR) is connected to each antennae element, which is a printed circuit monopole, via a T-resonator (TR). Resonances at 3.6 GHz and 4.8 GHz are provided by this design, making it appropriate for sub-6GHz 5G networks. To lessen mutual coupling, electromagnetic band gap (EBG) spacers are utilised between antenna elements. The antennae array's concerts are improved by the EBG spacers' moonquake fractal-shaped array design. The moonquake fractal EBG spacers are placed to achieve a -20dB mutual coupling reduction between antennae elements. This reduction in mutual coupling is important for maintaining good isolation and minimizing interference between elements. Four PIN diodes are connected to each antennae element to control the antennae's concerts . By using these diodes, different switching scenarios are tested to understand their impact on antennae behaviour. The projected array's concerts is both simulated and experimentally validated. Computer Simulation Technology Microwave Studio (CST-MW) is used for numerical simulations. This ensures that the theoretical design matches real-world concerts. Numerous concert metrics are considered, such as gain curves, radiation patterns, Envelope Correlation

Coefficient (ECC), and reflection coefficient (S11), isolation coefficients (S21), (S31), and (S41). The distance of separation between the planned antennae is equal to λ0/16, where λ0 represents the 3.6 GHz free space wavelength. The chosen spacing allows for a desired increase of 6.18dBi. Considerable progress has been made in terms of S-factors (S11, S21, etc.) and radiation patterns at the two resonant frequencies (3.6 GHz and 4.8 GHz), according to both simulated and measured results. In summary, the projected MIMO antennae array design incorporates advanced features such as the use of EBG spacers, PIN diode control, and specific resonant frequencies suitable for 5G communication networks. The combination of these elements aims to enhance the array's concerts in terms of isolation, radiation patterns, and other key metrics. The simulation and experimental validation further establish the effectiveness of the design in real-world scenarios.

Keywords: CPW, MTM, MIMO, EBG, SRR, TR.

TABLE OF CONTENTS

Pages

ABSTRACT .... **vi**

LIST OF TABLES.. **xi**

LIST OF FIGURES.. **xii**

ABBREVIATIONS.. **xiv**

LIST OF SYMBOLS.. **xvi**

1. INTRODUCTION **1**

1.1 INTRODUCTION 1

1.2 LITERATURE REVIEW 3

1.2.1 Reconfigurable Monopole Antennae in 5G Application 3

1.2.2 Design and Analyses EBG Structure 11

1.2.3 Reconfigurable Multi Input Multi Output [MIMO] in 5G Application............... 13

1.3 OBJECTIVE 15

1.4 PROBLEM STATEMENT.. 16

1.5 CONTRIBUTION 17

1.6 AIM OF THE WORK... 17

1.7 THESIS ORGANIZATION.. 18

2. SECOND CHAPTER.. **19**

2.1 BACKGROUND OF 5G WIRELESS NETWORK.. 19

2.2 ANTENNAE RECONFIGURATION:.. 20

2.2.1 Reconfiguration Types.. 20

2.2.2 Frequency reconfiguration.. 20

2.2.3 Polarization Reconfiguration 21

2.2.4 Radiation-pattern Reconfiguration.. 22
2.2.5 Compound Reconfiguration.. 22
2.3 RECONFIGURATION TECHNIQUES 22
2.3.1 Physical Reconfiguration.. 23
2.3.2 Electrical reconfiguration.. 23
2.3.3 Optical Reconfiguration.. 24
2.3.4 Material Change Reconfiguration.. 25
2.4 ANALYSIS OF PIN DIODE.. 25
2.5 GENERAL NOTATIONS AND COMPARISON.. 28
2.6 MIMO BASED ANTENNAE ARRAY 29
2.6.1 Applications of MIMO system 31
2.6.2 Standard MIMO Configurations... 33
2.7 MICROSTRIP ANTENNAE FEEDING TECHNIQUES 34
2.7.1. Coaxial Probe... 34
2.7.2. Coplanar Waveguide.. 34
2.7.3 Inductive Aperture Coupling 35
2.8 ARCHITECTURAL SCENARIO OF 3D ANTENNAE MIMO PROPAGATION 36
2.9 INTRODUCTION TO MAIN DESIGN OBJECTI.VES:................................. 36
2.9.1 Antennae Design and Geometrical Details... 37
2.9.2 Design Methodology... 38
2.9.3. Results Validations 40
2.9.4 S_{11} curves 40
2.9.5 Gain Curves 41
3. CHAPTER THREE... 42
3.1 INTRODUCTION 42

3.2. GEOMETRICAL INFORMATION AND ANTENNAE DESIGN........................ 43
3.3. DESIGN METHODOLOGY.. 44
3.3.1 Microstrip Line Design.. 45
3.3.2 Unit-cells Effects 45
3.3.3 TR Effects.. 47
3.3.4. CPW Effects.. 48
3.3.5 Switching Effects.. 49
3.4. RESULTS VALIDATIONS 52
3.4.1 In free Space Environments.. 52
3.4.2 In Close to Human Body.. 53
4. CHAPTER FOUR 57
4.1 INTRODUCTION 57
4.2. ANTENNAE ARRAY STRUCTURE AND GEOMETRICAL DETAILS 58
4.3 EBG SPACER DESIGN AND OPERATION DETAILS.. 59
4.4 DESIGN METHODOLOGY.. 62
4.5 RESULTS AND VALIDATION.. 65
5. CONCLUSION 69
5.1 CONCLUSIONS 69
5.2 FUTURE WORK.. 70
REFERENCES 72

LIST OF TABLES

Pages

Table 2.1: Comparison Between Different PIN and RF MEMS Switches [58] 24

Table 2.2: The Benefits and Restrictions of Antennae Reconfiguration Approaches are Described. [60]. 28

Table 2.3: Comparison Between of Different Techniques [42]. 29

Table 3.1: Comparison Between The Switching Scenarios Operation in Terms of Antenna Performance 50

Table 3.2: BER Evaluation at Different LDR Resistance Values. 51

Table 3.3: Analysing Antenna Performance in Two Distinct Antenna Settings. 54

Table 3.4: Comparison of This Research With Earlier Studies... 56

Table 4.1: Lumped Circuit Elements.. 61

Table 4.2: The Projected MIMO Array Concerts S With Respect to the Previous Published Results. 68

LIST OF FIGURES

Pages

Figure 2.1: Antenna Reconfigurable Types [46] 20

Figure 2.2: Reconfiguration Technique of Reconfigurable Antennas [51]. 23

Figure 2.3: Principle of PIN Diode [63]. 27

Figure 2.4: Point-To-Point MIMO System [64]. 29

Figure 2.5: Multiuser MIMO [65]. 30

Figure 2.6: Massive MIMO in (A) Uplink (B) Downlink [65]. 31

Figure 2.7: Coaxial Connector [69] 34

Figure 2.8: Co-Planer Waveguide [72] 35

Figure 2.9: Aperture Coupled Feed [72] 35

Figure 2.10: Scenario of MIMO Antenna Propagation [73]. 36

Figure 2.11: Antennae Geometry. 38

Figure 2.12: S_{11} Parameter of the Proposal Design 40

Figure 2.13: S_{11} Parameter Validation. 41

Figure 2.14: Gain Parameter Validation. 41

Figure 3.1: The Proposed Monopole Antenna Geometrical Details. 44

Figure 3.2: Antenna Performance With Changing L Value: (A) S_{11} Spectra And (B) Gain. 45

Figure 3.3: Antenna Performance With Different Cells Number: (A) S_{11} Spectra and (B) Gain. 47

Figure 3.4: Antenna Performance With and Without TR Structure: (A) S_{11} Spectra and (B) Gain. 48

Figure 3.5: Antenna Performance Varying the Ground Plane Length: (A) S_{11} Spectra and (B) Gain. 49

Figure 3.6: Antenna Performance With Different Switching Scenarios: (A) S_{11} Spectra and (B) Gain. 50

Figure 37: Fabricated Prototype Structure. 52

Figure 3.8: Antenna Performance Measurements With Different Switching Scenarios: (A) S_{11} Spectra and (B) Gain. 53

Figure 3.9: Antenna Radiation Pattern Measurements: (A) Experimental Setup, (B) 2.3 Ghz And (C) 4.4 Ghz 55

Figure 4.1: MIMO Antenna Geometrical Details: (A) Antenna Element Views and (B) 3D MIMO Array 59

Figure 4.2: The Projected EBG Structure.. 60

Figure 4.3: EBG Structure Based on Transmission Line. 60

Figure 4.4: Propose Equivalent Circuit Theory of EBG in ADS. 61

Figure 4.5: The Obtained Results From Both CST MWS and ADS Simulations: (A) S_{11} Spectra And (B) S_{12} Spectra 62

Figure 4.6: MIMO Antenna S11 Spectra And Radiation Pattenrs: (A) Without EBG and (B) With EBG Spacers.. 63

Figure 4.7: Coupling Between Antenna Elements: (A) Without EBG (B) With EBG. 64

Figure 4.8: Fabricated Prototype of MIMO Antennae Array... 65

Figure 4.9: Simulated and Measured S-Parameters of the Antenna At (A) All Diode OFF (B) All Diode ON. 66

Figure 4.10: Comparison of Coupling Between Simulated and Measured When All Diodes are: (A) OFF and (B) ON. 67

ABBREVIATIONS

MTM	:	Metamaterial
MIMO	:	Multi Input Multi Output
TR	:	T-Resonators
BER	:	Bit Error Rate
SRR	:	Split Ring Resonatot
ECC	:	Envelop Correlation Coefficient
RF	:	Radio Frequency
LDR	:	Light Dependent Resistor
5G	:	Mobile Fifth Generation
FR4	:	Flame Retardant Substrate
RHR	:	Right-Handed Rule
LHR	:	Left Hand Rule
CRLH	:	Composite Right Left-Handed
EBG	:	Electronic Band Gap
IoT	:	Internet of Things
PCB	:	Printed Circuit Boards
FSS	:	Frequency Selective Surface
GPS	:	Global Positioning System
LOS	:	Line Of Sight
WSN	:	Wireless Sensor Networks

CST	:	Computer Simulation Technology
HF	:	High Frequency
RIMS	:	Reconfigurable Intelligent Meta-Surface
D2D	:	Device –To-Device
LTE	:	Long Term Evolution
VSWR	:	Voltage Standing Wave Ratio
SISO	:	Single Input Single Output
WBAN	:	Wireless Body Area Network
WCDMA	:	Wideband Code Division Multiple Access
HFSWR	:	High Frequency Surface Wave Radar
SSR	:	Single Split Ring
TLM	:	Transmission Line Model
AAC	:	Antennae Array Correlation

LIST OF SYMBOLS

λ	:	Wave Length
ε	:	Permittivity
μ	:	Permeability
ε_r	:	Relative Permittivity
Γ	:	Voltage Reflection Coefficient
E	:	Electric-field\intensity
H	:	Magnetic-fields\Intensity
J	:	Current Density
D	:	Electric-flux\density
B	:	Magnetic-flux\density
ρ	:	Charge Density
U	:	Radiation Intensity
P_rad	:	Total Radiated Power

1. INTRODUCTION

1.1 INTRODUCTION

A reconfigurable intelligent meta-surface (RIMS) is a type of advanced material that can manipulate electromagnetic waves in innovative ways. These surfaces are designed to have highly tuneable properties, allowing them to change their behaviour depending on the signals passing through them. The potential applications of RIMS are many, Nevertheless, the development of 5G communication networks is one of the most exciting.

The next generation of cellular technology, or 5G, guarantees better data rates and lower latency, and greater reliability than previous generations. However, one of the challenges of 5G is that it uses higher frequencies than previous generations, which can be easily absorbed or blocked by obstacles such as walls or buildings.

This is where RIMS come in. By incorporating RIMS into 5G communication systems, it is possible to manipulate the behaviour of electromagnetic waves to overcome these obstacles. For example, RIMS can be designed to reflect or refract signals in specific directions, effectively steering the signals around obstacles. RIMS can also be designed to absorb unwanted signals, reducing interference and improving overall system concerts .

Moreover, RIMS can be reconfigured on-the-fly, allowing the system to adapt to changing conditions in real-time. This capability is particularly useful in dynamic environments where the signals are constantly changing, such as in urban environments or areas with high levels of electromagnetic interference.

Overall, the incorporation of RIMS into 5G communication systems has the potential to greatly improve the concerts and reliability of these systems, making it possible to realize the full potential of 5G technology. The major advancements in a Metamaterial-based antennae for WBAN applications will be reviewed in this thesis, includes wearable antennae based on meta-surfaces, reconfigurable wearable antennae based on CRLH TLs, and wearable antennae that use composite right/left-handed transmission lines. tuneable Metamaterial. [1].

These structures have increased wearable antennae concerts while having little to no negative effects on the human body, leading to more dependable wearable communication [2] [3].

Additionally, a number of meta-wearable antennae design processes are outlined, and applications of these strategies to wearable antennaes are examined. [4] . The idea, Right- and left-handed composite transmission line theory and applications (CRLH-TLs) have been thoroughly studied in this review work by taking into account how they might be included into antennae system designs [5].

It has been shown that CRLH-TLs with negative permeability (μ <; 0) and negative permittivity (ε <; 0) have unique properties not found in the natural world [6]. This leads to their being called "Metamaterial," man-made structures. [6]. These artificial structures include, for example, shunt left-handed (LH) capacitances (CR), series right-handed (RH) inductances (LR), and shunt left-handed (RH) inductances (L L).

Stubs or via-holes, undesired current flowing on the surface, and the gap between the surface and ground plane, respectively, are what make them all real [7][8]. Moreover, it is demonstrated that structures built with CRLH metamaterial-TLs generally outperform their conventional counterparts because of their increased efficiency, improved radiation patterns, wider bandwidth, lower profile, higher gain, and smaller dimensions—all of which make them easier to mass produce, simpler to use, and more accessible. [9]. A growing number of social sectors are adopting the Wireless Body Area Network (WBAN) [10].

Wearable antennas are a crucial part of these systems, but they face a number of difficult problems, such as electromagnetic coupling with the human body, physical deformations, and a wide range of operating environments. To overcome these obstacles, advanced design methods and techniques are urgently required. [1].

Recent research has concentrated on using metamaterial in wearable antennaes, which is a promising field with special benefits [11]. The key developments in wearable antennaes utilizing Wearable antennaes, right- and left-handed composite transmission lines (CRLH TLs), based on meta-surfaces, and reconfigurable wearable antennaes utilizing tuneable metamaterial will be discussed in this article for WBAN applications [12].

These structures have increased wearable antennae concerts while having little to no negative effects on the human body, leading to more dependable wearable communication [13]. Additionally, several meta-wearable antennae design approaches are outlined, and wearable antennae applications are discussed. [13]. Large number of antennaes on a single board with the ability to execute different jobs are a requirement for future wireless communication systems[14].

Size, weight, volume, and other restrictions are imposed by this, particularly for wireless portable and space applications [15]. Reconfigurable antennaes are the most recent advancement in antennae technology, replacing traditional fixed-form antennaes with changeable designs that may be adjusted to meet the demands of time-varying systems [16][17]. A discussion of various types, methods, and design strategies for reconfigurable antennae and antennae arrays will be presented in this study [18].

1.2 LITERATURE REVIEW

Consequently, the projected structure, the literature survey in this thesis is divided into three main sections: design and analysis of an EBG structure, Design and study of a reconfigurable MIMO antennae as well as a reconfigurable monopole antenna for usage in 5G applications.

1.2.1 Reconfigurable Monopole Antennae in 5G Application

(In 2013: Ding, X. and Wang, B.Z.) [19] A brand-new printed antenna with a Yagi-reconfigurable pattern was displayed. Four-four PIN diodes control the reflectors' length and the radiation pattern they emit. A circular wideband monopole with omnidirectional function drove the projecting antennae. The frequency range covered by the intended antennae was 3–4 GHz.

(Su, Zhen, et al. 2018.) [20], in a study conducted by Su et al. in 2018, they introduced a novel frequency-configurable Planar Inverted-F Antennae (PIFA) design utilizing a T-shaped monopole antennae. This unique antennae design offers configurability without requiring an external screen or additional printed components. The key innovation in this design is the integration of a vanadium dioxide (VO2) switch. The VO2 switch serves as a low-cost solution to enable frequency configuration in the antennae. The antennae can operate in two distinct modes facilitated by the VO2 switch: one at 2.7 GHz and the other in the 3.5 GHz frequency band. This switch allows the antennae to dynamically change its resonant frequency band. The result of this design is that the antennae can achieve a gain of 2.14 dBi specifically at the 3.5 GHz frequency band. This demonstrates the practicality and effectiveness of the frequency-configurable PIFA design. In summary, the study by Su et al. in 2018 introduced an innovative frequency-configurable PIFA design utilizing a T-shaped monopole antennae and a vanadium dioxide (VO2) switch. This design allows the antennae to operate at either 2.7 GHz or 3.5 GHz frequency bands, showcasing the ability to dynamically change its frequency band of operation. The antennae achieved a gain of 2.14 dBi at the 3.5 GHz frequency band, highlighting its practical application.

"(Jin, Guiping, et al. 2018) [21], in a study conducted by Jin et al. in 2018, they projected a straightforward and reconfigurable antennae design based on a four-arc dipole with a wireless feed network. This innovative design incorporates RF PIN diodes in the feeding network to enable the reconfigurability of the antennae's radiation pattern. The key feature of this antennae design is its ability to manipulate the principal radiation beam. By appropriately adjusting the settings of the RF PIN diodes, the antennae can switch between four similar directional radiation patterns. This means that the antennae's primary beam direction can be changed according to the desired application or scenario. The antennae's gain is reported to be 4.11 dBi, and it operates within a frequency range of 2.25 to 3.16 GHz. This frequency range indicates that the antennae design is suitable for applications in this specific frequency band. In summary, the study by Jin et al. in 2018 presented a novel reconfigurable antennae design featuring a four-arc dipole and a wireless feed network. The integration of RF PIN diodes allows for the manipulation of the antennae's radiation pattern, enabling it to switch between four distinct directional patterns. The antennae achieves a gain of 4.11 dBi and operates within the frequency range of 2.25 to 3.16 GHz. This design offers versatility in directing the antennae's radiation pattern for various applications.

In a study by Ikram et al. in 2018, they introduced an antennae system that operates across multiple frequency bands, specifically at sub-6 GHz (3.6 GHz) and in the millimeter-wave (mm-wave) band at 28 GHz. The antennae design is centered around a dipole antennae with two key properties. The first property involves the integration of components inspired by a tapered slot antennae and a standard dipole antennae operating at 3.6 GHz. This combination enables the antennae to function effectively in the sub-6 GHz frequency band. The second property of the design is the utilization of a tapered slot antennae to function as a high-gain end-fire antennae in the mm-wave band (28 GHz). This enables the same antennae structure to perform efficiently in both frequency bands. The concept behind this design is to achieve multi-band operation using a compact footprint. By combining the properties of the dipole antennae, tapered slot antennae, and end-fire antennae, the projected antennae system achieves coverage across two distinct frequency ranges.

Applications that need communication or sensing capabilities in both the mm-wave and sub-6 GHz frequency bands can benefit from this adaptability. In conclusion, the 2018 research by Ikram et al. describes a novel antenna system that functions in the sub-6 GHz and mm-wave (28 GHz) frequency ranges. To enable multi-band operation with a small footprint, the antennae design includes components of an end-fire antenna, a regular dipole, and a tapered slot antenna. The benefits of this method are adaptability to many frequency bands and wide-area coverage all within a single antenna design.

(Syrytsin, I., et. al., 2018) [23] The authors proposed an Ultra-wide end fire planar-phase antennae system with 1.2 mm spacing, which would provide a wider scanning angle phase for 5G mobile terminals. The proposed antennae, when arranged in a phased array with distinct radiation patterns for each mode, can reach an impedance bandwidth exceeding 8 GHz. Similar and more substantial embedded radiation patterns are produced in the arrays by these four modes. The overall even scanning pattern and cover efficiency of the observed and simulated phased array antennae were calculated in the 25–33 GHz frequency range. Despite a small deviation in coverage efficiency variance, the typical coverage efficiency over the frequencies range is rather similar, according to the data. In the specified frequency range, a coverage efficiency of about 50% is obtained with a threshold gain = 5 dBi.

(Diawuo et al. in 2018) [24] This paper makes the following suggestions, a feature low-cost and a high-gain mm – wave pattern antennae have been developed. This antennaes are indeed a 6 x 5 proximity-coupled of planar array designed in 5G a cellular applications. The suggested antennae configuration is efficient of providing broad-band properties and a low side lobe levels with a compaction size, as seen by the close results from simulations and measurements agree. higher a bandwidth of 27.5 GHz to 28.5 GHz, the antennaes have a gain of 21 dBi. It has a 9.8% impedance bandwidth between 26.04 GHz and 28.78 GHz.

A reconfigurable 5G and 4G operation band for radio frequency energy harvesters (RF-EH) in various wireless communication frequencies was described by (D. N. Elsheakh, 2019) [25]. The antennae's steerable beam pattern was built using such tunable graphene pads. The circular monopole fed by the CPW creates five rectangular strips with a 45° spacing angle that make up the projected antennas. These strips are connected to the monopole via graphene pads. The 5G frequencies that the proposed monopole antennae resonate at are 3.GHz to 7.8GHz. Elwi and colleagues (2020) proposed a basic reconfigurable antenna architecture consisting of a wireless feed network and four arc dipoles. The integration of RF PIN diodes within the feeding network is a crucial aspect of this design. These RF PIN diodes are strategically positioned to enable the reconfiguration of the antennae's radiation pattern. The primary focus of this antennae design is the ability to manipulate the main radiation beams. By appropriately controlling the RF PIN diodes, the antennae can be switched to achieve up to four distinct radiation patterns, each directed in a specific direction. This reconfigurability offers the advantage of adapting the antennae's radiation pattern according to the requirements of the application. The frequency operation range of the antennae spans from 2.25 GHz to 3.16 GHz, indicating its effectiveness in the sub-6 GHz frequency band. Furthermore, the antennae's gain reaches a maximum value of 4.11 dBi. In summary, the study by Elwi et al. in 2020 presents a fundamental reconfigurable antennae design featuring four arc dipoles and a wireless feed network. The strategic placement of RF PIN diodes within the feeding network allows for the manipulation of the antennae's main radiation beams. This results in the ability to switch between up to four radiation patterns directed in specific directions.

The antennae operates within the frequency range of 2.25 GHz to 3.16 GHz and achieves a maximum gain of 4.11 dBi. This design's reconfigurability enhances its versatility for various applications.

(S. Ullah, et al. 2020) [27], projected a narrow 5G reconfigurable antennae operating at sup 6 GHz. The antennae has been excited through the use of a CPW feed-specific waveguide port. The antennae works in four different areas. based on a Lumped elements' states (ON or OFF). A Cutting-phase technologies, such as the Internet of Things (I0T) and that use of wireless sensor networks (WSN) for device-to-device communications (D2D).

In the research conducted by Elwi et al. in 2020, a novel configuration of ultra-wideband (UWB) cylindrical metamaterial (MTM) antennaes is projected, with applications in radio frequency (RF) and Internet of Things (IoT) domains. The key aspects of this antennae design involve the utilization of Hilbert-shaped MTM unit-cellss for the antennae patch and the incorporation of an electromagnetic band gap (EBG) structure between the ground planes. The primary objective of using the Hilbert-shaped MTM unit-cellss is to enhance the bandwidth of the antennae. The specific design of these unit-cellss contributes to widening the frequency range over which the antennae can effectively operate. Furthermore, the introduction of an electromagnetic band gap (EBG) structure between the ground planes contributes to an increase in antennae gain. The EBG structure aids in shaping the radiation pattern and directing energy in desired directions, resulting in an improved gain characteristic. The operational frequency range of the projected antennae spans from 3.7 GHz to 13.8 GHz. The antennae's efficiency is notably high, achieving around 90% efficiency at 5.8 GHz. This efficiency value indicates that a significant portion of the input power is being radiated as electromagnetic energy, making the antennae an effective radiating element. In summary, Elwi et al.'s study in 2020 introduces a configuration of UWB cylindrical MTM antennaes suitable for RF and IoT applications. By employing Hilbert-shaped MTM unit-cellss and incorporating an EBG structure, the design achieves enhanced bandwidth and increased gain. The antennae operates within a frequency range of 3.7 GHz to 13.8 GHz, with a notable efficiency of around 90% at 5.8 GHz.

This design contributes to improved concerts in the specified frequency range, making it well-suited for a range of applications in RF and IoT domains.

In the research conducted by Wen, Sichao, and Yuandan Dong in 2020, a low-profile, broadband, vertically polarized antennae design is projected for indoor base station applications in the context of 4G/5G networks. The main objective of this antennae is to provide a monopole-like radiating pattern suitable for indoor environments. The antennae design is based on a standard monocone antennae equipped with internal matching circuits and a reactive load. This combination enables the antennae to exhibit a vertically polarized, monopole-like radiation pattern that is well-suited for indoor coverage.

The antennae is designed to operate within a frequency range of 1.66 to 3.95 GHz, which is relevant for both 4G and 5G applications. The antennae design is aimed at achieving a broad bandwidth, providing continuous monopole-like behavior within the working band. The antennae is engineered to exhibit omni-directional radiation patterns, making it suitable for indoor environments where signal coverage needs to be evenly distributed. The antennae's measured impedance, expressed as the voltage standing-wave ratio (VSWR), is reported to be 2.2 within the operating frequencies. The antennae's bandwidth achieves an 81% rating for the voltage standing-wave ratio (VSWR) within the specified frequency ranges.

Specifically, for 4G networks, the projected antennae operates within the frequency range of 1.7 to 2.7 GHz, while for 5G networks, it operates within the 3.3 to 3.8 GHz range, corresponding to the 5G N78 band. In summary, the study by Wen, Sichao, and Yuandan Dong in 2020 presents a vertically polarized, broadband antennae design suitable for indoor base station applications in 4G/5G networks. The antennae provides monopole-like radiating patterns with omni-directional radiation characteristics. It operates within the specified frequency ranges for 4G and 5G applications and achieves good impedance matching and broad bandwidth. This makes it a suitable candidate for providing reliable indoor coverage in indoor base station environments.

In the study conducted by Ciydem, M. and Miran, E.A. in 2020, a novel antennae design for 5G base stations operating at Sub-6 GHz is projected. This antennae design aims to achieve several key characteristics, including low cost, lightweight structure, low profile, and dual-polarizations. The antennae is designed to be cost-effective and lightweight, making it suitable for practical deployment in 5G base station setups. The antennae is designed with a flat and low-profile structure, which is advantageous for applications where space constraints are a concern. The antennae is capable of providing dual-polarized signals. This means that it can transmit and receive signals with two different polarization orientations, allowing for improved diversity and reliability in communication. The antennae design comprises several components, including a large radiating patch, a small parasitic patch, modified L-probe feeds, and a vertical metal wall. These components are strategically integrated to achieve the desired concerts characteristics. The main patch of the antennae is capacitive and is driven by two feeds, each with a 45-degree slant polarization. This feed configuration allows for dual-polarizations and diversity in signal reception. The projected antennae operates within the Sub-6 GHz frequency range, which is significant for 5G communication networks. The design's integration of multiple components and its modified feed configuration contribute to achieving dual-polarizations and improved signal diversity. These features are particularly important for enhancing the reliability of communication in 5G networks. In summary, the study by Ciydem, M. and Miran, E.A. in 2020 introduces a novel antennae design for 5G base stations operating at Sub-6 GHz. The design aims to provide a low-cost, lightweight, low-profile, and dual-polarization solution. With a combination of components including radiating and parasitic patches, modified feed arrangements, and a vertical metal wall, the projected antennae design enhances signal diversity and concerts for 5G communication applications.

In the study conducted by M. Aboualalaa in 2020, a dual-band slot antennae design for 5G sub-6 GHz frequencies is projected. The primary focus of this work is to achieve dual-band frequency operation within the sub-6 GHz range, which is relevant to 5G wireless applications. The antennae is designed to operate at two different frequency bands within the sub-6 GHz range. This dual-band capability allows the antennae to cover multiple frequency ranges, which is valuable for accommodating various communication standards and frequency allocations in 5G networks. The antennae's radiating element is a square slot. This slot structure contributes to the antennae's dual-band characteristics and radiation concerts . The antennae is fed using a coplanar waveguide (CPW) configuration. CPW feeds are commonly used in antennae designs due to their simplicity and concerts advantages. The dual-band operation is achieved by feeding the square slot antennae at two different positions using two separate feed lines. This approach allows for the excitation of different resonant modes, enabling the antennae to cover two distinct frequency bands. The projected antennae design exhibits good radiation characteristics and improved gain. The radiation efficiency of the antennae is reported to be over 93.5% in the required frequency bands. The antennae design is specifically intended for use in portable 5G wireless applications. This suggests that the design is well-suited for integration into handheld devices, IoT devices, and other portable communication solutions within the 5G ecosystem. In summary, the study by M. Aboualalaa in 2020 introduces a dual-band slot antennae design optimized for 5G sub-6 GHz frequencies. The antennae achieves dual-band operation by utilizing a square slot radiating element with CPW feeding at two different positions. The design aims for good radiation characteristics, enhanced gain, and high radiation efficiency. With its suitability for portable 5G wireless applications, the projected antennae offers a practical solution for communication needs in the 5G landscape.

(A. Bhattacharjee and S. Dwari, 2021) [32] We present a straightforward planar monopole antennae. complex re-configurability to be achieved. the structural reorganization of the ground plane and monopole element using just 8 pin diodes results in reconfigurable properties of operating frequency so, the frequency will be reconfigured in the sub-6 GHz band. For applications in (5G).

(H. Dildar., et al. 2021) [33], projected the frequency reconfigurable monopole antennaes with a low profile that is works in the microwave frequences band (1GHz -6 GHz). The FR-4 substrate is used to print the suggested construction. The operating modes of an antennae are changed by installing four pin diode switches between radiating patches. Voltage Standing Waves Ratio (VSWR) of the supplied antennae is less than 1.5. The designed antennae has an efficiency of 84% and a gain range of 1.2 to 3.6 dBi. It is also compatible with mobile devices of the fifth generation (5G).

A crucial element of 5G communication networks is multiple-input multiple-output (MIMO) technology, which enables simultaneous transmission and receipt of multiple data streams, boosting data throughput and enhancing system capacity. Multiple antennaes are utilized at the transmitter and receiver in conventional MIMO systems to enable the transmission and reception of multiple streams of data. Reconfigurable MIMO antennaes are a type of advanced antennae technology that can be dynamically adjusted to optimize their concerts . These antennaes can be adjusted in real-time to adapt to changes in the radio environment, such as changes in frequency, signal strength, or interference. In 5G applications, reconfigurable MIMO antennaes can be used to improve system concerts and capacity. By dynamically adjusting the antennae configuration, it is possible to optimize the transmission and reception of data, ensuring that the system is operating at maximum efficiency. Reconfigurable MIMO antennaes can also be used to overcome some of the challenges associated with 5G communication, such as interference from other wireless systems or obstacles that block or absorb radio signals. By adjusting the antennae configuration, it is possible to steer the transmission and reception of data around obstacles or interference sources, improving system reliability and concerts. Overall, reconfigurable MIMO antennaes are a powerful tool for optimizing 5G communication systems. By dynamically adjusting the antennae configuration, it is possible to overcome many of the challenges associated with 5G, while also improving system capacity and concerts.

1.2.2 Design and Analyses EBG Structure

(Alaa H. Radhi et. al., 2016) [34] The projected fractal structure based on the electromagnetic band gap (EBG) can aid in reducing the connection between microstrip antennae because of its ability to greatly slow down surface wave propagation in a certain frequency band. To improve isolation, two rounds of the planner EBG between two PIFA were used in a recently found one-layer unit-Planar fractal based on EBG (UPF-EBG) structure. The measurements of the PIFA antennae are 40 mm, 1.6 mm, and 68 mm. It operates at the wireless Long-Term Evolution (LTE) MIMO frequency of 2.65 GHz.

A compact periodic lattice EBG structure is connected to improve themutual coupling between an H-plane connected PIFA array is investigated through a thorough concerts study. As a result, the mutual coupling has been reduced by more than 30 db.

(Elwi, Taha in 2018) [35] projected a idea based on a printed slotted patch with an electromagnetic band Gap (EBG) layer for wideband applications, which is coated on a dielectric substrate in the shape of a lotus. The substrate for the dielectric is a Roger RT/droids. 5880 layer. The substrate's back profile is covered with an EBG layer to deliver a high gain bandwidth product across a wide frequency range. A flared-shaped coplanar waveguide (CPW) structure supplies the antennae.

(Ismail, M. F. et al. 2018) [36] It was suggested to set up an EBG in an array arrangement between two micro strip antennaes to provide polarization and radiation characteristics that are changeable. While the polarization reconfigurable elements are created by connecting the square patch edge to a PIN diode, The EBG structure reflection wave is what gives the pattern reconfigurable properties. The beam pattern on EBG structures may be changed from 0 to 14 degrees with a gain of 7.2 dBi at 2.4 GHz by turning a PIN diode (in ON and OFF states).

(Dey, Soumik, and Sukomal Dey in 2020) [37] projected a unique electro- magnetic band gap (EBG) for a Fabric Perot cavity antennae (FPCA) that is circularly polarized. The projected EBG creates a frequency band gap in the sub-6 GHz range between 3.07 and 4 GHz. The unit-cells's overall diameter is 0.071 GHz, 0.071 GHz, and 0.018 GHz, where 0 is the free space wavelength at the 3.53 GHz center frequency. Using a 7 7 EBG lattice as a partially reflecting surface (PRS) will increase the circularly polarized (CP) antennae's directivity using metamaterials. Peak gain of the main CP antennae at 3.66 GHz is 7.51 dBi as opposed to 9.67 dBi for the FPCA loaded with the EBG defaulter.

The unit-cells's overall diameter is 0.071 $\lambda 0 \times 0.071 \lambda 0 \times 0.018 \lambda 0$, where $\lambda 0$ the free space wavelength at the 3.53 GHz center frequency. Using a 7* 7 EBG lattice as a partially reflecting surface (PRS) will boost the circularly polarized (CP) antennae's directivity using metamaterials.

Peak gain of the main CP antennae at 3.66 GHz is 7.51 dBi, compared to 9.67 dBi for the EBG defaulter loaded FPCA. One advantage of EBG structures is that they can reduce interference between closely spaced antennaes. In a MIMO system, To send and receive, many antennaes are utilized. signals simultaneously, and interference between the antennaes can degrade system concerts . By using EBG body to separate that antennaes, it is possible to reduce interference and improve system concerts . EBG structures can also be used to be improve the radiation efficiency of MIMO antennaes. Radiation efficiency refers to the ability of an antennae to convert electrical energy into electromagnetic radiation. In some cases, the radiation efficiencies of a MIMO antennae could be reduced due to mutual coupling through the antennaes. By incorporating EBG structures into the antennae design, it is possible to reduce mutual coupling and improve radiation efficiency. Another advantage of EBG structures is that they can be used to improve the directivity of MIMO antennaes. Directivity refers to the ability of the antennaes to transmitting or receiveing signals in a specific direction. By using EBG structures to steer the radiated pattern of the antennae, it is possible to improve the directivity and focus the transmission or reception of signals in a specific direction. Overall, EBG technology is a powerful tool for improving the concerts of MIMO antennaes in 5G communication systems. By using EBG structures to reduce interference, improve radiation efficiency, and enhance directivity, it is possible to optimize the concerts and capacity of 5G communication systems.

1.2.3 Reconfigurable Multi Input Multi Output [MIMO] in 5G Application

(Wong, Kin-Lu, et al. in 2020) [38] Projected a fabrication 3-Three wideband monopole patch antennaes combined into a Y/shape body for (MIMO) that is operation between (3300~4200) MHz for 5G application. Each element of these antennaes has waves with monopole like radiation patterns and Good concerts . They obtained radiation pattern is broadside direction and measured antennae efficiency for better 88% in the 5G band.

(Serghiou, Demos, et al in 2020) [39] For 5G smartphone applications, a manufactured 88 MIMO antennae that runs at (sub-6 GHz) spectrum frequencies has been projected. Each antennae is a folded monopole that can operate in the (3100–3851 MHz) low band and (4800–6000 MHz) high band frequency ranges. In terms of Envelope Correlation Coefficient (ECC), overall efficiency, channel capacity, and Mean Effective Gain (MEG), they achieved good concerts .

(N. O. Parchin , 2020) [40] A brand-new MIMO broadband antenna system is currently available. with regard to sub-6 GHz fifth-generation (5G) mobile communications. Four pairs of symmetrically positioned compact coplanar waveguide (CPW) antennae are placed on the four corners of the smartphone in the suggested design (PCB). The antennae are fed with different polarizations. as a result. The proposed architecture provides isolation, dual-polarized full radiation coverage, and appropriate efficiency. A broad impedance bandwidth (S11 -10 dB) covering the frequency range of 3.3 to 6 GHz is also possessed by each antennae radiator. Furthermore, the intended design works effectively even in the absence of human hands.

(Xu, Zhan, and Changjiang Deng in 2020) [41] It has been projected that a newly constructed MIMO antennae operating in the 3500 MHz frequency range will be used with 5G wireless devices. The necessary Feed signals are provided by a small two-port feed network. Enough bandwidth to handle the 3400-3600 MHz range is measured at 750 MHz (3.06-3.81 GHz) and 340 MHz (3.33-3.67 GHz) for the two ports. The port isolation in the overlap bandwidth is greater than 14 dB.

In the research conducted by Chen, Shu-Chuan, et al. in 2020, a multi-input multi-output (MIMO) slot antennae system for fifth-generation (5G) tablet computers is projected. The focus of this study is on sub-6 GHz frequency operation, which is relevant for 5G communication. Each antennae element in the MIMO system is constructed using a slot structure. Slot antennaes are known for their compact and planar design, making them suitable for integration into portable devices like tablet computers. The spacing between the two slot antennaes within a single device is enhanced using an ungrounded full-wavelength strip resonator. This resonator configuration aids in achieving the desired isolation between the antennae elements. The ungrounded full-wavelength strip resonator design contributes to an increased intra-unit isolation, improving it by approximately 3.5 dB at the mid-band frequency. Improved isolation is essential in MIMO systems to minimize interference between antennae elements. The MIMO antennae system supports the frequency band of 3400 to 3600 MHz, which is relevant for 5G communication. The observed isolation within the operational band is reported to be greater than 11 dB. Additionally, the observed antennae efficiency exceeds 40%, indicating that a significant portion of the input power is being radiated effectively. All of the measured complex E-field radiation patterns' envelope correlation coefficients (ECCs) are less than 0.23. In a MIMO system, ECCs are used to evaluate the correlation between the radiation patterns of various antennae elements. Good independence between antennae elements is indicated by low ECC values, which is advantageous for preserving the integrity of MIMO communication. In summary, the study by Chen, Shu-Chuan, et al. in 2020 presents a MIMO slot antennae system designed for 5G tablet computers operating in the sub-6 GHz frequency range. The design employs slot antennae elements, enhanced spacing using an ungrounded resonator, and achieves improved isolation and efficiency. The antennae system supports the 3400-3600 MHz frequency band and is suitable for 5G mobile communications due to its low ECC values, which are essential for fast and reliable transmission.

A reconfigurable multi-input multi-output (MIMO) antennae is a type of antennae system that can dynamically adjust its configuration to optimize its concerts . MIMO technology is an important component of modern wireless communication systems, as it allows for the transmission and reception of multiple data streams simultaneously, increasing data throughput and improving system capacity. Reconfigurable MIMO antennaes take this technology one step further by incorporating the ability to adjust the antennae configuration in real-time. This allows the antennae system to adapt to changing conditions in the radio environment, such as changes in frequency, signal strength, or interference. One advantage of reconfigurable MIMO antennaes is that they can optimize the transmission and reception of data in real-time, ensuring that the system is operating at maximum efficiency. By dynamically adjusting the antennae configuration, it is possible to adapt to changing conditions in the radio environment, ensuring that the system is always operating at peak concerts .

Reconfigurable MIMO antennaes can also be used to overcome some of the challenges associated with wireless communication systems, such as interference from other wireless systems or obstacles that block or absorb radio signals. By adjusting the antennae configuration, it is possible to steer the transmission and reception of data around obstacles or interference sources, improving system reliability and concerts . Overall, reconfigurable MIMO antennaes are a powerful tool for optimizing wireless communication systems. By incorporating the ability to adjust the antennae configuration in real-time, it is possible to adapt to changing conditions in the radio environment and overcome many of the challenges associated with wireless communication systems.

1.3 OBJECTIVE

A few prerequisites must be met in order to meet the state-of-the-art in antenna design, considering how modern communication networks have recently grown [1]. The idea that artificial materials might emerge and change over time revolutionized microwave research. [1]. As a result, one of the most crucial components of cellular transmission lines and wireless communication systems is an antenna. Dipoles/monopoles, slot/horn, loop, microstrip, reflector, helical, dielectric/lens, log periodic, and frequency-independent antennas are among the nine types of antennas that have been developed in the last 50 years for use in communication and navigation systems. Every variety is better than the others for a specific purpose. Reconfigurable antenna designs most frequently use microstrip antennas due to their low cost, light weight, and ease of manufacturing [2]. The first known example of reconfigurable antennas was shown in the D. Schubert patent [2] from 1983. The US Defense Advanced Research Projects Agency (DARPA) funded the "Reconfigurable Aperture Program (RECAP)" in 1999 to investigate the application of reconfigurable antennae. [3]. Reconfigurable antennae have also been reported for use in cognitive radio, MIMO systems, broadband networking, and other applications. Thus Reconfiguring an antenna involves changing its radiating characteristics, polarization, or frequency.

The majority of antennae re-configurability techniques redistribute antennae currents, modifying the effective aperture's electromagnetic fields. [4]. The most often produced reconfigurable type antennas in recent years have been reconfigurable patch antennae, which are easy to manufacture and integrate into small electronic devices like laptops and mobile phones. A standard reconfigurable patch antenna is made up of several different metalized sections connected by switches or tuning elements and carried on a plane. [4].

Different metalized components can come into contact with one another by dynamically shifting the switch states, which will alter the antennae's overall radiation efficacy [5]. On the other hand, Multiple Input Multiple Output (MIMO) antennas are used to boost wireless channel capacity. [5]. For aspects of spatial diversity, the approved MIMO technology provides an efficient, high data rate split into multiple lower-rate streams. MIMO antennae are essential to several wire-free communication technologies, such as WLAN, 3G, LTE, and WIMAX (4G). Several researchers have developed MIMO antennae in a number of frequency bands that are covered by different types of [6]. Many wireless communication systems require MIMO antennas with a small footprint, high gain, and concerts, as well as CP radiation and a wide impedance bandwidth [7]. Furthermore, it has been proposed that MIMO systems can lessen the effects of multipath fading [8]. Nonetheless, the most notable disadvantage, particularly with portable contemporary MIMO devices and systems, would be the strong coupling of adjacent antennae [9]. Mutual coupling, a term for electromagnetic losses brought on by surface wave interactions between antennae elements, needs to be decreased in MIMO systems in order to improve antennae impedance matching and radiation characteristics [10, 11]. Here, mutual coupling can be considered surface wave leakage, although it depends largely on the antennae form, array design, and spacing distances [12].

1.4 PROBLEM STATEMENT

Due to the recent interest in meta-surfaces layers for different modern applications including, 5G systems, hyperthermia, MRI, and wireless power transfer; a great research impact is moved toward pushing the limits of such technologies. This can be realized from the unique properties of such layers in comparison to other metamaterial categories. Therefore, an intelligent meta-surface will be projected for such study to realize several achievements such as antennae beam forming, polarization reconfiguration, and direct antennae modulation. As a result, multiple modulation states can be performed with different carriers for multiplexing and transmitting multiple data streams that increases the system capacity and efficiency. Consequently, the research being conducted is By regulating the frequency band and radiation pattern and utilizing EBG structures to lessen the isolation between antennae MIMO elements, an advanced antenna works in MIMO systems. These innovative techniques offer programmable radiation patterns and frequency ranges for improved antennae concerts for 5G networks with sub-six (6-GHZ lower bands) frequency bands.

1.5 CONTRIBUTION

The major objective of such view is to design a high gain antennae over a certain bandwidth with direct antennae modulation process to realize intelligent beam forming process. Thus, the resulted beam forming would be applicable for many applications including the OFDM technology with high data rate processing to suit the current state of the art. The first objective of such view is to design a high gain antennae over a certain bandwidth with direct antennae modulation process to realize intelligent beam forming process. Thus, the resulted beam forming would be applicable for many applications including the OFDM technology with high data rate processing to suit the current state of the art.

1.6 AIM OF THE WORK

Designing monopole antennae for 5G networks at lower frequency bands—up to 6-GHZ—is the goal of that effort. The projected antennae would be excited with a CPW feed based on a new technique (left gap on one side of the ground plane and monopole antennae) to maintain asymmetrical radiation patterns towards one direction and design MIMO configuration for 5G application, as summarized in these sentence:

a. Using four PIN diodes, create a new compact multiband frequency and radiation pattern reconfigurable monopole antennae for 5G mobile devices with a broader range of re-configurability from 1 to 10 GHz and a (-10 dB) reflection coefficient.

b. Create a Matching Impedance Circuit (MIC) by placing a fractal structure adjacent to the monopole from a specific angle in order to reduce surface waves.

c. Introduce the PIN diodes that are used to regulate the radiation pattern and frequency resonance of an antennae under various switching conditions.

d. Improve the Gain-Bandwidth High Product (GBWHP) to meet the demands of 5G systems.

e. To meet the needs of the 5G systems, create a 4_element reconfigurable MIMO antennae for wireless technologies. The frequency band re-configurability ranges from 1 to 6GHz, and all of the antennae parts are the same size.

f. Add an EBG structure to the projected antennae structures in the MIMO scheme to reduce mutual coupling.

1.7 THESIS ORGANIZATION

This thesis is arranged into five chapters as follows:

CHAPTER1 Contains the thesis' introduction. The motivation, literature review, problem statement, and work goal are the four areas that were covered in this study.

In CHAPTER 2, a broad overview of the reconfigurable single antenna and reconfigurable antennae in the 5G MIMO configuration is provided. The topics covered include an introduction, background information, various types of reconfigurable antennae, design and feeding schemes, the present EBG structure design and analysis, and reconfigurable MIMO at 5G.

In CHAPTER 3, the construction design, results, and analysis of a microchip-based monopole antenna for 5G applications are presented.

CHAPTER4 The fabrication design, outcomes, and analysis of the MIMO system in 5G applications are discussed.

CHAPTER5 Concludes this thesis, and some recommendations for future work.

2. SECOND CHAPTER

This chapter covers the theoretical underpinnings of MIMO and 5G wireless networks, as well as technology related to antenna reconfiguration and applications.

2.1 BACKGROUND OF 5G WIRELESS NETWORK

Fifth-generation wireless (5G), the most recent iteration of communication systems, aims to dramatically boost wireless network speed and responsiveness [43]. Data may presently transfer over wireless broadband connections at multiple gigabits per second (Gbps), with some estimates putting peak speeds as high as 20 Gbps. These speeds, which have a latency of less than 1 millisecond (ms) and are faster than landline network rates, are very advantageous for real-time applications. With 5G, data transmitted across wireless systems will increase significantly because of enhanced antenna technology and more available capacity. Providers have also been investing in mobile networks [43]. In contrast, fifth-generation (5G) networks were starting to be installed by telecommunications firms in 2018 to meet the growing data demands of consumers and businesses. It is expected that the introduction of 5G networks will enable service providers to expand their offerings to consumers (e.g., virtual reality and streaming video applications), support the growing Internet of Things and smart homes, support advanced industrial applications (e.g., industrial sensors and monitoring systems), participate in advanced data analytics, and take advantage of technological advancements (e.g., autonomous vehicles, smart city applications). Spectrum is another factor driving the 5G rollout. The electromagnetic spectrum is used by all wireless communication techniques [44], [45]. A spectrum is the set of radio frequencies utilized for airborne communication. Multiple spectrum bands are used in 5G. Low-band (below 1 GHz), mid-band (1 GHz–6 GHz), and high-band millimeter spectrum are all used in the 5G standard. In order to deliver extremely fast services in densely populated locations, 5G requires the deployment of 5G technologies that use high band spectrum (mmW). Current users gain from the addition of new features, faster service, and increased capacity and coverage that come with the implementation of 5G technology in the mid-band spectrum. Many Internet of Things applications require wide-ranging coverage, which 5G technology, when utilized in a low-band spectrum, might supply Furthermore, since wireless communications work best at frequencies lower than 6 GHz, the majority of portable electronic devices, including cell phones, run at those frequencies. For example, frequencies in this region of the spectrum can very well travel long distances, spanning large areas, and they can easily pass through obstacles like walls. But as more people use mobile devices for increasingly varied purposes[45],[43], all parties engaged in 5G technology development acknowledge that spectrum in three major critical frequency ranges is necessary for 5G to function as intended.

a. Sub-1 GHz for complete coverage in urban, suburban, and rural areas, as well as for in-building IoT device and service coverage.
b. 1-6 GHz for increased bandwidth, especially in the 3.3–3.8 GHz range, which is expected to provide the foundation for a large number of the initial 5G services.
c. Above 6 GHz, BMW will focus on providing ultra-high wideband speeds.

2.2 ANTENNAE RECONFIGURATION:

2.2.1 Reconfiguration Types

Based on the characteristics of the reconfiguration methods, there are four categories that can be applied to reconfigurable antennas like shown in Figure (2.1) [46].

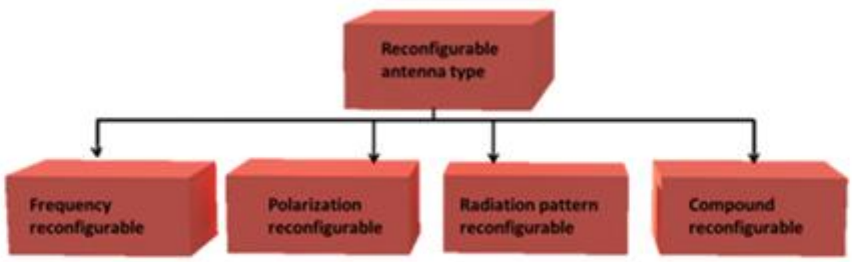

Figure 2.1: Antenna Reconfigurable Types [46].

2.2.2 Frequency Reconfiguration

When a system runs in various frequency bands in today's communication systems, individuals can observe a range of circumstances. The simplest example is when signals are received on one frequency by a transceiver and transmitted on another. Instead of utilizing a different antenna for each band in this case, a frequency-reconfigurable antenna might be employed to lower system costs and simplify the design and operation of the system. The primary goal of antenna design is to maintain the desired frequency. overall operating frequency bands, the radiation and polarization patterns are measured. Given that the antennae's physical size cannot typically be altered, this is a challenging undertaking. During the procedure, adjustments are straightforward. Of course, using mechanical devices to manage antennae concerts is never required.

The alternative, though, is to employ switches to modify the antennae's physical attributes. The electrical system and the current distribution of the antennae need to be adjusted. By modifying the antennae length in response to surface current velocity, a frequency reconfiguration can be accomplished [46]. The frequency reconfiguration procedures fall into three types. Ultimately, mechanical and electrical methods are utilized to control the properties of the material that was used to create the antennae. The antennae construction, which serves as an example for these techniques, showed how to mechanically tune a metamaterial unit-cell's overall thickness to change the resonance frequency [47]. The benefits of mechanical frequency reconfiguration systems include linear behavior, minimal inter-modulation harmonics, low loss rate, and wide frequency coverage. Their main problem, though, is that they are limited by things like bulky constructions and sluggish actuator switch rates. Most contemporary programs are incompatible with it. Electrical methods are routinely used to switch PIN-diodes and FETs. These systems have one disadvantage over mechanical ones, although being much faster: in order to regulate the switching components, they require an extremely complex biasing network.

2.2.3 Polarization Reconfiguration

The antennaes can change their polarization state while maintaining a steady frequency and radiation pattern in this form of re-configurability. MIMO antennae systems favor reconfigurable antennaes with various polarization patterns. These are achieved by changing the surface morphology of the antennae's feeding network, which alters the direction of the electric field. So theoretically, there is a 3 dB power loss when an antennae is communicating with merely a linearly polarized antennae. A vertically polarized antennae is effectively shielded from its surroundings. These antennae radiation patterns stand out because they cover the ground level from horizon to horizon. Polarization that can be changed is being implemented. These antennae provide excellent line-of-sight (LOS) without path mismatching, hence improving the radio connection budget [48].

2.2.4 Radiation-pattern Reconfiguration

An additional crucial subject in smart antennas is the reconfiguration of the radiation pattern. This statement describes antennae gain control in both the azimuth and elevation planes as well as beam-steering methods. By simply concentrating the signal, the reconfigurable antennas of the radiation-objective pattern enhance link quality. This results in superior antennae gain control inside a specific coverage region or in a specific direction. The main strategy for putting these properties into practice is current control. spread of the antennae, changing frequency behavior and matching of the antennae impedance. Therefore, while altering the antennae's beam or power, matching attributes must be taken into consideration [49]. Moreover, the fundamental challenge for a pattern reconfigurable antennae is to provide beam-switching capabilities with little use of parasitic elements, an antenna array, or simple switching circuits, all while maintaining good pattern variety. [43]. This work indicates that producing high-quality pattern reconfigurable variety with low-profile printed antennae is a difficult task. You may view an illustration of this technique in [50]. This type of reconfigurability is achieved by adjusting the electric field orientation through modifications to the interactions between the antennae's surface structure and feeding network [49].

2.2.5 Compound Reconfiguration

Additionally, compound reconfigurable antennaes can be set up to function with different characteristics. They have the ability to modify each frequency's frequency and polarization phase as well as the shape of their radiation pattern to produce a variety of reconfigurable processes. Furthermore, numerous designers provide various antennae characteristic configurations [51]. To provide pattern and polarization variation, two orthogonally oriented strips were used, and such compound antennae designs are given special design requirements in [52].

2.3 RECONFIGURATION TECHNIQUES

It is simple to select a reconfiguration strategy that consistently yields the needed functionality or characteristic in order to obtain the necessary reconfiguration functionality.

In order to achieve reconfiguration using the reconfigurable antennae, four universal methodologies are required. This makes it possible to employ the matched antennae for a real-world wireless communication task that calls for a flexible RF frontend. are displayed in [50] (Figure 2.2).

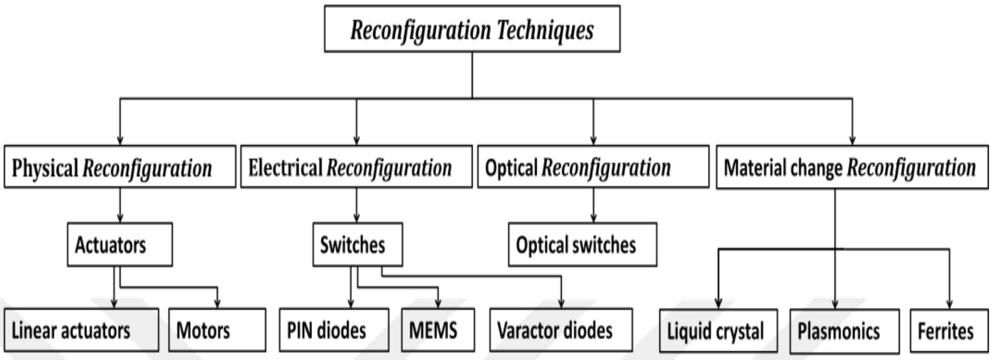

Figure 2.2: Reconfiguration Technique of Reconfigurable Antennas [51].

2.3.1 Physical Reconfiguration

Mechanical Reconfiguration techniques employ both linear actuators and motors [51]. They require rotating mechanisms like servo motors but lack biasing networks like electrical reconfiguration approaches. as shown in [53].

2.3.2 Electrical Reconfiguration

That is, re-configurability can be attained with a range of switching techniques that find the ideal balance between complexity, effectiveness, and cost, such as image silicon [54], varactor diodes [55], PIN diodes [56], RF MEMS, or optical switches [57]. As a result, [58] provided a detailed comparison utilizing those switches. Electrical switches have certain features and a number of limitations, as listed in Table 2.1 below, despite the fact that they provide active reconfiguration procedures.

Table 2.1: Comparison Between Different PIN and RF MEMS Switches [58].

Electrical Propertious	Units	PIN Diodes	RF MEMS
Voltage	V	3-5	20-100
Current	Ma	3-20	0
Power Consumption	mW	5-100	0.05-1
Switching Speed	Sec	100nSec	1-200µSec
Isolation (1-10 GHz)	dB	Hisgh	Very High
Loss (1-10 GHz)	dB	0.3-1.2	0.05-0.2

2.3.3 Optical Reconfiguration

Antennae reconfiguration optically refers to the process of using optical signals to modify the operating characteristics of an antennae. This can be achieved by using a variety of techniques, such as optically controlled reflectors or phase shifters, to modify the properties of the antennae. One possible approach to optically reconfiguring an antennae is to use optically controlled reflectors to change the direction of the antennae's radiation pattern. These reflectors can be made of materials that change their optical properties in response to an applied voltage or current, allowing the direction of the reflected signal to be controlled. Another approach is to use optically controlled phase shifters to modify the phase of the signal being transmitted or received by the antennae. This can be used to change the direction of the radiation pattern or to adjust the phase of the signal to compensate for signal distortion or interference. Optically reconfigurable antennaes have several advantages over traditional antennaes. They can be designed to be smaller, lighter, and more efficient than traditional antennaes, making them ideal for use in applications where space and weight are at a premium. They can also be rapidly reconfigured to adapt to changing operating conditions, making them ideal for use in dynamic environments. Overall, the use of optical signals to reconfigure antennaes has the potential to revolutionize the design and concerts of antennaes, enabling them to be more flexible, efficient, and adaptable to changing conditions. The use of optical switching technology is supported by embedded photoconductive switching systems in antennaes as well. When the antennae construction is only exposed to a laser beam, the photo detector switches become conductive [59]. Most of these techniques are explained. in [59], and [60].

2.3.4 Material Change Reconfiguration

Material change reconfiguration refers to the process of modifying the physical properties of a material in order to alter its functionality or concerts . This can be achieved through a variety of techniques, including changes in temperature, pressure, or electromagnetic fields. One example of material change reconfiguration is shape memory alloys (SMAs), which are metals that can "remember" their original shape and return to it after being deformed. By applying heat or other stimuli, SMAs can be reconfigured to change their shape, making them useful for a variety of applications, such as actuators, sensors, and medical devices. Another example of material change reconfiguration is the use of smart polymers, which are polymers that can change their physical properties in response to changes in their environment, such as temperature, pH, or light. By changing the environmental conditions, smart polymers can be reconfigured to alter their stiffness, shape, or other properties. Material change reconfiguration has many potential applications in various fields, including aerospace, biotechnology, and robotics. For example, reconfigurable materials could be used to create adaptive structures that change shape in response to changing environmental conditions, or in soft robotics to create soft, flexible robots that can change their shape and function depending on the task at hand. Overall, material change reconfiguration has the potential to enable the development of new materials and devices with unprecedented levels of functionality and adaptability. Magnetic ferrites can be used to construct reconfigurable antennaes [61]. Liquid crystals and smart materials like grapheme are examples of reconfiguration techniques based on material change. [62].

2.4 ANALYSIS OF PIN DIODE

A PIN diode is a type of diode that consists of a p-type semiconductor material, an intrinsic or un-doped semiconductor layer, and an n-type semiconductor material, forming a PIN structure. It is a type of photo-detector and is commonly used in electronic circuits for high-frequency switching, attenuation, and phase shifting. The intrinsic layer in the PIN diode is designed to be wider and have a lower doping concentration compared to the p-type and n-type layers, allowing it to have a higher resistance and lower capacitance. This makes the PIN diode suitable for use in applications requiring high speed and low noise, such as in microwave and RF circuits. PIN diodes work by varying their forward bias current to control their impedance and capacitance. When a forward bias voltage is applied, the diode becomes conductive, allowing current to flow through it. When a reverse bias voltage is applied, the diode becomes non-conductive, and its impedance increases. One of the key advantages of PIN diodes is their ability to handle high levels of power without being damaged. They are also highly responsive to changes in voltage, making them ideal for use in switching and modulation applications. Additionally, they have a wide range of frequency response, making them useful in a variety of high-frequency circuits. Overall, PIN diodes are an important component in electronic circuits, especially in applications that require high-speed switching and low noise. They are commonly used in RF and microwave circuits, telecommunications, and radar systems, among others. In this section of the work, the author introduces an analysis of PIN diodes, which is an essential component of the projected research as they are used to control the antennae's concerts. At radio and microwave frequencies, a PIN diode is a kind of semiconductor device that functions as a variable resistor. The study is provided to clarify how these PIN diodes work in relation to the antenna design. Within the range of microwave frequencies, the PIN diode functions as a variable resistor. It has two settings, ON and OFF, and functions like a switch. These states can be attained by applying either forward or reverse bias to the PIN diode. The PIN diode has low impedance when it is forward-biased, which occurs when it is in the ON state. The diode acts like a short circuit due to its low impedance, which permits current to pass through it. On the other hand, the PIN diode experiences reverse biasing in the off state, which results in high impedance. The diode functions as an open circuit in this state, blocking the flow of current. As shown in Figure 2.3, the PIN diode is composed of three regions: an intrinsic (I) area in the middle, a severely doped n-region, and a heavily doped p-region. Because of its construction, the diode can act as a variable resistor in response to an applied bias. The PIN diode functions almost like a constant capacitance when reverse-biased. The PIN diode acts as a variable resistance with fluctuating current flow when it is forward-biased. This analysis of the PIN diode's characteristics and behavior is crucial for understanding how it functions as a switch in the context of the projected antennae design. By controlling the bias applied to the PIN diodes, the antennae's concerts can be modified effectively, achieving the desired outcomes. This section provides essential information to readers about the principles behind using PIN diodes to control the antennae's behavior, ensuring a clear understanding of the projected research's technical foundation.

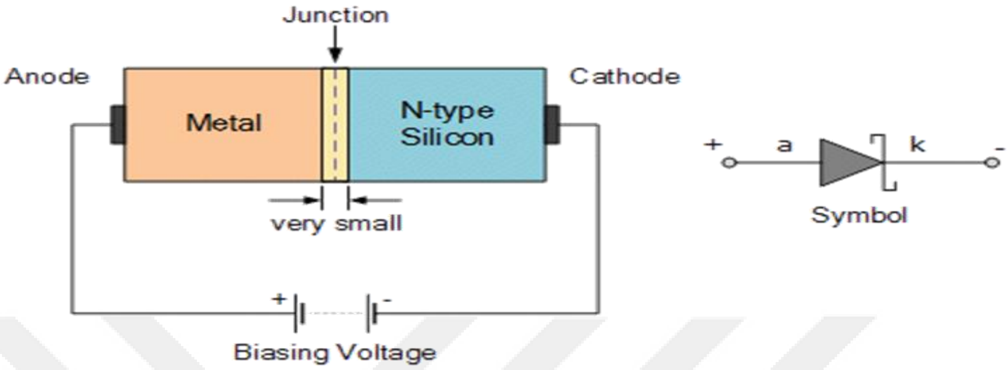

Figure 2.3: Principle of PIN Diode [63].

PIN diodes are utilized in physics for a number of applications, such as radio frequency attenuators, microwave attenuators, and microwave switches. A few examples of these uses are listed below. [63]:

a. These diodes are employed in RF, microwave, and variable microwave attenuators due to their low capacitance.

b. They have been utilized in photovoltaic cells and photodetectors, and PIN photodiodes are used in switches and fiber optic network cards.

c. These diodes can be utilized as an RF switch and for RF protection circuits.

d. Gamma and X-ray photons can also be located using the PIN photodiode. In addition, PIN diodes are used in microwave and antenna applications because of their high reliability, high voltage capability of over 2000 volts, high current capability of over 25 amps continuous, high surge current capability of over 500 amps, low distortion of less than -60 dBc at 455 kHz, high power gain of over 10,000:1, fast switching speed of less than 100 ns, small physical size, and availability of a range of thermal packaging [64].

2.5 GENERAL NOTATIONS AND COMPARISON

There are numerous wireless systems that can use the reconfigurable antennaes, including [60], [61]:

a. Based on cellular, personal, and millimeter-wave communications networks as well as 5G networks.
b. Wireless sensors and health monitoring technologies are part of IoT networks.
c. MIMO mobile phones with fields-based Cognitive Radio Application.
d. Frequency modulation reconfigurable antennae elements based on radar systems for communications in space.
e. Terahertz communication technology.
f. Reusable antennae for wireless local area networks based on frequency bands.

Table 2.2: The Benefits And Restrictions of Antennae Reconfiguration Approaches are Described. [60].

Reconfiguration	Advantages	limitations
Electrical Reconfigurati	➢ Ease of implementatio ➢ Low-cost	➢ Complex structure ➢ Requires biasing systen
Optical Reconfiguration	➢ No need the use of bias lines. ➢ No intermodulation distortion.	➢ No need the use of bias lines. ➢ No intermodulation distortion.
Mechanical-reconfiguration	➢ No need of active elements ➢ No need of biasing system	➢ Slow response ➢ Requires power source
Smart-Materials-reconfiguration	➢ Low-profile ➢ Lighter weight	➢ Low efficiency ➢ Limited application

The author used a comparative study between the discussed methodologies to order to compare the strategies further as in Table 2.53

Table 2.3: Comparison Between of Different Techniques [42].

Re-configurability	Advantages	Disadvantages
Varactor	Continuous tuning Nonlinear Small energy	Small range of tuning Very slow
Physical	No biasing	Slow response, High cost , High power need, large bulk
RF PIN	Less necessary driving voltage	On linear A high DC bias voltage Poor quality
Optical	Linear Properties High reliability	Complex, Loss behavior, Active mechanism
RF MEMS	Insertion loss is low, isolation i linearity is great, power loss is l and a DC supply is not utilized	High control voltage (50-100 V), Low switching velocity, Poor dependability Short lifespan
Smart materials	Size as it has high relative permittivity and permeability	Low efficiency

2.6 MIMO BASED ANTENNAE ARRAY

To solve the data throughput constraint suffered by traditional Single-Input-Single-Output (SISO) wireless communications, Multiple-Input-Multiple-Output (MIMO) technology was created. in circumstances of signal fading, multipath, and interference [65]. To send more data simultaneously, MIMO technology employs multiple transmitters and receivers. MIMO divides communication systems into three categories:

a. The data throughput constraint observed by traditional Single-Input-Single-Output (SISO) wireless systems led to the development of Multiple-Input-Multiple-Output (MIMO) technology. communications under conditions of interference, multipath, and signal-to-fade to fade [66].

MIMO technology uses To transfer more data simultaneously, use numerous transmitters and receivers. MIMO categorizes three main kinds of communication systems, as shown in (Figure 2.4) .

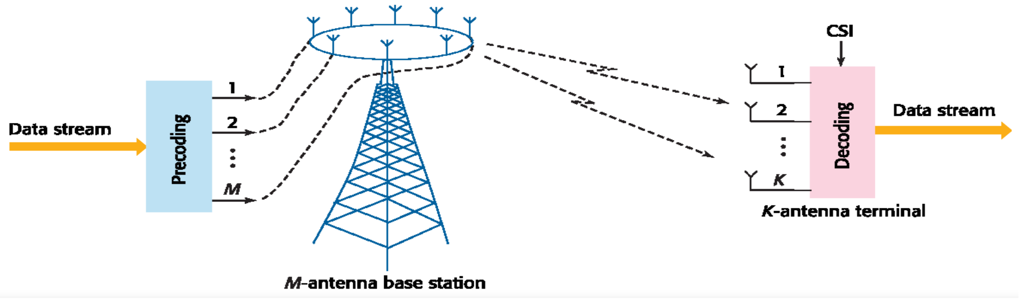

Figure 2.4: Point-To-Point MIMO System [64].

b. 2. The concept underlying the other form, multiuser MIMO, is that one base station can employ a single time-frequency resource to service several terminals simultaneously. As seen in (Figure 2.5), multiuser MIMO is produced from point-to-point setup by splitting the number of antennae on the terminal sides.

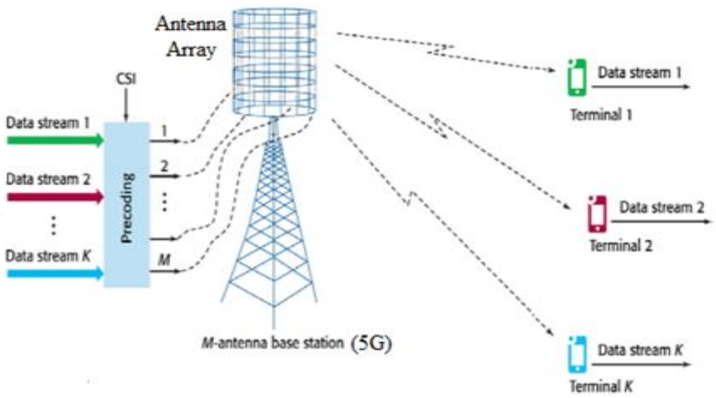

Figure 2.5: Multiuser MIMO [65].

c. Lastly, Massive MIMO: This technology prevents base stations from collaborating in any way since each base station has an enormous number of antenna terminals. as seen in Figure 2.6.

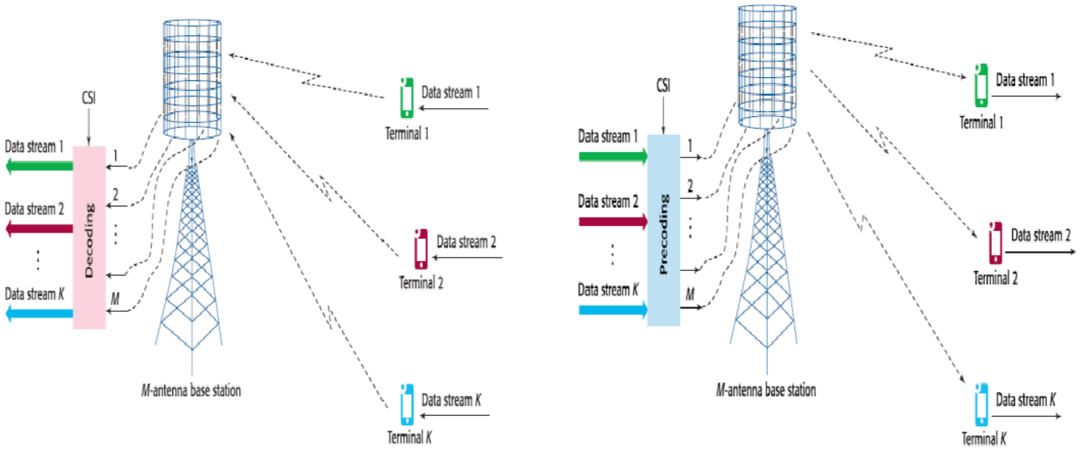

(a) (b)

Figure 2.6: Massive MIMO in (a) Uplink (B) Downlink [65].

5G antennae offer several advantages, including improved efficiency, fewer interference, faster speeds, lower latency, and more capacity for connected devices. As smartphones and other mobile terminals become more ergonomic and multipurpose, antennae reduction is crucial to boost MIMO channel capacity for 5G at sub-6 GHz [66].

2.6.1 Applications of MIMO System

Numerous applications make use of MIMO systems. Another use that is quickly expanding in a variety of industries, such as wearable computing, healthcare, and military organizations, is wireless body area networks (WBAN). The human body has a high dielectric constant in the microwave. range The human body has low microwave conductivity, a significant loss tangent, and a high dielectric constant. Because of this, dispersion from the body and its surrounds as well as polarization mismatch can reduce an antennae's gain and radiation efficiency when it is employed on or within the human body. Multi-input, multi-output (MIMO) systems were a potent method for enhancing overall concerts and mitigating multipath fading [66]. A thin mobile device with support for wide resonant modes at 0.77 GHz for LTE WiBro (Wireless Broadband) functioning requires band 13 and 2.35 GHz, as well as a broad resonant mode of around 2 GHz for wideband code division multiple access. (WCDMA) operations has been used in another MIMO application [65]. For laptop computer applications, better signal transmission and reception has been sought for using the 2.4/5.2/5.8 GHz band as an additional application for Tri-band WLAN MIMO operation. For WLAN MIMO operation, a small WLAN antenna array with superior antennae isolation and radiation efficiency is needed. Furthermore, a dual-band strip resonator is placed between two WLAN laptop computer antennae in order to collect near-field radiation from one to the other and improve isolation in the WLAN bands [66]. Wi-Fi 802.11n is another use for MIMO [67]. Mesh networks, including 4G and 5G [68] and Muni Wireless [58]. RFID and the Digital Home [60] [61]. However, there are several benefits to using the MIMO system to reduce size. One such benefit is the construction mobile phone apps for the original self-antennae element consist of two vertical stubs the 5G (MIMO) system. Without the use of extra isolation devices or decoupling procedures, an 8-antennae MIMO system is capable of achieving very excellent isolation and antennae efficiency [67]. Utilizing chip-based The experimental demonstration of LED arrays as wavelength-selective, high-concerts, and self-powered photo detectors (PDs) [68] made possible gain-based micro-LED in (LED) arrays for a variety of multipurpose devices, including micro-displays, solar cells, photo detectors, and data transmitters using 405 nm violet laser diodes (LDs) as transmitters, multiple-input multiple-output (MIMO) visible light communications at high speeds. An in-depth examination of the ambiguity function in radar applications serves as the foundation for a method for constructing a 2-D-array for multiple inputs and outputs (2-D-MIMO) in 3-D imaging. An investigation is conducted into the uncertainty throughout the whole angular field of view function. Consequently, the influence of any invasive signals beyond the domain of interest is considered, thereby enhancing the reliability of the results. A genetic algorithm developed to enhance a four transmitter and eight receive element 2-D-MIMO sparse array guarantees an angular resolution of 8 and 5.9 on the azimuth and elevation angles, respectively, as well as an ambiguity-free region span in azimuth and elevation angles greater than 120. High-frequency surface wave (HFSWR) radars are utilized in conjunction with space-time adaptive processing (STAP) in an HFWSR configuration to improve the resolution and accuracy of coastal radars as well as the identification of sluggish objects. MIMO is also used through radar to provide multiple benefits for mitigating multipath caused by propagation effects and fading environments in many different applications Therefore, MIMO antennaes with the capacity to transmit waves in a number of patterns and polarizations have become crucial in recent years in modern telecommunication systems. The concerts of MIMO systems can be negatively impacted by increases in mutual coupling because of how they can affect antennae properties. The reciprocal coupling in the digital domain can be optimized to somewhat improve concerts . However, using methods like defective complementing split ring resonator, ground structure, parasitic or slot element, and decoupling networks, which may circumvent reciprocal coupling effects through physical implementation, is the most basic and efficient strategy [69].

2.6.2 Standard MIMO Configurations

For simultaneous transmission and reception of various data streams, MIMO radio employs many antennaes. The number of antennae needed for a radio is decided by the manufacturer based on what they think would function best for transmission and reception with their particular hardware and software.

a. Typically, 22 MIMO is used (two transmit antennaes, two receive antennaes)
b. MIMO uses three transmit and three receive antennaes (three transmit antennaes, three receive antennaes).
c. another type of MIMO Four send antennaes and four receive antennaes (four transmit antennaes, four receive antennaes).
d. third type of MIMO Eight send and eight receive antennaes (eight transmit antennaes, eight receive antennaes).

For MIMO radios, a variety of antenna options are available based on the customer's preference for configuring the radio system in accordance with the particular needs of that application. Antennae for MIMO applications generally fall into two categories. into the subsequent groups:

a. The most prevalent kind of antennaes are vertically polarized dipoles. These are the same antennaes used in SISO systems, with the exception of the MIMO system employing two or more of the same antennae. Practically any omnidirectional antennae may be utilized as long as it satisfies the specifications for the required frequency bands, gain, RF power handling, and other system factors.
b. Products that have several antennaes in a single unit. Each of these antennaes' two or more RF connections links to a separate antennaes inside the vehicle. These are The two elements are typically offset from one another by 90 degrees (orthogonally) and produced with slant left and slant right polarization. This provides more antennae polarization variety for active RF situations without adding difficulty to the end user's system installation.

2.7 MICROSTRIP ANTENNAE FEEDING TECHNIQUES

2.7.1. Coaxial Probe

It is among the simplest ways to send microwave energy. The probe can be used as the inner conductor of a coaxial wire or, in the case of coaxial line feeding, to supply power to a microstrip antenna through a slot in the common ground plane from a triple line (strip-line). an ordinary microstrip antenna connected by a type N coaxial cable. The coaxial center conductor is soldered to the patch metallization after passing through the substrate, and a coaxial connection is fastened to the back of the printed circuit board. The feed point position is selected to obtain the best impedance match for the given mode. The primary method of excitation of the patch is the coupling of the feed current to the patch modes like shown in (Figure 2.7) [69].

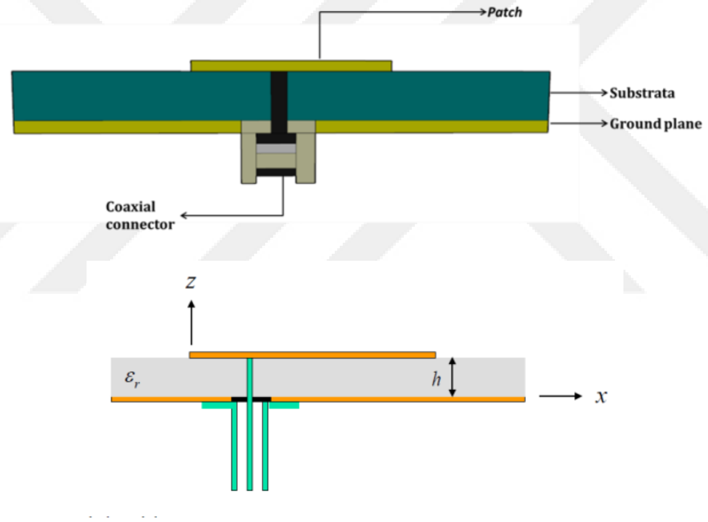

Figure 2.7: Coaxial Connector [69].

2.7.2. Coplanar Waveguide

Cheng P. W. invented the coplanar waveguide in 1969 [70], primarily to include non-reciprocal elements like gyrators and isolators into planar transmission line circuits. In the simple design of the ordinary coplanar waveguide antennae, the GND plane is only partially composed of the two parts that are pictured, and it lies above the dielectric substrate.

As seen in (Figure 2.8).Coplanar waveguides, a kind of electrochemical planar transmission line that uses circuit board technology, are used to transfer microwave signals. On a smaller scale, monolithic microwave-integrated switches also contain coplanar waveguide transmission lines.[69]

On the other hand, A (CPW) has a single conducting route printed into a dielectric substrate in addition to two return conductors—one on each side of the track. Since they are all three on the same dielectric substrate, they are all coplanar [71].

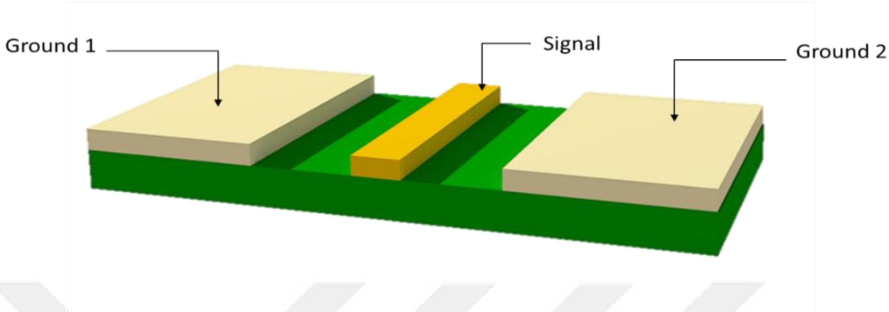

Figure 2.8: Co-Planer Waveguide [72].

2.7.3 Inductive Aperture Coupling

Two unique substrates are present in aperture coupled feed and are separated from one another by a ground plane [72]. This technique uses a slot in a ground plane to link the microstrip patch and feed line [72]. With the aperture-coupled feeding technique, interference is reduced and pure polarization is achieved.(Figure 2.9) shows this feeding technique.

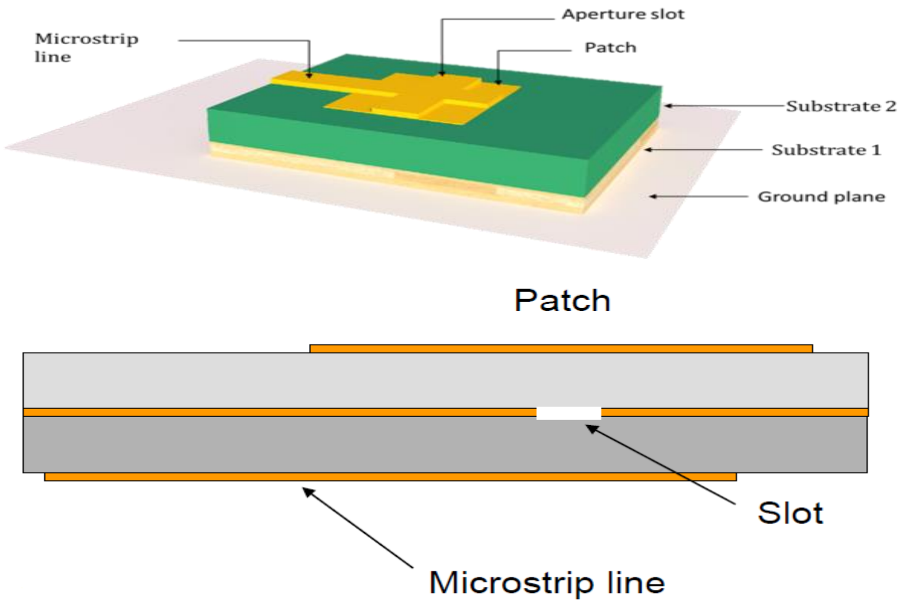

Figure 2.9: Aperture Coupled Feed [72].

2.8 ARCHITECTURAL SCENARIO OF 3D ANTENNAE MIMO PROPAGATION

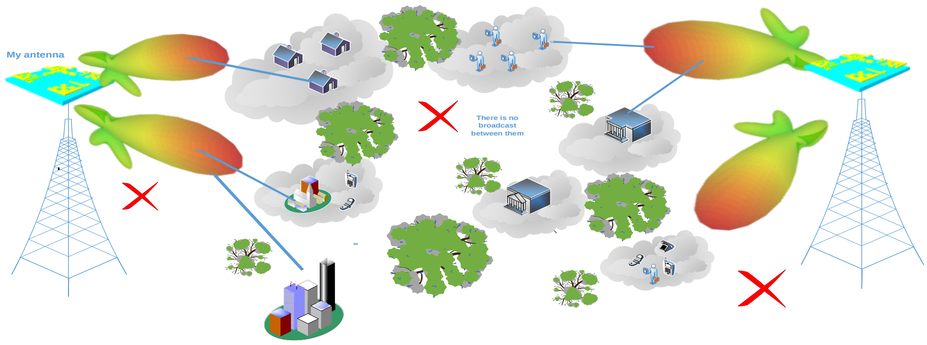

Figure 2.10: Scenario of MIMO Antenna Propagation [73].

The author depicts a 5G communication scenario using an antennae operating between two sectors in this illustration. It demonstrated how the user receives directional antennae propagation without experiencing any propagation loss. This specifically applies to the transceiver method's antennae control inside the constrained frequencies of sub 6 GHz [73].

2.9 INTRODUCTION TO MAIN DESIGN OBJECTI.VES

The growth of mobile communication systems has reached a point where ultra-high data rates in the gigabits-per-second region are required[74]. Researchers have been challenged by the growing demand for high-speed communication, and the answer that has emerged as a result is to enhance physical communication in the millimetre-wave frequency above 6 GHz [74]. As a result, the existing congested spectrum must be abandoned in favour of a new, limitless capacity accessible in the millimetre-wave range[72].

For DSRC-band applications, It has been suggested to use a low-profile fractal antennae and related array[74]. The projected single element is a freshly built right-handed circularly polarized (RHCP) fractal antennae developed from the Koch-snowflake 1st-iteration. Additionally, a ground plane defect with a diagonal slit was employed to resonantly align the structure at the required frequency while minimizing cross-polarization over the operational frequency [73]. Metamaterial surfaces are essential for suppressing surface waves and achieving in-phase reflection, which improve antennae concerts [74]. In that study, the concerts of a metamaterial-based antennae and a fifth-generation (5G) antennae design for 5G communication system applications were compared. Metamaterial surfaces are utilized as reflectors to increase antennae gain because of their high impedance and in-phase reflecting properties [75]. The antennae's efficiency falls significantly as a result of a conventional conducting ground plane's insufficient surface wave suppression.

The integrated MIMO antennae system for 5G wireless communication services combining Long Term Evolution (LTE) and Millimetre-Wave (mm-wave) technologies is demonstrated in this paper[76]. An LTE MIMO with two elements The four-element 5G MIMO configuration and a rectangular[78] antennae make up the projected design. Moreover, the ground plane exhibits spherical flaws. The suggested structure is constructed on a 0.76mm-thick Rogers RO4350B substrate for experimental confirmation. [79]. The substrate measures a total of 110 mm by 75 mm. The proposed structure might operate at frequencies in the range of 5.29–6.12 GHz (LTE 46 and 47 bands) and 26-29.5 GHz (5G mm-wave).[77]. The isolated ground-radiation antennae (iGradiANT) is used in a 5G multiple-input multiple-output (MIMO) antenna array, illustrating its applications. [79]. It is inherently isolated from another neighboring antenna element. GradiANT is made possible by merely enhancing a standard ground-radiation antenna with a small out-of-ground loop (GradiANT). Because of this, the projected GradiANT may support both an in-ground loop-type current mode and an out-of-ground loop-type current mode, which oversee approaching energy cancellation and dangerous radiation, respectively, in contrast to existing GradiANTs. [77].

In this paper, We suggest a millimeter-wave (mm-wave) operating Structure of metamaterial (MTM) with reconfigurable capability [80]. The MTM's reconfigurable feature with two configurations is accomplished using four switches [81]. These two arrangements have various refractive indices, which are utilized to steer the antennae's radiation beam in the desired directions [81]. Operating at 28 GHz, the projected planar dipole antennae is in the 5th generation (5G) spectrum. A microstrip printed antennae for 5G applications is presented [83]. It is covered with meta-material unit-cellss and features dipole arms on the substrate's front and back planes. on each side. The optimal locations in relation to the dipole arms are where the meta-material cells are located [81].

2.9.1 Antennae Design and Geometrical Details

To feed a micro strip line, the suggested antennae is built from a coplanar waveguide. The micro strip line is invoked to excite a T-resonator that is connected to one split ring resonator (SSR) unit-cells[79]. By stimulating harmonic plasmatic surface waves, To lengthen the electrical antennae effectively, the projected SSR is employed to shorten the antennae length. [84]. When compared to these based on direct connection, the antennae bandwidth is greatly increased by the T-resonator's inductive excitation of the SSR [83]. Every unit-cells is built through a succession of fractal size reductions that improve a current route motion on a patch surface [79]. The antennaes size are reduced to the same extent lambda/5.

2.9.2 Design Methodology

The suggested antennae dimensions are parametrically investigated in this part to understand the impacts of changing them with regard to the antennae concerts . The numerical analysis used for the parametric investigation is based on CST MWS[83]. The suggested antennae is organized. consist of 8 cell with a coplanar feed as seen in (Figure 2.11).

The suggested patch is printed without a ground plane on a FR4 substrate. With a height of 1.67 mm, the substrate dielectric constant is 4.3. It is believed that given a limited space, the cell geometry will increase the effective height (length).

The T-Resonator's benefits include expanding the bandwidth and supporting the antennaes to cut down on patch losses.

A transmission line is used to deliver power from the RF source to an antenna component. The load is being used to adjust the antenna radiation to the open space impedance. The coplanar waveguide feed is anticipated to match power throughout a large frequency range with little dispersion effects.

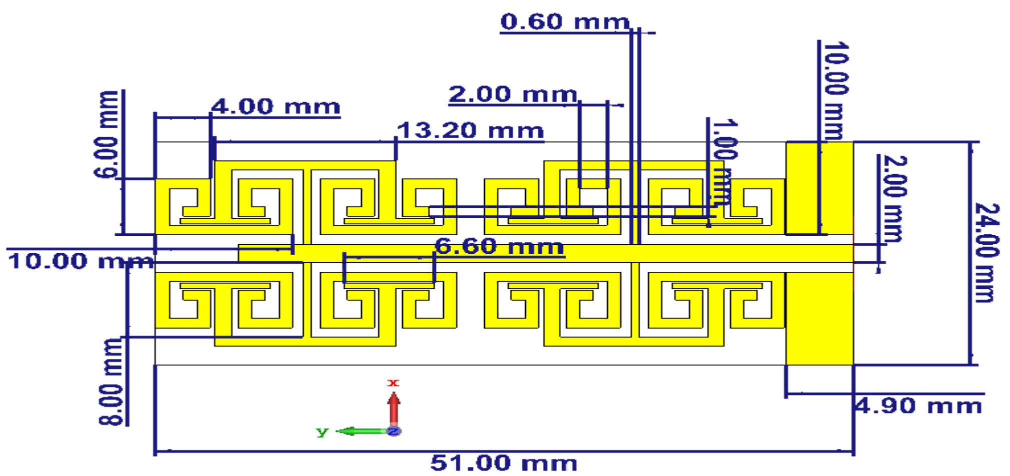

Figure 2.11: Antennae Geometry.

This section displayed the simulation results of Antennae design in many parameters such as S-factors, Gain and Directivity, we selected two bands (0.1 GHz and 6 GHz) as resonate frequencies because it has a good result in S11 and gain together. The CST microwave studio software is used to carry out the simulation. A coplanar waveguide with a transmission line on top of the substrate and a printed ground plane structure excites the antennas, as will be covered later[9]. Thus, as shown in (Figure 2.12(a)), the authors used their parametric analysis on the ground plane length to realize the impacts of that on the antennae S11 spectrum. The obtained results reveal that, in relation to the ground plane, the antennas exhibit no fluctuation in frequency resonance. However, there is a 0.5mm step in the length change (L) from 4 to 5 millimeters. On the other hand, the matching impedance is significantly affected by the initial resonance mode. The authors next conducted the same investigation on the distance gap (G) between a ground plane and a transmission line, ranging from 2 to 1 millimeters in steps of 0.5 millimeters, as shown in Figure 2.12 (b)). According to the findings in [86], the antennae bandwidth decreases with decreasing the distance between the transmission line and the ground plane. However, changing the antennae diameters generally affects the antennae resonances. As mentioned in [85], this is because the coplanar gap significantly affects the antennae matching impedance. Lastly, as shown in Figure 2.12(c), the ground plane width (W) is adjusted from 10 mm to 8 mm in steps of 1 mm to examine the impact on the S11 spectrum. It is found that the projected antenna show insignificant variations with respect to W variation.

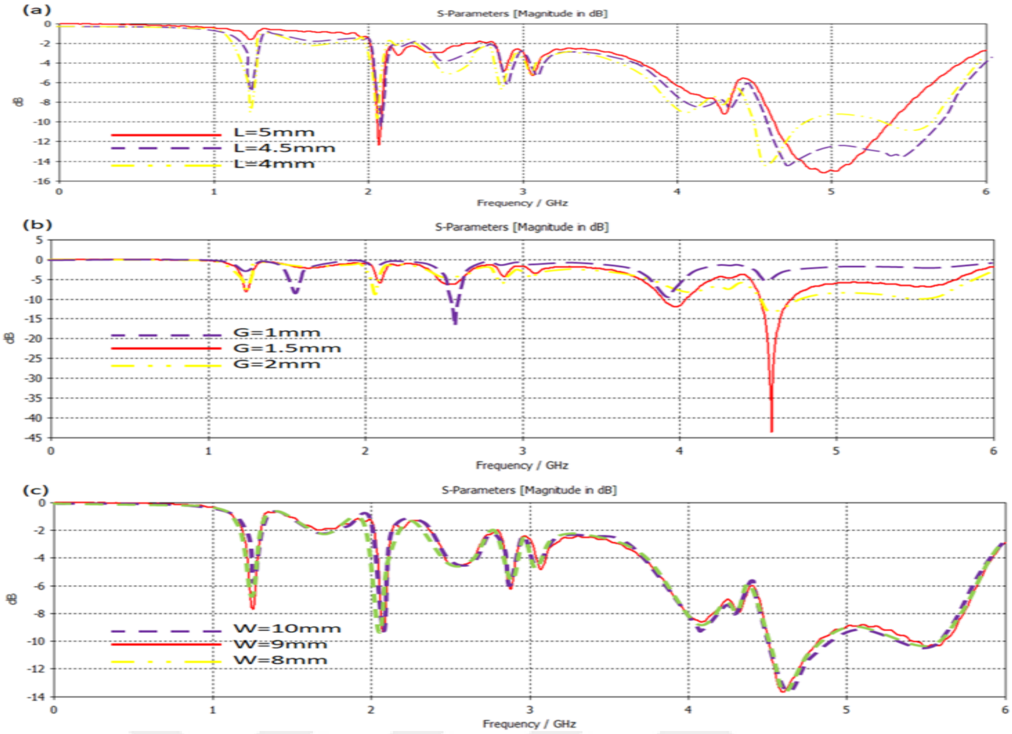

Figure 2.12: S_{11} parameter of the Proposal Design.

2.9.3. Results Validations

The suggested antennae findings are quantitatively assessed using CST MWS and HFSS in this part. The proposel antennae concerts in terms of S11 and gain curves are evaluated with in the frequency band between 3GHz to 6GHz, with the sub-6GHz, to suit the 5G applications. Nevertheless the antennaes radiation patterns are evaluated at 3.7GHz, 4.6GHz, 5.2GHz, and 5.9GHz. This analysis is conducted as following:

2.9.4 S_{11} curves

S_{11} is one of most important factors to describe the relationship between input and output power coupling [81]. S_{11} curve describes the return loss that realizes the matching between the input impedance of the antennae patch and the RF source. From Fig. 2.13, it is found that projected antennae S_{11} is about -10dB and -44dB at 2.5 GHz and 4.8GHz, respectively. For validation HFSS software package is invoked as seen in (Figure 2.13).

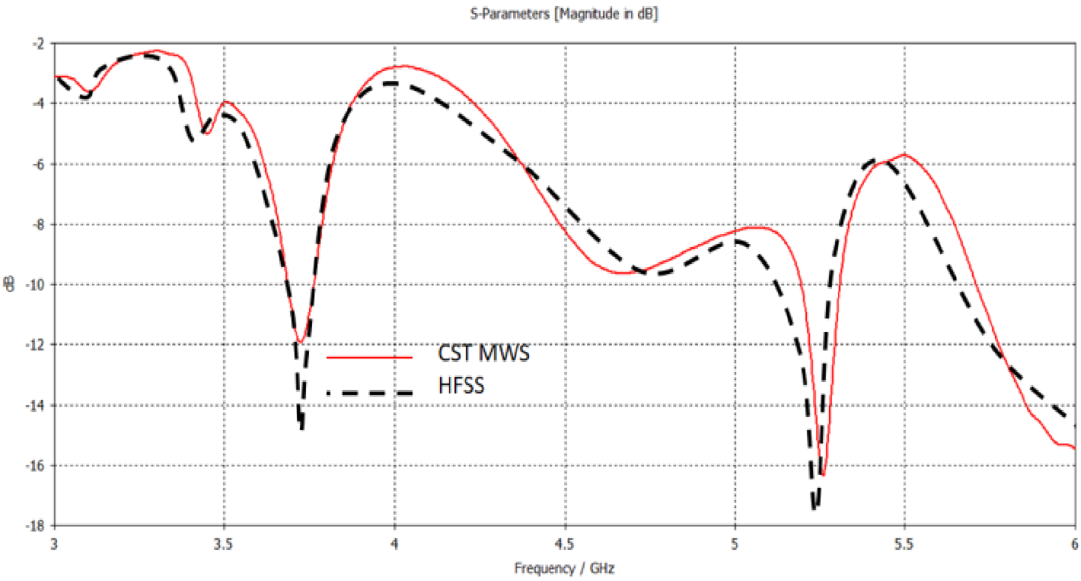

Figure 2.13: S_{11} Parameter Validation.

2.9.5 Gain Curves

The antennae gain is the efficiency of power transmitted in a certain direction with a specific reference point [88]. If the antennae radiates in all directions is called Omni-directional antennae [80]. When the antennae radiates at a specific direction is called directional antennae. In Fig. 2.14, the antennae gain curves pf the projected antennae from 0.5 GHz to 6 GHz. The obtained results are validated numerically using HFSS software package as seen in (Figure 2.14) .

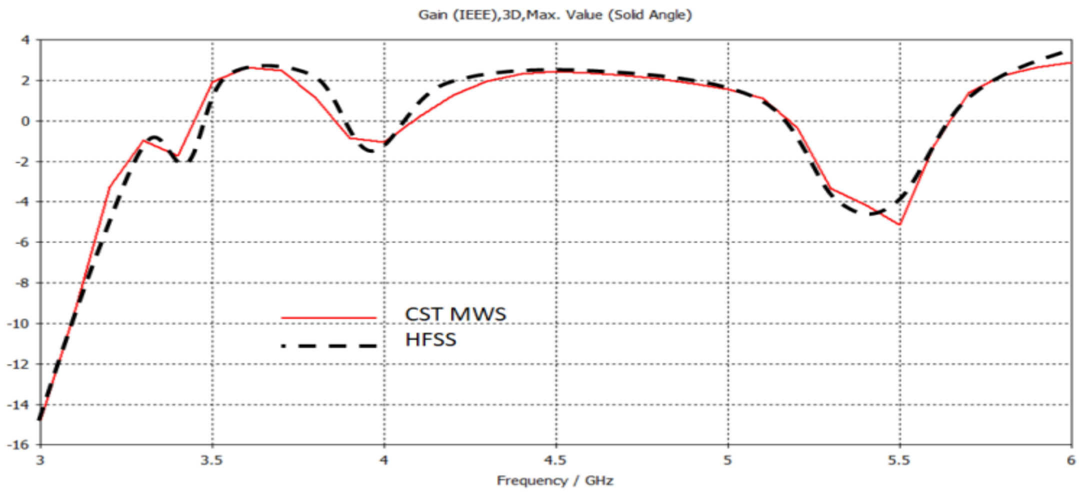

Figure 2.14: Gain Parameter Validation.

3. CHAPTER THREE

3.1 INTRODUCTION

Mobile communication networks are now being created quickly to meet the demands of mobile communication services [89]. However, Gigabit per second or higher data rates are necessary for the advancement of the present mobile communication systems [90]. As a result, one of the most crucial requirements was the necessity to create contemporary antennaes designs to support the wireless communication systems. [91]. Due to restrictions on antennae size, scientists in such situations have great hurdles in developing antennaes with a broad and increased gain [90]. However, by using a variety of strategies, numerous researchers were able to overcome the limitations mentioned. The authors in [92] created a composite right-left microstrip antennae with a higher gain-bandwidth result for RF energy harvesting [93] at 2.45GHz and 5.8GHz. A low-profile MTM array-based fractal antennae architecture was developed for modern Wi-Fi systems [94]. For 5G mobile devices at 3.5GHz only, a circularly polarized fractal Koch-snowflake patch with ground plane MTM defects was projected [93] [95].

Aside from that, MTM was crucial in the development of antennae systems because of its peculiar characteristics based on extraordinary electromagnetic constitutive parameters [97]. Therefore, the scientists in [96] adjusted the beam steering capacity by using two semiconductor switches in combination with specific MTM inclusions on their antenna patch. A alternative method based on applying an MTM layer on top of an antennae patch was published in [97] in order to boost antennae gain at Wi-Fi bands. In [98], the MTM structure was developed and applied to the antennae ground plane in order to lessen the back lobe effects at 3.4GHz. A further MTM introduction was proposed in [99] to ensure antennae surface wave propagation in the direction of the end-fire to boost gain and bandwidth. In order to attain a gain boost specifically at 4.6GHz for 5G communication networks, an MTM antenna design was ultimately published in [98].

As of [99], A microstrip antenna array at 28GHz bands for 5G networks was reported using 4X4 components; however, the band they selected had restricted propagation, which was not considered in their analysis. Another suggestion published in [100] called for the usage of a triple-band, dual polarization printed circuit antenna array for 5G applications. For 5G systems, a high gain-bandwidth antenna array was produced by positioning four antennae components on a 3D profile and dividing them using MTM defects. The projected antennae in [101] was, however, quite complex and was not appropriate for low-profile devices [102]. Additionally, a different design based on an optical switch-equipped reconfigurable antennae element that was projected in [100]. Without considering the examination of the array systems. For the same purpose, a microstrip antenna design with a limited gain at a single frequency band was published in [101].

This research proposes an antennae design based on an innovative MTM-array for the development of a small antennae structure for 5G communication networks. To ensure features of in-phase reflection The recommended MTM arrays are placed parallel to a copper wire to offer high impedance response and defense against surface wave retardation caused by antennae edges. Such a method may result in gains-bandwidth improvements over conventional printed antennae setups, as will be shown subsequently. Section 3.2 describes the antennae's geometrical features, while Section 3.3 goes into the antennae design techniques. Section 4 contains a validation of the obtained results. The conclusion of the paper is found in Section 5.

3.2 GEOMETRICAL INFORMATION AND ANTENNAE DESIGN

According to (Figure 3.1), the suggested antennaes is built from CPW to feed a microstrip line. The microstrip line is used to excite TR, which is connected to a single split ring resonator (SSR) unit-cells [100]. The proposed SSR is used to shorten the antennae by inducing the harmonic plasmonic surface waves that prolong the effective electrical antennae. [103]. The projected TR structures inductively excite the SSR, resulting in a significantly larger antennae bandwidth for the suggested SSR than for those based on direct connection [102]. Each unit-cell is constructed through a fractal sequence of size reductions, improving the present route motion on the patch surface [105]. Likewise, the antennae have shrunk to λ/5 in size. A transmission line with a 2mm diameter was made in order to accomplish a 50Ω Circuit matching and surface current motion transfer to the required TR [102]. [99] states that the current movement is pushed in the direction of the anticipated SRR by coupling effects on the proposed TR. The suggested CPW approach is presented to prevent the surface wave retardation that results from the usage of the transmission line junction and causes opposing interferences and inductive losses. The matching circuit's capacitive effects can be used to eliminate these effects [98]. The projected TR is presented to reduce the antennae edge surface waves that have a detrimental impact on radiation efficiency [99]. The microstrip patch has a height of 1.67 mm, a dielectric constant of 4.3, and is printed on a Taconic RF-43 substrate without a ground plane.

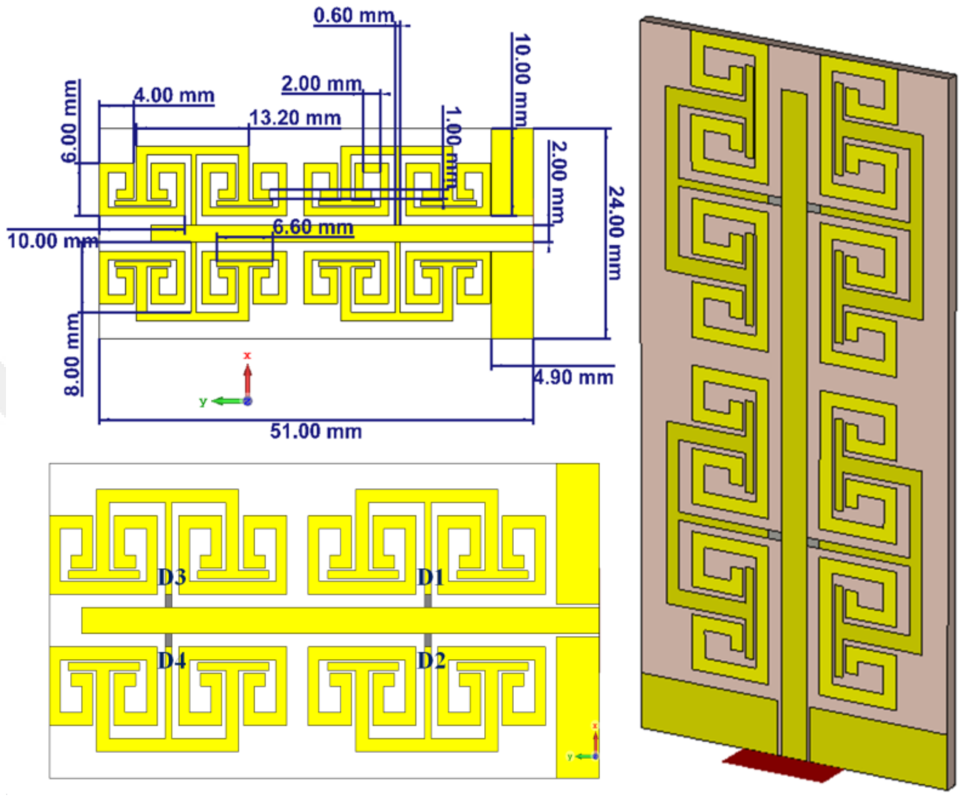

Figure 3.1: The Proposed Monopole Antenna Geometrical Details.

3.3. DESIGN METHODOLOGY

The suggested antennae dimensions are parametrically investigated in this part to understand the impacts of changing them with regard to the antennae concerts. The numerical analysis used for the parametric investigation is based on CST MWS [97]. The proposed antenna structure, shown in Figure 3.1, calls for printing the recommended patch on the substrate without the need of a ground plane. Because of the geometry of the cell, the effective length is assumed to increase within a limited space. The recommended TR has the advantage of supporting the antennae while lowering patch losses and boosting bandwidth [106]. Power for the antennae component is sent over the transmission line from the RF source. Use a matching load to match the antennae radiation to the free space impedance. [107]. It is believed that the recommended CPW feed will match the power with minimal phase retardation and dispersion effects over a wide frequency range [99].

3.3.1 Microstrip Line Design

The authors changed the transmission line length from 30 to 50 mm for parametric analysis in order to monitor S11 and gain curves. Such research is done to confirm the impact of altering the transmission line's length on the concerts of the antennae. (Figure 3.2(a)) displays the assessed S11 curves for the three microstrip lengths under consideration. According to research, the antennae frequency resonance shifts toward lower frequency bands when transmission line length increases due to an increase in electrical length [106]. However, it is observed that the antennae gain increases fast with antennae length due to an increase in surface current. [101]. The transmission line with a length of 50mm was therefore thought to be the best option by the authors since it exhibits a frequency resonance at 3.6GHz with an S11 of -25dB and gain of 3.1dBi.

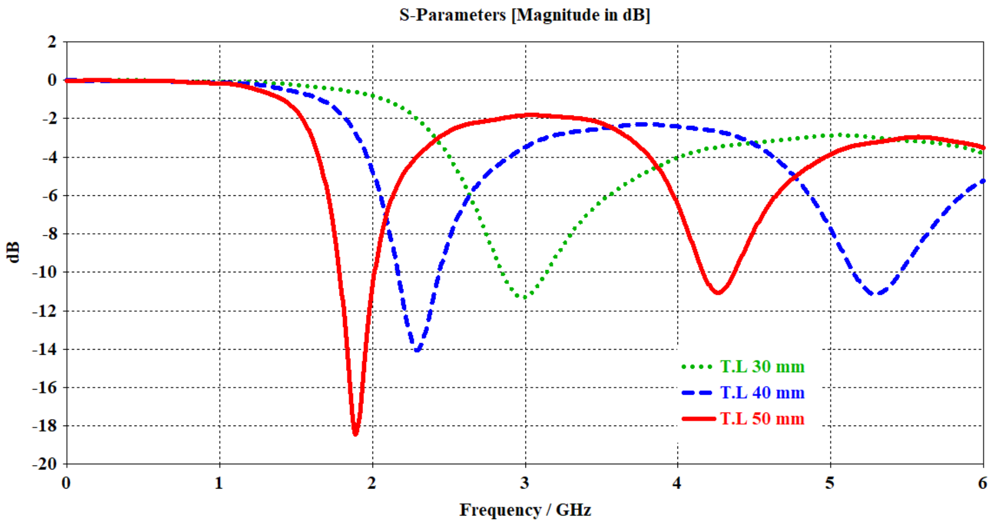

Figure 3.2: Antenna Performance With Changing L Value: (A) S_{11} Spectra and (B) Gain.

3.3.2 Unit-cells Effects

The proposed antennae are constructed in the shape of a butterfly using four unit-cells and SRR geometry. To ascertain the effects of adding them to the antennae concerts, the scientists employed a parametric study based on CST MWS. In this simulation, the first unit-cells were integrated into an antenna design. The authors then compared the results, in terms of S11 and the gain curves, to those of identical antennae designs based on (two, three, and four) unit-cells. We found that the antennae at the first cell display multiple frequency bands within the required frequency range, as shown in (Figure 3.3(a)). A definite rise in the antenna resonance modes is seen as the unit-cells count is increased. This is because the current motion at the intersections of the transmission line and the unit-cellss has faded. This fading is brought on by the projected unit-cellss' inductive addition, which chokes the current [106]. Due to the parallel connected between the fading spots, which is produces an efficient electromagnetic aperture coupling with the free space impedance, it is discovered that the antennae gain increases quickly. [102]. This is made possible by the planned transmission line's unit-cellss being connected in a serial fashion. The majority of the current motion in such a link is in the same direction as the suggested unit-cellss. Additionally, by combining the unit-cells in this way, two components from the transmission line opposite one another produce antiparallel equalized forces that don't change the direction of the current motion [102] in order to maintain the initial frequency resonance at 3.5GHz. However, their combination produces a succession of connection outcomes that add their individual impacts to one another. The suggested unit-cells is a capacitive inclusion, therefore by adding more of them and multiplying them, the equivalent capacitor may be significantly reduced [108], expanding the specific working frequency band [99]. As a result, it is discovered that the antennae gain at 3.5GHz is around 5.5dBi. (Figure3.3(b)).

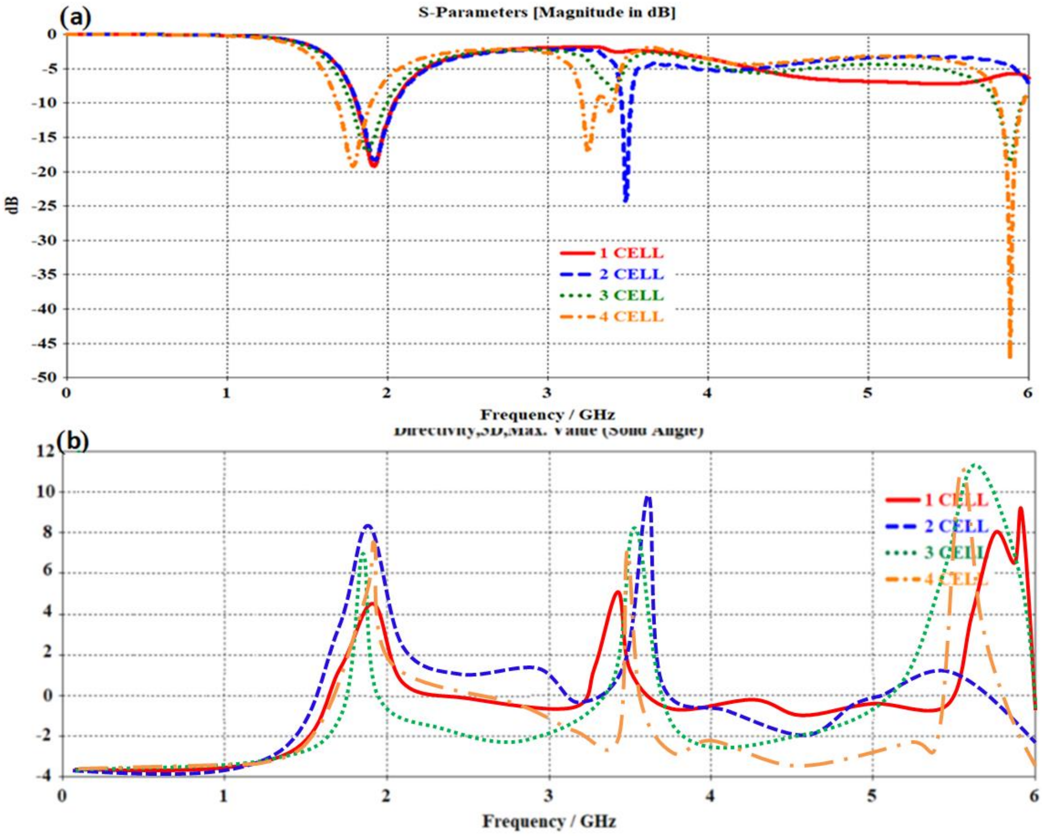

Figure 3.3: Antenna Performance With Different Cells Number: (A) S_{11} Spectra and (B) Gain.

3.3.3 TR Effects

In this part, the planned TR introduction's impacts on antennae concerts are quantitatively quantified. At the resonance frequency, electromagnetic energy is conducted to pair inductively [105]. It is found that the effects of the inductive coupling, which store the collected charges on the conductor's edges, allow the proposed TR to achieve an improvement in bandwidth. [104]. As a result, as illustrated in Figure 3.4(a), the antennae bandwidth is increased with a negligible drop in antennae gain. After incorporating the suggested TR structure, it is discovered that the antennae gain has risen up to 6.8dBi at this point. Such an increase in The inductive component of the suggested TR structure's charge accumulation cancellation is what is responsible for the antennae gain. [104].

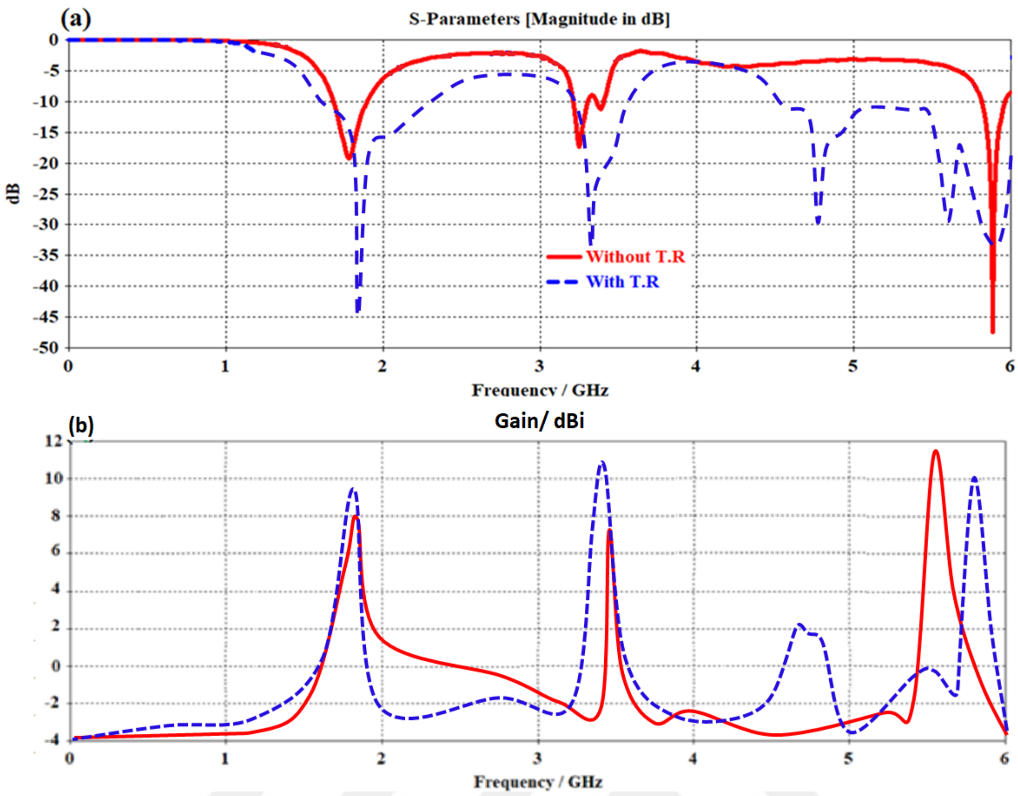

Figure 3.4: Antenna Performance With and Without TR Structure: (A) S_{11} Spectra and (B) Gain.

3.3.4. CPW Effects

As seen in (Figure 3.1), the projected antennae is supplied by a CPW arrangement. In an effort to optimize the antennae concerts, the scientists investigated the effects of altering the recommended CPW dimensions on S11 and gain curves. The antennae demonstrate a significant improvement when the distance between the antennae patch and the ground plane section of the projected CPW is adjusted, as shown in (Figure 3.5(a)). Antennae gain is shown to be improved by decreasing the air gap between the projected patch and the projected CPW ground plane. This is because of the electrostatic capacitive connection between the ground plane and the antennae components being eliminated [105]. With S11 below -10dB at 4.9mm distance, the antennae is discovered to give five primary bands at 1.6GHz, 2.6GHz, 3.9GHz, 4.5GHz, and 5.85GHz. Nevertheless, as demonstrated in (Figure 3.5 (b)), various adjustments at various frequency bands have an impact on antennae gain. However, it is discovered that the antennae bandwidth at 4.9mm distance is greatly increased compared to other lengths.

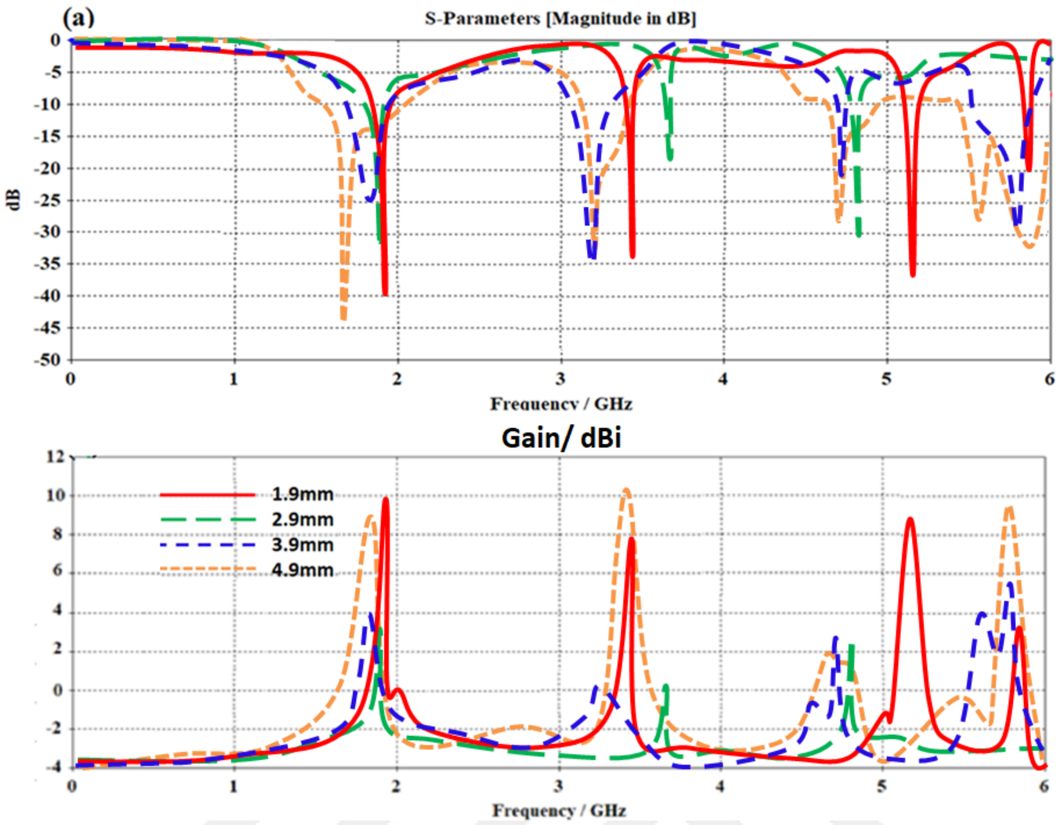

Figure 3.5: Antenna Performance Varying the Ground Plane Length: (A) S_{11} Spectra and (B) Gain.

3.3.5 Switching Effects

Four LDR diodes are added to the suggested antennae to manage the frequency resonances, reconfiguring the antennae's concerts . We discovered that this method is highly useful for regulating the produced frequency bands by regulating the current motion. [108]. As seen in Table 3.1, we only chose four examples for our study. The antennae concerts are shown in terms of S11 and gain curves in Figure 3.5. It is found that changing the diode's functioning has very little effect on the antennae gain because of coupling effects between the antennae transmission line and the proposed SRR unit-cells. The remaining examples are not included in this study due to space constraints. It is crucial to remember that in order to obtain a logic_1, the LDR diode must be activated by applying a biasing voltage. Turning off the LDR diode can result in the production of a logic_0.

Table 3.1: Comparison Between The Switching Scenarios Operation in Terms of Antenna Performance.

R_1	R_2	R_3	R_4	Frequency/ GHz @ S_{11}≤-10dB	Gain/ dBi
0	0	0	0	1.8, 3.3, 4.8, 5.5, 5.8	9.8, 10.8, 2, 0, 9.9
1	1	0	0	2.5, 3.9, 4.8	2.7, 4.1, 3.8
0	0	1	1	1.3, 2.1, 2.8, 3.9, 4.8, 5.8	1.7, 2.7, 2.3, 4, 3.5, 3.7
1	1	1	1	2.5, 3.9, 4.8	2.9, 4, 11.6

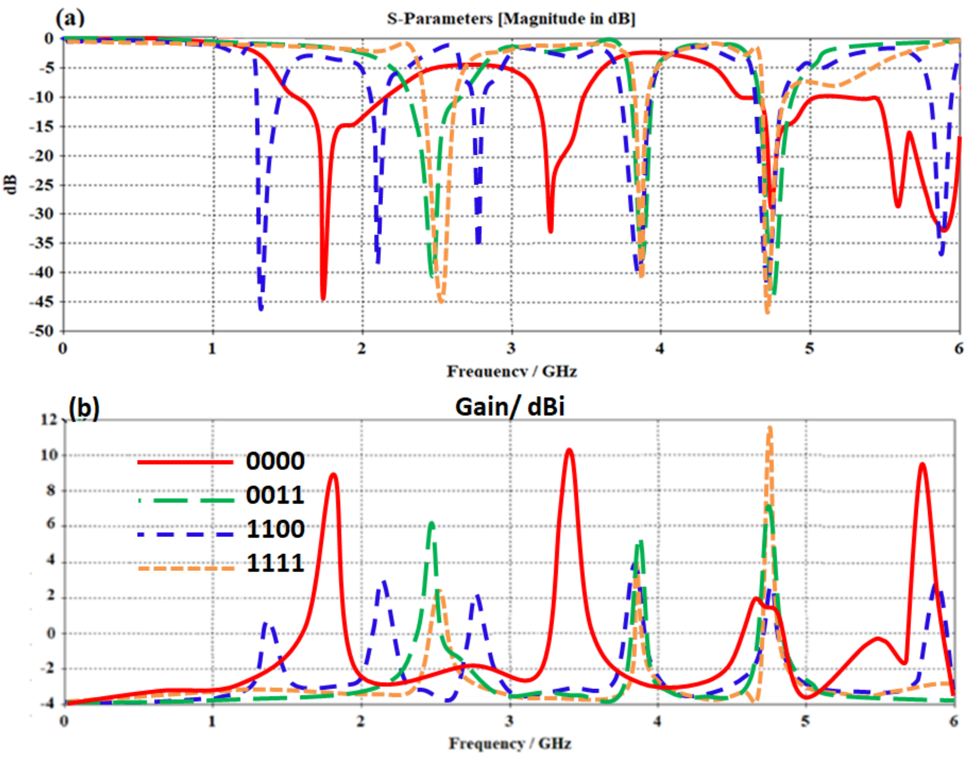

Figure 3.6: Antenna Performance with Different Switching Scenarios: (A) S_{11} Spectra and (B) Gain.

This section examines the suggested antennae concerts based on LDR switches using an alternative research method that entails varying the LDR resistance value from 0 to 700. In this study, the resistance values of all LDR resistors are adjusted simultaneously to switch the proposed antennae. This is because the antennae gain in such study is varied. Where it is found that the recommended antennae gain gradually drops as the resistance value listed in Table II is increased, for example, at 4.5 where the gain is highest, from 11.6 dBi to 2 dBi. This is the outcome of the resistance fluctuation affecting the surface current's velocity [109]. Consequently, the antennae gain at each LDR value is taken into account while computing the BER values. In such a process, a computer simulation and numerical analysis of the QAM modulation method are used to assess the BER from the MATLAB platform. The number of bits that differ in the comparison and how that number compares to all the bits. When comparing sent and received data, the function determines which bits to compare first based on their sizes.

The AGWN channel for (8, 16, 32, and 64)-QAMs is taken into account when the simulation is done. The considered AGWN channel in a MATLAB function is generated from a random source. The highest bit count that may be achieved is 1107, while the maximum bit error is 100. As shown in Table II, the objective is to evaluate each QAM index with respect to BER against the variance in LDR resistance. The results demonstrate that when the LDR value increases, modulation concerts improve in terms of BER as QAM order decreases.

Table 3.2: BER Evaluation at Different Ldr Resistance Values.

LDR/ Ω	**Gain/ dBi**	**BER@QAM-8**	**BER@QAM-16**	**BER@QAM-32**	**BER@QAM-64**
0	11.6	0.0894	0.0921	0.1164	0.1313
100	10.1	0.1034	0.1171	0.1234	0.1431
200	8.6	0.1091	0.1198	0.1391	0.1595
300	6.2	0.1178	0.1281	0.1498	0.1618
400	5.5	0.1412	0.1521	0.1609	0.1732
500	4.1	0.1569	0.1692	0.1760	0.1860
600	3.2	0.1678	0.1773	0.1802	0.1971
700	2	0.1756	0.1851	0.1977	0.2056

3.4. RESULTS VALIDATIONS

This section compares measurements to the projected antennae findings that were quantitatively assessed using CST MWS. The S11 and gain curves of the suggested antennaes are assessed up to 6GHz. As a result, the suggested antennae is created and put to the test experimentally. Wet chemical etching is used to create the antennae, and the finished prototype is seen in (Figure3.7).

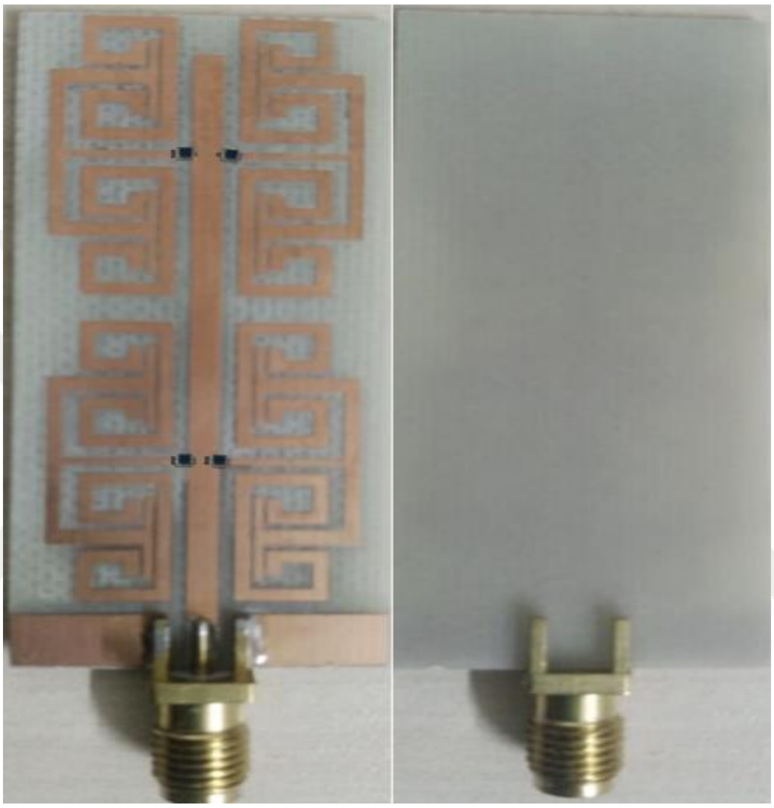

Figure 37: Fabricated Prototype Structure.

The concerts of the antennae is evaluated in two distinct situations to fully convey the significance of portable uses of such an antennae.

3.4.1 In free Space Environments

This section includes an experimental test of the proposed antennas to evaluate the gain and S11 curves at two LDR levels. The recommended antennae's S11 curves are observed to have a great reaction to the switching operation when all LDR resistance values are changed from OFF state, logic_0, to ON status, logic_1, as shown in (Figure 3.8 (a)). Covering all LDR resistance with lids is necessary to achieve the OFF condition of this operation. Without cover lids to turn ON, all of the LDR resistances are lighted for the ON state. It follows that when all of the LDR resistors are turned on with light, the proposed antennae gain spectrum achieves a gain of 11.6dBi. But as Figure 3.8(b) illustrates, the gain drops to 2dBi at 4.5GHz when all LDR resistors are disabled. It is found that there are not many differences between the simulated findings and the measurements.

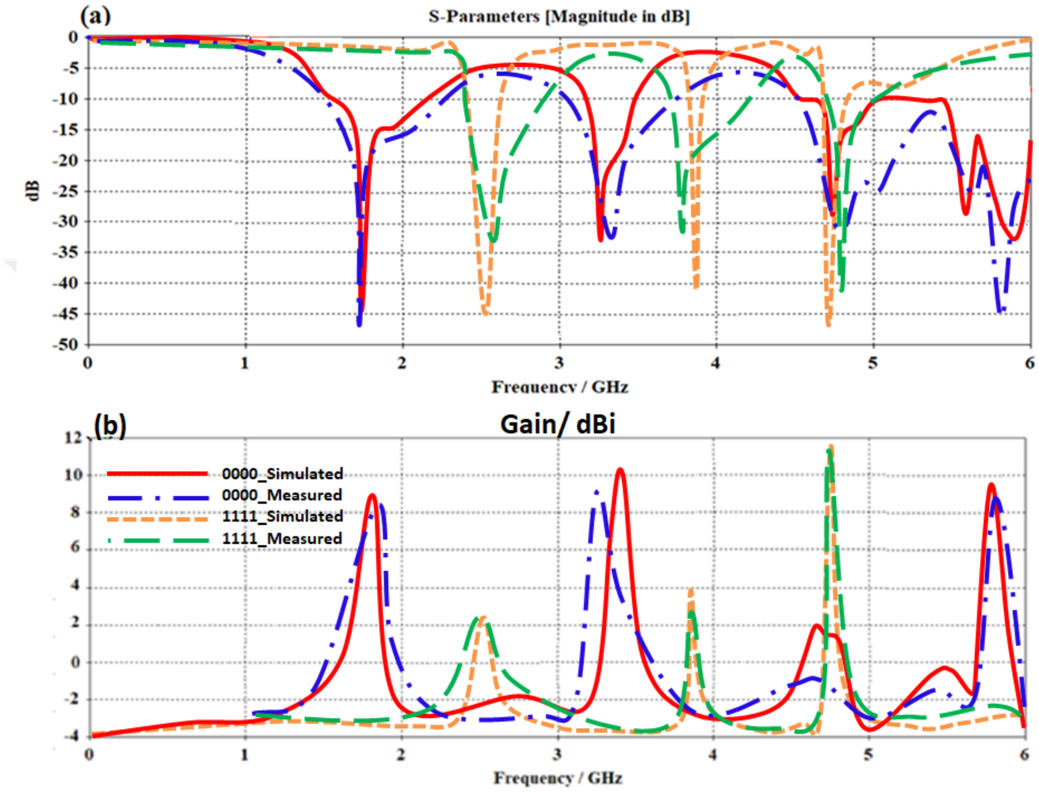

Figure 3.8: Antenna Performance Measurements with Different Switching Scenarios: (A) S_{11} Spectra and (B) Gain.

3.4.2 In Close to Human Body

The antennae concerts are then evaluated in close proximity to the human body, as seen in (Figure 3.9(a)), with respect to S11 and radiation pattern. The antennae are put straight against the subject's skin to measure the S11 and gain curves. Afterwards, the measured results for the prototype placed in close proximity to the human body are compared with the case when the antennas are in free space. Thus, as shown in (Figure 3.9(b)), the antennae structure is located during the measuring operation utilizing the human phantom model. The results show that the projected antennae's S11 spectrum is moderately affected by positioning the antennae close to the body (Figure 3.9(c)).

In (Figure 3.8(b)) the observed antennae gain spectrum is displayed. According to research, the suggested antennae exhibits a decline in antennae gain as a result of losses caused by human tissues [109]. Table 3.3 lists the antennae gain and bandwidth reductions. In general, the degradations are seen to be tolerable given the proximity of the antennae to the human body.

The observed antennae radiation patterns are discovered to be considerably different from those obtained when the antennae is placed in a free space environment, as illustrated in (Figure 3.9(a)). It is important to note that for both antennae position situations at azimuth, the antennae radiation patterns are observed with OFF statues case at 2.3GHz, 3.7GHz, and 4.4GHz (theta=0°) and zenith (theta=90°) planes.

Table 3.3: Analysing Antenna Performance in Two Distinct Antenna Settings.

In the free space		**On the human body**	
Frequency/ GHz	**Gain/ dBi**	**Frequency/ GHz**	**Gain/ dBi**
2.5	2.9	2.3	2.1
3.9	4	3.7	3.3
4.8	11.6	4.4	9.6

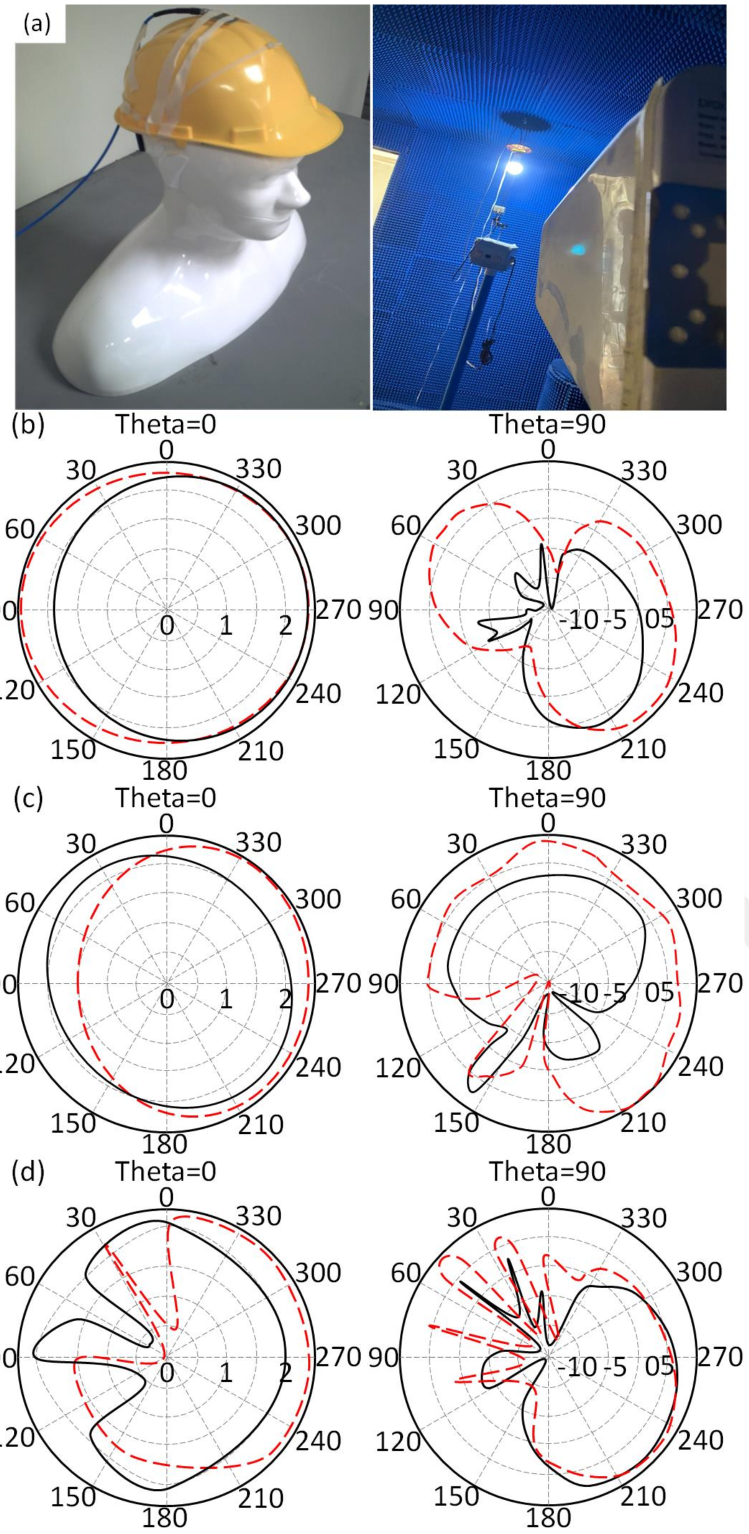

Figure 3.9: Antenna Radiation Pattern Measurements: (A) Experimental Setup, (B) 2.3 Ghz and (C) 4.4 Ghz.

Table 3.4 compares the antennae concerts s in terms of frequency of operation, gain, size, and the process of reconfiguration. It's discovered that the Comparing the suggested antennae to others described in the literature, it achieves an exceptional size reduction and great concerts.

Table 3.4: Comparison of this Research with Earlier Studies.

Previous work	Frequency/GHz	Antenna dimensions/ mm^2	Gain
[13]	5.5	21×17.5	3
[14]	5.01–6.12	25×20	3
[17]	2.5/3.5/5.5	32×20	1.67
[18]	2.4/5.2/5.8	20×22	3
[19]	3.5/5.5	35×39	2.2
This work	2.5, 3.9, 4.8	51×24	2.9, 4, 11.6

4. CHAPTER FOUR

4.1 INTRODUCTION

Recently, an improvement in wireless communication technology was established to continue development in the channel capacity of modern wireless communication networks [110]. Therefore, such advancements may include MIMO and antennae concerts reconfiguration technologies [111]. This is developed to improve the signal quality, and quality of service, and minimize fading effects [110]. Later, several researchers introduced reconfigurable MIMO antennae arrays to realize smart wireless devices [111]. Therefore, such antennae systems achieve high gain properties through many bands depending on switching scenarios [112]. However, reconfigurable MIMO antennaes for sub-6GHz 5G mobile terminals are investigated for beam and frequency reconfigurations using PIN diodes to switch between two PIFA elements [113]. In [114], the authors presented a low-profile antennae that directs the main antennae beam to five distinct directions at sub-6GHz bands [115]. Another MIMO antennae was based on two reconfigurable elements that were controlled by RF MEMS switches for sub-6GHz bands to achieve excellent radiation efficiency and high diversity. In [115], enhancing MU-MIMO transmission techniques by using reconfigurable antennaes was achieved to reduce channel estimation overhead and difficulty while achieving superior concerts . However, rapid developments in wireless technology sparked interest in multi-band reconfigurable antennaes as devices and satellites are innovating toward miniaturization with limited space at Cube Sat application and 5G systems that promise high data rates [116]. The authors in [117] presented a reconfigurable MIMO antennae using the liquid metal technique between adjacent elements at sub-6GHz frequency bands. Nevertheless, a quad-frequency bands-based reconfigurable MIMO antennae was projected to achieve frequency reconfigurations by controlling 8-PIN diodes at sub-6GHz [111]. In [115], the authors projected MIMO antennae configuration to enhance the curvesl efficiency with better channel capacity over 10b/s/Hz at 6GHz. A new differential frequency technique based on a reconfigurable antennae of four dipoles was projected in [112] by controlling four PIN diodes to operate at 3.5GHz and 5.8GHz. In [113], a reconfigurable MIMO antennae system was projected for 5G and WLAN applications by using a PIN diode to achieve dual operating bands at 3.4GHz to 4.1GHz and 4.99GHz to 5.16GHz. Moreover, a dual monopole frequency reconfigurable MIMO system for sub-

6GHz 5G terminals was presented in [114] to achieve tunable resonant frequencies and maximize the realized gain.

In this effort, a design of a reconfigurable MIMO antennae array of printed circuit monopoles coupled to SRR through TR structure. Each antennae element is exited with CWP feed port to provide two frequency bands at 3.6GHz and 4.8GHz. The projected EBG spacer is designed as a moonquake fractal-shaped array to increase the mutual coupling reduction between the antennae elements. Four PIN diodes are connected to each antennae element to control the antennae concerts . The projected EBG spacers are introduced between the antennae elements to improve the isolation quality for MIMO applications.

4.2. ANTENNAE ARRAY STRUCTURE AND GEOMETRICAL DETAILS

In this paper, a MIMO antennae array is projected for sub-6GHz 5G systems. Each antennae element contains a monopole feed line with CWP structure to represent the excitation part of the antennae. The antennae monopole is structured as a transmission line to be separated from SRR resonators that are fetched to the projected monopole through TR stubs capacitive [115]. The projected SRR is constructed as fractal geometry of the 2nd order to be matched inductively with the antennae monopole structure that enhances the bandwidth [116]. On the other side, the matching circuit is connected to TR stubs through four PIN diodes to control the antennae concerts . The antennae elements are spaced with EBG spacers based on complementary SRR-based moonquake (CSRRM) fractal inclusions Without a metallic back panel, all antennae components are printed on FR4 substrate with

εr =4.3 and $\tan\delta$ =0.025. The size of the resultant antennae array is 30×30×30mm3. However, lowering the antennae's surface area might significantly ameliorate of the fringing effects. The MIMO antennae structure is shown in (Figure 4.1) with all geometrical details.

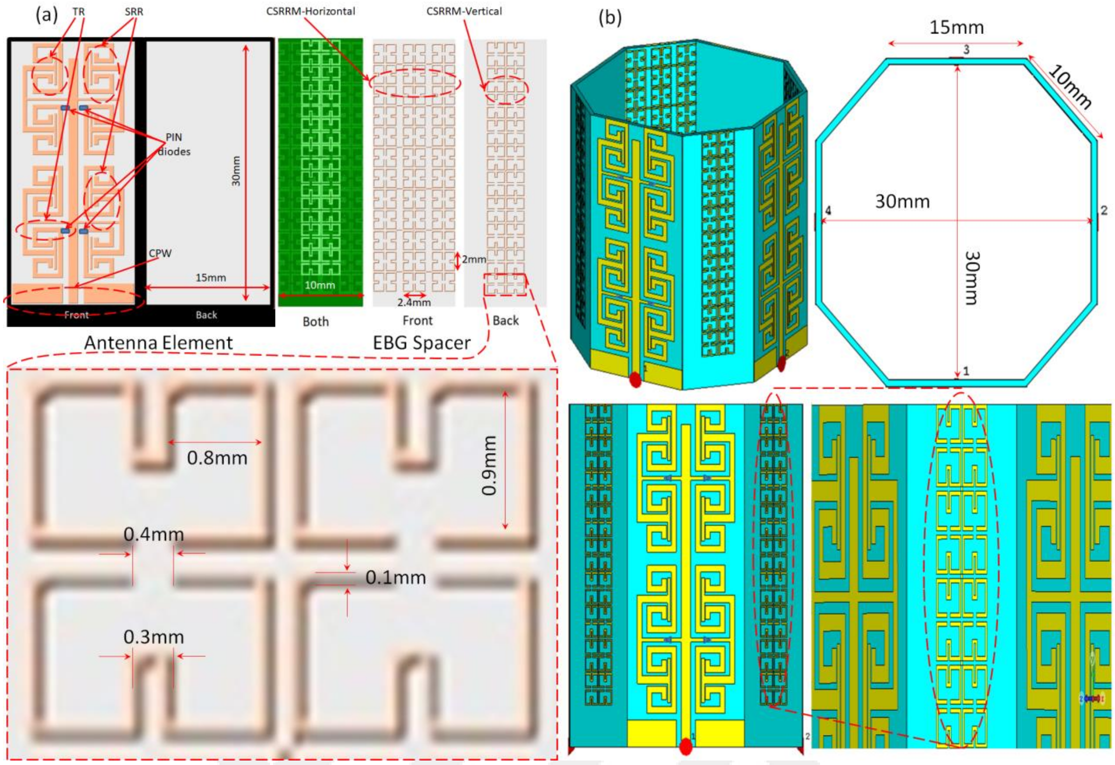

Figure 4.1: MIMO Antenna Geometrical Details: (A) Antenna Element Views and (B) 3D MIMO Array.

4.3 EBG SPACER DESIGN AND OPERATION DETAILS

In this section, the projected EBG structure is to reduce the coupling between the antennaes convergent and to improve antennae gain enhancements [117]. The projected EBG spacers are integrated on the same substrate surface of dimension 10×30mm^2 with antennae elements. Also, the projected EBG spacer contains 10 unit-cellss to produce a high reject band gap with minimum insertion losses. Therefore, the projected EBG unit-cells occupies an area of 2×2.4mm^2 with a separation distance of 0.4mm between each individual unit-cells. For more details about the projected EBG spacers are seen in (Figure 4.2).

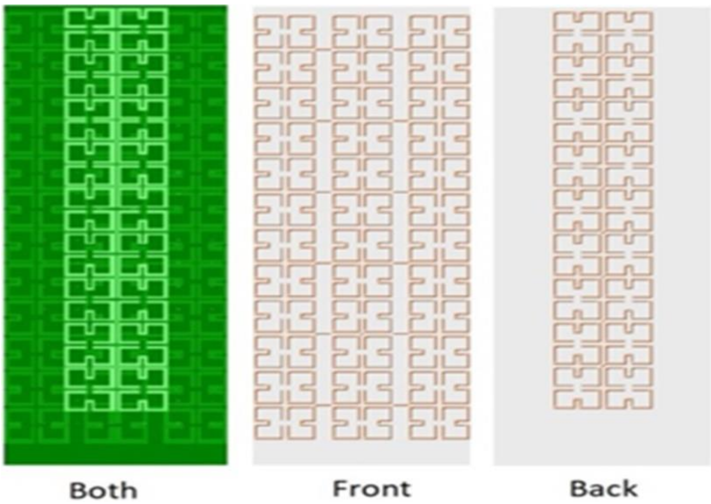

Figure 4.2: The Projected EBG Structure.

The projected EBG structure concerts s in terms of S-factors are investigated using a transmission line study based on full-wave analysis using CST MWS environment. To describe the performances in terms of S11 and S12 curves, the projected EBG spacer is situated on a transmission line. The projected EBG spacer is regarded as a load in this analysis and is coupled directly to the transmission line printed on a FR4 substrate [117] as illustrated in Figure 4.3. The transmission line has TEM excitation.

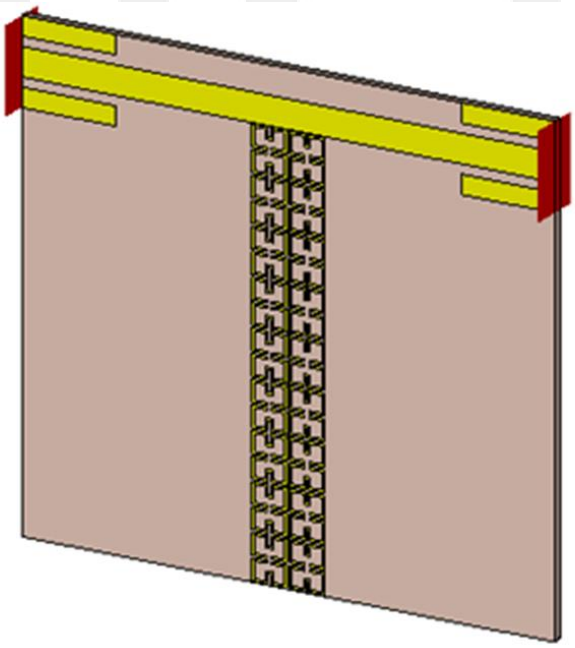

Figure 4.3: EBG Structure Based on Transmission Line.

Nonetheless, the author offers a circuit concept based on the Transmission-Line-Model (TLM) in (Figure 4.4). The series combination of L R t presents the T-stub, and the parallel combination of LCR shows the remaining portion of the unit-cells. The link between the unit-cells and the transmission line is represented by the (Ct Re) branch. As a result, Table 4.1 lists and evaluates the fundamental circuit values.

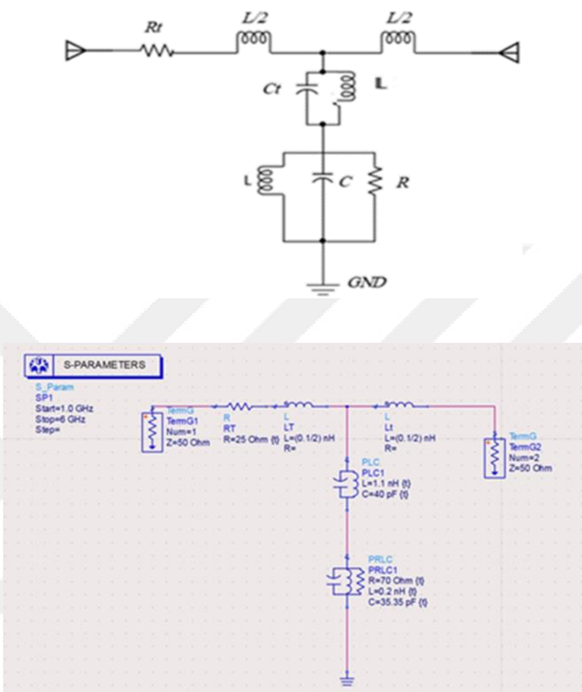

Figure 4.4: Propose equivalent circuit theory of EBG in ADS.

Table 4.1: Lumped Circuit Elements.

Lumped element	Value
L_T	0.1 nH
R_T	50 Ω
C_T	40 pF
L_1	1.1 nH
C	35.35 pF
R	70Ω
L	0.2 nH

To calculate the S-factors for the projected EBG spacer, the authors applied TLM analysis for the calculations as presented in the S-factors in (Figure 4.5) in terms of S_{11} and S_{12} curves.

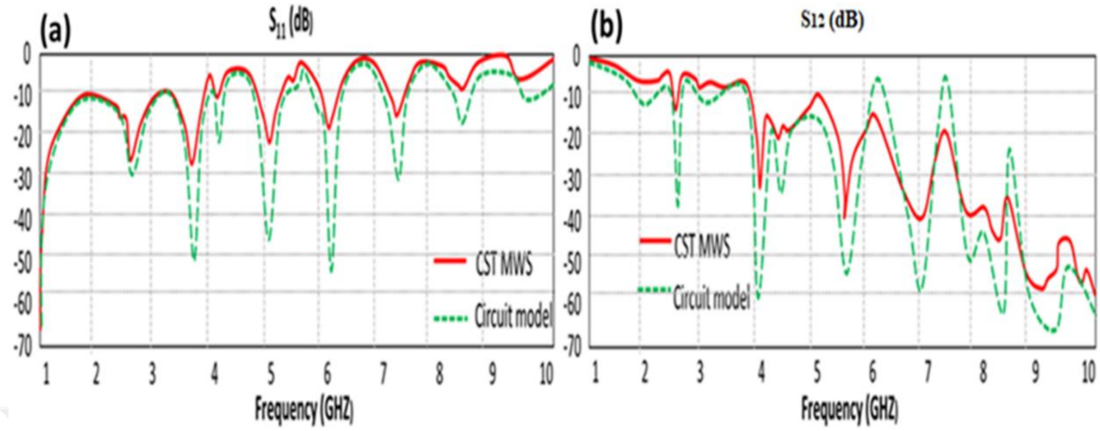

Figure 4.5: The Obtained Results From Both CST MWS and ADS Simulations: (A) S_{11} Spectra and (B) S_{12} Spectra

4.4 DESIGN METHODOLOGY

In this section, the authors discussed the results of the projected antennae array with and without EBG spacers. Therefore, a numerical simulation based on CST MWS in terms of reflection curves and radiation patterns with and without EBG is shown in Figure 4.6. The projected antennae concerts in terms of reflection curves for S11, S22, S33, and S44 curves are evaluated in with and without EBG spacer introduction.

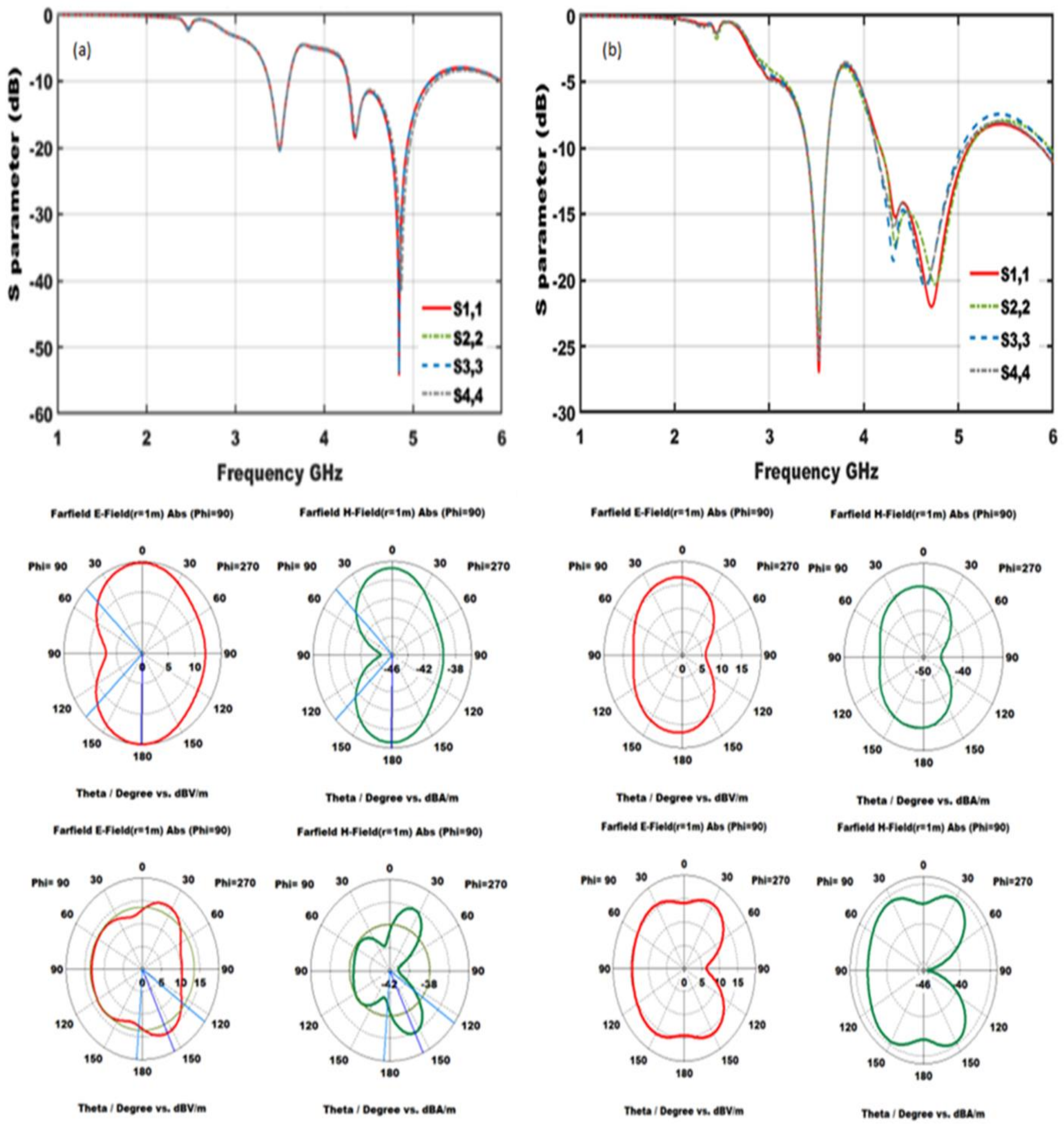

Figure 4.6: MIMO Antenna S11 Spectra and Radiation Pattenrs: (A) Without EBG and (B) With EBG Spacers.

It is found that the projected antennae array shows excellent matching at 3.5 GHz and 4.8 GHz. Such matching enhancement is attributed to the capacitive coupling-based electrostatic charge accumulation in which the energy is stored in the antennae near field [118]. Furthermore, to study the isolation between the projected antennae elements, the projected antennae elements are oriented around a fixed centre and spaced with EBG spacers. Moreover, the obtained radiation patterns at 3.5 GHz and 4.8 GHz in E- and H-planes are mostly oriented toward the Omni-direction from the array without EBG. After introducing the projected EBG spacers, the antennae radiation patterns at E- and H-planes are found to almost tower in the opposite direction from the array centre at the same frequency band of interest. Therefore, the authors evaluated the coupling between the antennae elements in terms of S12, S13, and S14 curves with and without EBG as shown in (Figure 4.7).

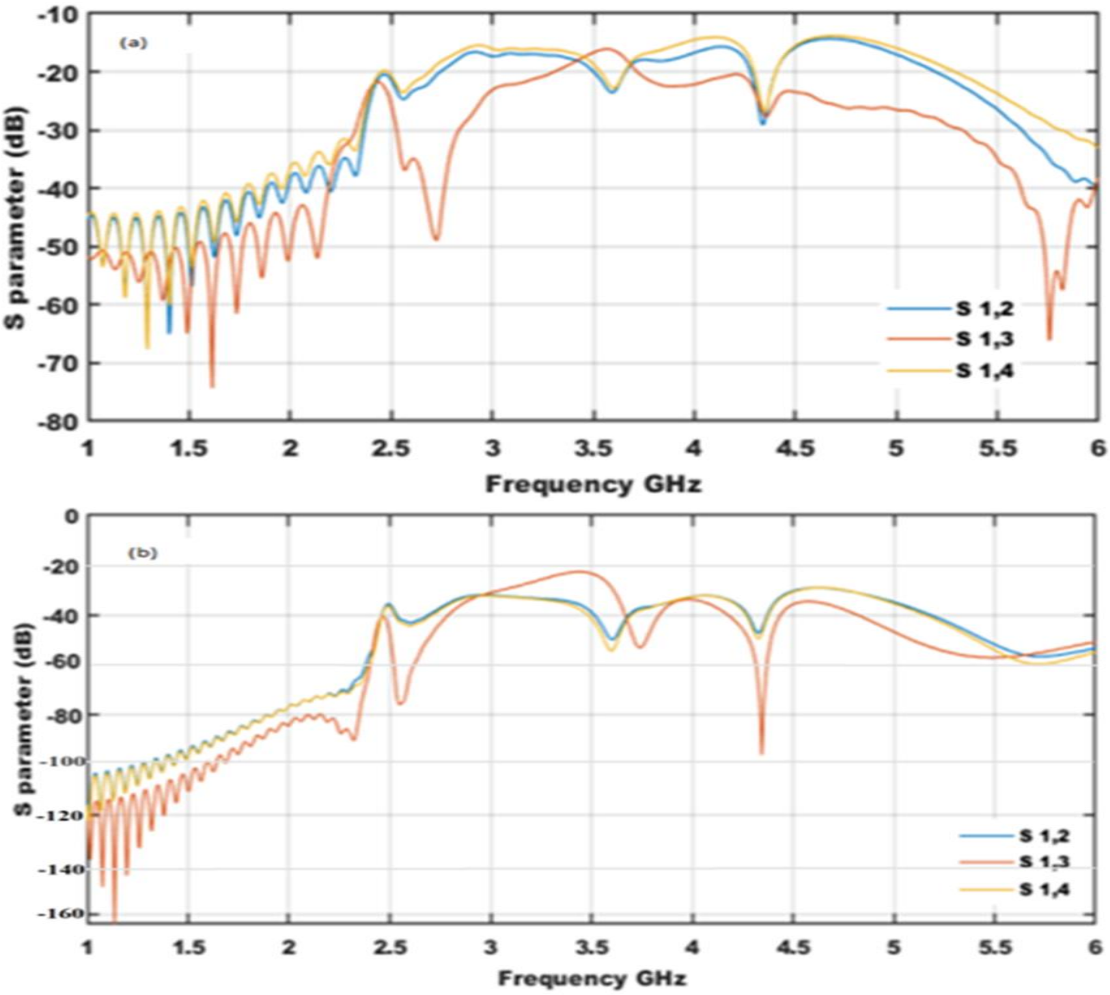

Figure 4.7: Coupling Between Antenna Elements: (A) Without EBG (B) With EBG.

To achieve excellent coupling reduction below -20dB, the authors projected EBG spacers between the antennae elements to increase antennae gain and reduce radiation interference between antennae parts. As will be demonstrated later, the suggested EBG structure is used to completely improve the overall concerts by suppressing the antennae surface waves.

The EBG spacer structure that is being employed has dimensions of 10 x 30 mm. As previously said, the planned EBG array structure is composed of ten unit-cells, as the manufactured prototype will be shown in the following section.

4.5 RESULTS AND VALIDATION

The MIMO antennae prototype is constructed in this part using FR4 substrate of 3D structure as shown in (Figure 4.8). The antennae is measured in terms of S-factors and radiation patterns using a Professional Network Analyzer (Agilent PNA 8720). Therefore, the projected antennae array concerts is located inside an RF anechoic chamber to ensure far-field shielding and path loss reduction. Therefore, the projected antennae array system is exposed for MIMO measurements by calibrating the reflection and space losses by using open, short, 50Ω, and through-calibration process.

Figure 4.8: Fabricated Prototype of MIMO Antennae Array.

For further analysis, While all PIN diodes are OFF, compare the concerts of the manufactured antennae to its simulated results in terms of S-factors and radiation patterns. and ON at the resonant frequencies of 3.3GHz and 4.5GHz are evaluated and presented in (Figure 4.9). It is observed a significant variation can be achieved between the switching scenarios of the PIN diodes. These changes are ascribed to the capability of manipulating the PIN diodes' operation to modify the surface current on the antennae construction [110]. The scientists discovered a negligible difference between the simulated and measured findings that could be caused by the effects of soldering SMA and PIN diodes.

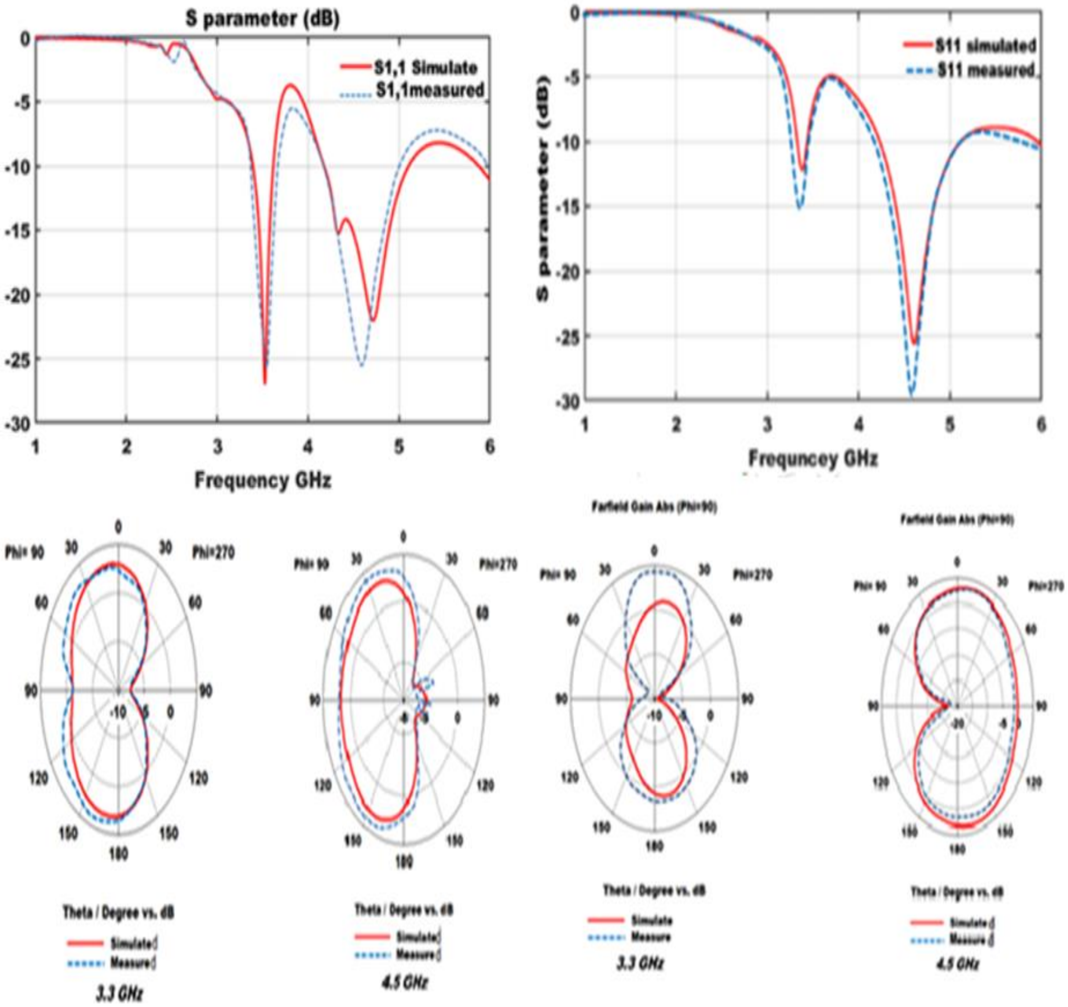

Figure 4.9: Simulated and Measured S-Parameters of the Antenna At (A) All Diode OFF (B) All Diode ON.

The results of the simulation and measurement of the radiation patterns were in good agreement, with only a little variation brought on by the capacitive coupling between antennae elements, which has a considerable impact on the surface current dynamics. However, the measured and simulated coupling curves are presented in Figure 10 to show the effects of coupling when each diode is both ON and OFF.

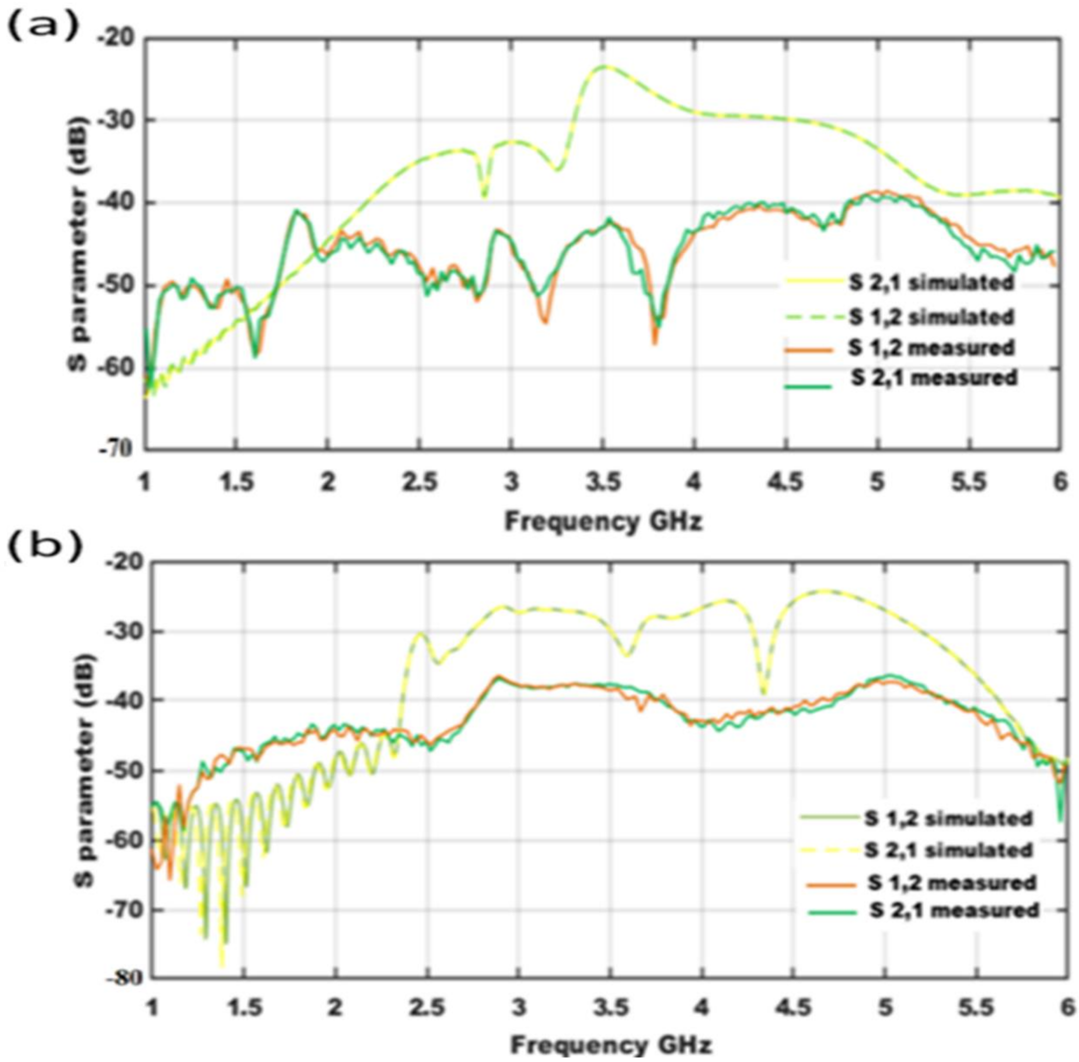

Figure 4.10: Comparison of Coupling Between Simulated and Measured When All Diodes are: (A) OFF and (B) ON.

The observed result is found to have a negligible difference [119] curves with the predicted S11 result in CST MWS. Subsequently, the antenna array concerts are described in Table 4.2 and compared to other relevant data. It has been noted that when compared to antennae found in the literature, such an antennae achieves good performance. In this instance, the gain curves, S11, and emission patterns of the recommended antennae are controlled by four PIN diodes. Furthermore, the results inspire us to have high expectations for such antennaes as viable candidates for 5G portable devices.

Table 4.2: The projected MIMO Array Concerts S With Respect to the Previous Published Results.

Previous work	**Frequency/GHz**	**Antennae size/mm^3**	**Separation Distance**	**Gain/dBi**
[11]	5.5	21×7.35×2	$\lambda_0/3$	3
[13]	5.01–6.12	25×12×1.6	$\lambda_0/4$	3
[14]	2.5/3.5/5.5	32×12×1	$\lambda_0/3.5$	1.67
[16]	2.4/5.2/5.8	20×12×2	$\lambda_0/7$	3
[17]	3.5/5.5	35×19×2	$\lambda_0/6$	2.2
The Projected Work	3.5/4.8	25×25×30	$\lambda_0/16$	6.18

5. CONCLUSION

5.1 CONCLUSIONS

This study's recommended antenna is designed for 5G usage in sub-6GHz bands. The design of the antennae makes use of MTM technology to enable size reduction down to /8 at 3.5GHz. The antennae has an average gain of 6.1dBi to 8dBi and displays four operational bands with S11-10dB at 3.7GHz, 4.6GHz, 5.2GHz, and 5.9GHz. In order to regulate the frequency of the surface current flow and guarantee that the antennae have high reconfiguration mechanisms, four LDR diodes are connected to the TR structure. Consequently, the antennae's performance and characteristics suggested that it would be a strong candidate for 5G networks that use sub-6GHz frequencies. Excellent agreement is found between the measured results and the S11 and gain curves of the antennas concerts, as well as the radiation patterns evaluated using numerical simulations. The investigation's final finding states that the recommended antennae are an excellent option for portable wireless devices' short- and medium-range wireless communications.

In this paper, a MIMO array structure based on four elements that are based on EBG is projected for 5G applications at sub-6GHz frequency bands. It is found that the projected MIMO antennae operates at 3.6GHz and 4.5GHz. The projected antennae elements are spaced with EBG array structure It is created to improve antennae element coupling and provide the greatest gain improvement with the best polarization radiation pattern. Moreover, with the introduction of the projected EBG spacers, the antennae gain is increased from 1.14dBi to 6.18dBi. Experimentally, the projected antennae array-based EBG spacers show a better total efficiency of about 65% in comparison to the identical one without EBG spacers to show 30%. Therefore, it is substance to mention that the EBG spacers reduced the mutual coupling between the antennae elements. The projected antennae array concerts is controlled by using four PIN diodes to yield radiation pattern reconfiguration with a negligible shift in the frequency bands.

5.2 FUTURE WORK

The projected antennae array designs are discussed in this thesis for MIMO applications at sub-6GHz. The projected antennaes designed based on self-powered technology. Therefore, the projected designs are discussed based on tow man aspects of mutual coupling reduction and size miniaturization. As a future research study, the author is willing to apply several research aspects as following:

a. The projected antennae designs designed based on rigid substrates that limit their use for flexible devices. As a part of the future research, the author is attending to apply different types of flexible substrate for foldable electronic devices.

b. The use of nanomaterial printed technology as a wearable smart clothes would an excellent candidate for future research. This technology became very desirable at sub-6GHz frequencies and modern wireless technology.

c. The effects of specific absorption rates on the human tissue during the long exposure to antennae terminal became a very effective parameter in the antennae design. Therefore, a part of the future research, the use of MTM structure to shield the human tissue from the antennae radiation could be a promising future research.

d. The applications of RF harvesting technology would be conducted in the future to collect the electromagnetic energy from several resources and feeding the modern wireless networks.

e. Apply a study of realize the advantage of the Proposal design on enhancing the channel concerts s through measuring a channel capacity and bit error rate. After that, realizing the mean effective design parameters to optimized the channel concerts through the antennaes design parameters.

f. Study the possibility of using the direct antennae technology in the projected designs and apply the use of antennae concerts reconfiguration through electronic switches.

g. Apply the use of the neural network analysis to enhance the antennae concerts and optimize the designs through training the network by input data from the numerical software package.

h. Conducting the use of beam steering to minimize the effects of beam squint in the MIMO array study specifically at millimetre wave propagation. Also, study the possibility of implementing such antennae arrays for millimetre bands.

REFERENCES

[1] N. Cohen, Fractal antennae and fractal resonator primer, Chapter 8 in J. A. Rock and M. van Frankenhuijsen [Eds.], Fractals and Dynamics in Mathematics, Science, and the Arts: Theory and Applications, vol. 1. World Scientific, 2015.

[2] Ahmed, Hayder Salah. *Fractal Based Multi-Band Reject Filter*. Diss. University of Technology, 2015.

[3] Hayder S. Ahmed, Ali J. Salim, Mohammed R. Hussan, Hussain A. Hammas, Mahmood T. Yassen, Saad Mutashar and Jawad K. Ali," Design of Compact Dual-Mode Fractal Based Microstrip Band Reject Filter, " ARPN Journal of Engineering and Applied Sciences, vol. 13, no. 7, pp.2395-2399, April 2018.

[4] Juan de Dios Ruiz, Fe´ lix L. Martı´nez, and Juan Hinojosa," 1D Koch Fractal Electromagnetic Bandgap Microstrip Structures With r/a Ratios Higher Than 0.5," MICROWAVE AND OPTICAL TECHNOLOGY LETTERS, vol 53, no. 3,pp. 646-649, March 2011

[5] Shrivishal Tripathi, Akhilesh Mohan, Sandeep Yadav," A Compact Koch Fractal UWB MIMO Antennae with WLAN Band-Rejection," IEEE Antennaes and Wireless Propagation Letters, vol. 14, pp. 1565 – 1568, 12 March 2015.

[6] Mayur P. Satpute, and Prof. Sachin S. Khade," A Novel Shape Octagonal Koch Fractal MIMO Antennae for WLAN and WiMAX Application," 2016 World Conference on Futuristic Trends in Research and Innovation for Social Welfare (Startup Conclave), Coimbatore, India, 29 Feb.-1 March 2016.

[7] Shrivishal Tripathi, Akhilesh Mohan, and Sandeep Yadav," A Compact Octagonal shaped Fractal UWB MIMO Antennae with 5.5 GHz Band-notch Characteristics," 2014 IEEE International Microwave and RF Conference (IMaRC), Bangalore, India, 15-17 Dec. 2014.

[8] W. Roh et al., “Millimeter-wave beamforming as an enabling technology for 5G cellular communications: Theoretical feasibility and prototype results*,” IEEE*

Commun. Mag., vol. 52, no. 2, pp. 106–113, Feb. 2014.

[9] J. G. Andrews et al., “What will 5G be?,” IEEE J. Sel. Areas Commun., vol. 32, pp. 1065–1082, June 2014.

[10] P. Wang, Y. Li, L. Song and B. Vucetic, “Multi-gigabit millimeter wave wireless communications for 5G: from fixed access to cellular networks,” *in IEEE Communications Magazine, vol. 53, no. 1, pp. 168-178, January 2015.*

[11] S. Gupta, Z. Briqech, A. R. Sebak, and T. A. Denidni," Mutual-Coupling Reduction Using Metasurface Corrugation for 28 GHz MIMO Applications," *Antennaes and Wireless Propagation Letters*, pp. 1-4, 2017.

[12] Falconer, Kenneth (2003). Fractal Geometry: Mathematical Foundations and Applications. John Wiley & Sons. xxv. ISBN 978-0-470-84862-3.

[13] T. A. Elwi, “Printed Microwave Metamaterial-Antennae Circuitries on Nickel Oxide Polymerized Palm Fiber Substrates,” *Nature Scientific Reports*, volume 9, number 2174, pp. 1-14, January 2019,

[14] T. A. Elwi and A. M. Al-Saegh, “Further realization of a flexible metamaterial based antennae on indium nickel oxide polymerized palm fiber substrates for RF energy harvesting”, International Journal of Microwave and Wireless Technologies, Cambridge, Volume 5, issue 4, pp. 1-9, May 2020,

[15] T. A. Elwi, D. A. Jassim, H. H. Mohammed, “Novel miniaturized folded UWB microstrip antennae-based metamaterial for RF energy harvesting,” International Journal of Communication Systems, Volume 1, issue 2, January 2020,

[16] T. A. Elwi, Z. A. AL-Hussain, O. Tawfeeq, “Hilbert Metamaterial Printed Antennae based on Organic Substrates for Energy Harvesting”, IET Microwaves, Antennaes & Propagation, volume 12, number 4, pp.1-8, June 2019,

[17] T. A. Elwi, “Novel UWB Printed Metamaterial Microstrip Antennae based Organic Substrates for RF-Energy Harvesting Applications,” AEU - International Journal of Electronics and Communications, volume 101, pp. 1-10, January, 2019,

[18] Z. Al-Dulaimi, T. A Elwi, and D. Cagdas Atilla (2020) Design of a Meander Line Monopole Antennae Array Based Hilbert-Shaped Reject Band Structure for MIMO Applications, IETE Journal of Research, DOI: 10.1080/03772063.2020.1743207.

[19] Elwi, T.A. A Miniaturized Folded Antennae Array for MIMO Applications. *Wireless Pers Commun* **98,** 1871–1883 (2018). https://doi.org/10.1007/s11277-017-4950-4

[20] Elwi, T. , Abbas, Z. , Noori, M. , Al-Naiemy, Y. , Salih, E. and Hamed, M. (2014) Conformal Antennae Array for MIMO Applications. *Journal of Electromagnetic Analysis and Applications*, **6**, 43-50. doi: 10.4236/jemaa.2014.64007.

[21] Z. Al-Dulaimi, T. A. Elwi, D. C. Atilla and C. Aydin, "Design of Fractal Based Monopole Antennae Array with Ultra-Mutual Coupling Reduction for MIMO Applications," *2018 18th Mediterranean Microwave Symposium (MMS)*, 2018, pp. 39-42, doi: 10.1109/MMS.2018.8611858.

[22] S. H. Ghadeer, S. K. Abd.Rahim and T. A. Elwi, "Solar Panel Integrated 3D MIMO Antennae Array for Modern Communication Systems," *2021 International Conference on Advanced Computer Applications (ACA)*, 2021, pp. 112-115,

[23] H. Almizan, Z. A. A. Hassain, T. A. Elwi and S. M. Al-Sabti, "Controlling Gain Enhancement Using a Reconfigurable Metasurface Layer," *2021 12th International Symposium on Advanced Topics in Electrical Engineering (ATEE)*, 2021, pp. 1-6.

[24] A. I. Imran, T. A. Elwi, and Ali J. Salim, "On the Distortionless of UWB Wearable Hilbert-Shaped Metamaterial Antennae for Low Energy Applications," Progress In Electromagnetics Research M, Volume 101, pp. 219-239, March 2021.

[25] S. M. Obaid, T. A. Elwi, and M. Ilyas, “Fractal Minkowski-Shaped Resonator for Noninvasive Biomedical Measurements Blood Glucose Test,” Progress in Electromagnetics Research c, Volume 107, pp. 143-156, December 2020,

[26] T. A. Elwi, “A Further Realization of a Flexible Metamaterial-Based Antennae on Nickel Oxide Polymerized Palm Fiber Substrates for RF Energy Harvesting”, Wireless Personal Communications, Volume 10, no. 12, pp.1-15, August 2020,

[27] Y. Alnaiemy, T. A Elwi, L. Nagy, “An end fire printed monopole antennae based on electromagnetic band gap structure,” Automatika, volume 61, issue 3, pp. 482-495,

[28] T. A. Elwi, “Remotely Controlled Reconfigurable Antennae for Modern Applications”, Microwave and optical letters, Volume 6, issue 1, pp. 1-19, April 2020,

[29] T. A. Elwi, “Further Investigation on Solant-Rectenna based Flexible Hilbert-Shaped Metamaterials”, IET Nanodielectrics, Volume 4, issue 12, pp. 1-12, March 2020,

[30] T. A. Elwi and A. M. Al-Saegh, “Further realization of a flexible metamaterial based antennae on indium nickel oxide polymerized palm fiber substrates for RF energy harvesting”, International Journal of Microwave and Wireless Technologies, Cambridge, Volume 5, issue 4, pp. 1-9, May 2020,

[31] Z. Al-Dulaimi, T. A. Elwi, and D. C. Atilla, “Design of a Meander Line Monopole Antennae Array Based Hilbert-Shaped Reject Band Structure for MIMO Applications,” IETE Journal of Research, Volume 66, issue 1, pp. 1-10, March 2020,

[32] M. A. Jawad, M. A. Elwi, E. Y. Salih, T. A. Elwi, and Zulkifly Abbas, “Monitoring the Dielectric Properties and Propagation Conditions of Mortar for Modern Wireless Mobile Networks,” Progress in Electromagnetic Research Letters, Volume 89, pp. 91-97, January 2020,

[33] T. A. Elwi, D. A. Jassim, H. H. Mohammed, “Novel miniaturized folded UWB microstrip antennae-based metamaterial for RF energy harvesting,” International Journal of Communication Systems, Volume 1, issue 2, January 2020,

[34] A. M. Al-Saegh and T. A. Elwi, “Direct extraction of rain-induced impairments on satellite communication channel in subtropical climate at K and Ka bands”, Telecommunication Systems, Volume 22, number 8, November 2019,

[35] Y. Alnaiemy, T. A. Elwi, L. Nagy, “Mutual Coupling Reduction in Patch Antennae Array Based on EBG Structure for MIMO Applications”, Periodica Polytechnica Electrical Engineering and Computer Science, Volume 1, number 4, pp.1-11, September 2019,

[36] H. M. Al-Sabbagh, T. A. Elwi, Y. Al-Naiemy, and H. M. Al-Rizzo, “A Compact Triple-Band Metamaterial-Inspired Antennae for Wearable Applications”, Microwave and Optical Technology Letters, Volume 11, number 2, October 2019,

[37] Z. A. Abdul Hassain, A. R. Azeez, M. M. Ali, and T. A. Elwi, “A Modified Compact Bi-Directional UWB Tapered Slot Antennae with Double Band-Notch Characteristics”, ADVANCED ELECTROMAGNETICS, Volume 8, number 4, September 2019,

[38] T. A. Elwi, A. J. Salim, A. N. Alkhafaji, J. K. Ali, and A. S. A. Jalal, “Complex Constitutive Characterizations of Materials in the X-Band Using a Non-Destructive Technique”, Special Issue of the 8th International Advances in Applied Physics and Materials Science Congress (APMAS 2018), ACTA PHYSICA POLONICA A, Number 4, Volume 135, August 2019,

[39] T. A. Elwi, Z. A. AL-Hussain, O. Tawfeeq, “Hilbert Metamaterial Printed Antennae based on Organic Substrates for Energy Harvesting”, IET Microwaves, Antennaes & Propagation, volume 12, number 4, pp.1-8, June 2019,

[40] H. S. Ahmed and T. A. Elwi, “On the design of a reject band filter for antennaes mutual coupling reduction”, International Journal of RF and Microwave Computer-Aided Engineering, volume 11, number 3, pp.1-11, April 2019,

[41] G. M. Hatem, A. J. Salim, T. A. Elwi, H. T. Ziboon, J. H. Majeed and J. K. Ali, 2019, “Wunderlich Curve Fractal Dipole Antennae for Dual-Band Wearable RFID Applications,” Journal of Engineering and Applied Sciences, volume 14, Issue 4, pp. 1093-1099, March 2019,

[42] B. I. Halim and A. Boutejdar, "Design and Improvement a Novel Microstrip Antennae Using Array of Composite Right/Left Handed Transmission Line (CRLH-TL) Technique for Multiband Applications," 2019 IEEE International Symposium on Phased Array System & Technology (PAST), 2019, pp. 1-5, doi: 10.1109/PAST43306.2019.9021028,

[43] Xie, S.; Li, J.; Deng, G.; Feng, J.; Xiao, S. A Wide-Angle Scanning Leaky-Wave

Antennae Based on a Composite Right/Left-Handed Transmission Line. Appl. Sci. 2020, 10, 1927.

[44] Alibakhshikenari, M., Virdee, B.S., Althuwayb, A.A. et al. Bandwidth and gain enhancement of composite right left handed metamaterial transmission line planar antennae employing a non foster impedance matching circuit board. Sci Rep 11, 7472 (2021),

[45] M. Comisso and R. Vescovo, “Fast 3D pattern synthesis with polarization and dynamic range ratio control for conformal antennae arrays,” *International Journal of Antennaes and Propagation*, vol. 2014, Article ID 106741, 9 pages.

[46] Dahri, M. H., Jamaluddin, M. H., Seman, F. C., Abbasi, M. I., Ashyap, A. Y., Kamarudin, M. R., & Hayat, O. (2020). A Novel Asymmetric Patch Reflectarray Antennae with Ground Ring Slots for 5G Communication Systems. *Electronics*, *9*(9), 1450.

[47] Mei, P., Zhang, S., & Pedersen, G. F. (2020). A Low-Cost, High-Efficiency and Full-Metal Reflectarray Antennae with Mechanically 2-D Beam-Steerable Capabilities for 5G Applications. IEEE Transactions on Antennaes and Propagation, 68(10), 6997-7006.

[48] Wang, Z., Pan, X., Yang, F., Xu, S., & Li, M. (2020). Real-Time Mode Switching and Beam Scanning of High-Gain OAM Waves Using a 1-Bit Reconfigurable Reflectarray Antennae. *Electronics*, *9*(12), 2181.

[49] Yang, J., Wang, P., Sun, S., Li, Y., Yin, Z., & Deng, G. (2020). A novel electronically controlled two-dimensional terahertz beam-scanning reflectarray antennae based on liquid crystals. Frontiers in Physics, 8, 435.

[50] Luyen, H., Zhang, Z., Booske, J. H., & Behdad, N. (2019). Wideband, Beam-Steerable Reflectarrays Based on Minimum-Switch Topology, Polarization-Rotating Unit-cellss. IEEE Access, 7, 36568-36578.

[51] Zhang, H., Chen, X., Wang, Z., Ge, Y., & Pu, J. (2019). A 1-bit electronically reconfigurable reflectarray antennae in X band. IEEE Access, 7, 66567-66575

[52] Xu, H., Xu, S., Yang, F., & Li, M. (2020). Design and Experiment of a Dual-Band 1 Bit Reconfigurable Reflectarray Antennae With Independent Large-Angle Beam Scanning Capability. *IEEE Antennaes and Wireless Propagation Letters*, *19*(11), 1896-1900.

[53] Baladi, E., Xu, M. Y., Faria, N., Nicholls, J., & Hum, S. V. (2021). Dual-Band Circularly Polarized Fully Reconfigurable Reflectarray Antennae for Satellite Applications in the Ku Band. *IEEE Transactions on Antennaes and Propagation*.

[54] Niu, T., Zhang, J., Cheng, L., Cao, P., Cui, R., & Mei, Z. (2020, March). Reconfigurable Terahertz Reflectarray Based on Graphene Radiating Patches. In *2020 14th European Conference on Antennaes and Propagation (EuCAP)* (pp. 1-4). IEEE.

[55] Sun, S., Li, W., & Shi, X. (2019, May). A Reconfigurable Graphene Reflectarray for Generation of OAM in THz Band. In *2019 International Conference on Microwave and Millimeter Wave Technology (ICMMT)* (pp. 1-3). IEEE.

[56] T. A. Elwi and A. M. Al-Saegh, "Further realization of a flexible metamaterial based antennae on indium nickel oxide polymerized palm fiber substrates for RF energy harvesting", International Journal of Microwave and Wireless Technologies, Cambridge, Volume 5, issue 4, pp. 1-9, May 2020.

[57] Roo-Ons, M.; Shynu, S.; Ammann, M.; McCormack, S.; Norton, B. Transparent patch antennae on a-Si thin-film glass solar module. Electron. Lett. 2011, 47, 85–86.

[58] Liu, X.; Jackson, D.R.; Chen, J.; Liu, J.; Fink, P.W.; Lin, G.Y.; Neveu, N. Transparent and nontransparent microstrip antennaes on a CubeSat: Novel low-profile antennaes for CubeSats improve mission reliability. IEEE Antennaes Propag. Mag. 2017, 59, 59–68.

[59] Alwareth, H.; Ibrahim, I.M.; Zakaria, Z.; Al-Gburi, A.J.A.; Ahmed, S.; Nasser, Z.A. A Wideband High-Gain Microstrip Array Antennae Integrated with Frequency-Selective Surface for Sub-6 GHz 5G Applications. Micromachines 2022, 13, 1215.

[CrossRef] [PubMed]

[60] Raza, U.; Sadiq, U.; Rizwan, U.; Iftikhar, U.D.; Babar, K.; Muhammad Altaf Hussain, K.; Ladislau, M. Wideband and High Gain Array Antennae for 5G Smart Phone Applications Using Frequency Selective Surface. IEEE Access 2022, 10, 86117–86126. [CrossRef]

[61] Ravi, K.C.; Kumar, J.; Elwi, T.A.; Ali, M.M. Compact MIMO Antennae for 5G Applications. In Proceedings of the 2022 IEEE ANDESCON, Barranquilla, Colombia, 16–19 November 2022; pp. 1–6. [CrossRef]

[62] Ghaffar, A.; Awan, W.A.; Hussain, N.; Ahmad, S.; Li, X.J. A Compact Dual-Band Flexible Antennae for Applications at 900 and 2450 MHz. Prog. Electromagn. Res. Lett. 2021, 99, 83–91. [CrossRef]

[63] Al-Gburi, A.J.A.; Ibrahim, I.M.; Zakaria, Z.; Abdulhameed, M.K.; Saeidi, T. Enhancing Gain for UWB Antennaes Using FSS: A Systematic Review. Mathematics 2021, 9, 3301. [CrossRef]

[64] Ahmed, H.S.; Ahmed, Z.S.; Zamel, R.S.; Elwi, T.A. Compact MIMO Antennae Array for 5G Applications based Novel Hayder-Koch Fractal Geometry. In Proceedings of the 2022 International Telecommunications Conference (ITC-Egypt), Alexandria, Egypt, 26–28 July 2022; pp. 1–5. [CrossRef]

[65] Awan, W.A.; Ghaffar, A.; Hussain, N.; Li, X.J. CPW-fed dual-band antennae for 2.45/5.8 GHz applications. In Proceedings of the 2019 8th Asia-Pacific Conference on Antennaes and Propagation (APCAP), Incheon, Republic of Korea, 4–7 August 2019; pp. 246–247.

[66] Alibakhshikenari, M.; Virdee, B.S.; Azpilicueta, L.; Naser-Moghadasi, M.; Akinsolu, M.O.; See, C.H.; Liu, B.; Abd-Alhameed, R.A.; Falcone, F.; Huynen, I.; et al. A comprehensive survey of “metamaterial transmission-line based antennaes: Design, challenges, and applications. IEEE Access 2020, 8, 144778–144808. [CrossRef]

[67] Bayat, M.; Shahi, H.; Mazloum, J. Dual-band balanced-to-single-ended crossover based on composite right-and left-handed transmission lines. Electron. Lett. 2020, 56,

380–382. [CrossRef]

[68] Althuwayb, A.A. MTM-and SIW-inspired bowtie antennae loaded with AMC for 5G mm-wave applications. Int. J. Antennaes Propag. 2021, 2021, 6658819. [CrossRef]

[69] Lee, S.; Lee, J.; Choi, S.; Lee, Y.H.; Chung, J.Y.; Hwang, K.C.; Park, Y.B. Design and Characterization of VHF Band Small Antennae Using CRLH Transmission Line and Non-Foster Matching Circuit. Appl. Sci. 2020, 10, 6366. [CrossRef]

[70] Song, K.; Zhang, F.; Fan, M.; Zhu, Y.; Fan, Y. Compact broadband bandstop filter based on composite right/left handed transmission line. Electromagnetics 2017, 37, 196–202. [CrossRef]

[71] Caloz, C.; Itoh, T. Novel microwave devices and structures based on the transmission line approach of meta-materials. In Proceedings of the IEEE MTT-S International Microwave Symposium Digest, Philadelphia, PA, USA, 8–13 June 2003; Volume 1, pp. 195–198.

[72] Haleem, M.; Elwi, T.A. Circularly Polarized Metamaterial Patch Antennae Circuitry for Modern Applications. Int. J. Emerg. Technol. Adv. Eng. 2022, 12, 44–50. [CrossRef] [PubMed]

[73] Ghadeer, S.H.; Abd, S.K.; Alibakhshikenari, M.; Virdee, B.S.; Elwi, T.A.; Iqbal, A.; Al-Hasan, M. An innovative fractal monopole MIMO antennae for modern 5G applications. AEU-Int. J. Electron. Commun. 2022, 159, 154480, ISSN 1434–8411. [CrossRef]

[74] Al-khaylani, H.H.; Elwi, T.A.; Ibrahim, A.A. Optically remote-controlled miniaturized 3D reconfigurable CRLH-printed MIMO antennae array for 5G applications. Microw. Opt. Technol. Lett. 2022, 65, 603–610. [CrossRef]

[75] Ismail, M.M.; Elwi, T.A.; Salim, A.J. A Miniaturized Printed Circuit CRLH Antennae-based Hilbert Metamaterial Array. J. Commun. Softw. Syst. 2022, 18, 236–243. [CrossRef]

[76] Shirkolaei, M.M.; Ghalibafan, J. Unbalanced CRLH behavior of ferrite-loaded waveguide operated below cutoff frequency. Waves Random Complex Media 2020, 32, 755–770. [CrossRef]

[77] Hussain, M.; Rizvi SN, R.; Awan, W.A.; Husain, N.; Hameed, A. On-Demand Frequency Reconfigurable Flexible Antennae for 5Gsub-6-GHz and ISM Band Applications. In WITS 2020; Springer: Singapore, 2022; pp. 1085–1092.

[78] Ibrahim, A.A.; Abdalla, M.A.; Budimir, D. Coupled CRLH transmission lines for compact and high selective bandpass filters. Microw. Opt. Technol. Lett. 2017, 59, 1248–1251. [CrossRef]

[79] Caloz, C.; Itoh, T.; Rennings, A. CRLH metamaterial leaky-wave and resonant antennaes. IEEE Antennaes Propag. Mag. 2008, 50, 25–39. [CrossRef]

[80] Liu, N.; Liang, Y.; Zhu, L.; Zhou, H.; Fu, G. A low-profile dual-band shorted patch antennae with enhanced-bandwidth and multifunctional beams under reshaped modes. Int. J. RF Microw. Comput. Eng. 2021, 31, e22726. [CrossRef]

[81] Sharma, N.; Bhatia, S.S. Comparative analysis of hybrid fractal antennaes: A review. Int. J. RF Microw. Comput. Eng. 2021, 31, e22762. [CrossRef]

[82] Malallah, R.; Shaaban, R.M.; Al-Tumah, W.A.G. A dual band star-shaped fractal slot antennae: Design and measurement. AEU-Int. J. Electron. Commun. 2020, 127, 153473. [CrossRef]

[83] Daniel, R.S. A CPW-fed rectangular nested loop antennae for penta band wireless applications. AEU-Int. J. Electron. Commun. 2021, 139, 153891. [CrossRef]

[84] Patanvariya, D.G.; Chatterjee, A.; Kola, K.; Naik, S. Design of a linear array of fractal antennaes with high directivity and low cross-polarization for dedicated short range communication application. Int. J. RF Microw. Comput. Eng. 2020, 30. [CrossRef]

[85] Kola, K.S.; Chatterjee, A.; Patanvariya, D. Design of a compact high gain printed octagonal array of spiral-based fractal antennaes for DBS application. Int. J. Microw.

Wirel. Technol. 2020, 12, 769–781. [CrossRef]

[86] Sawant, K.K.; Kumar, C.S. CPW fed hexagonal micro strip fractal antennae for UWB wireless communications. AEU-Int. J. Electron. Commun. 2015, 69, 31–38. [CrossRef]

[87] Khalaf, O.I.; Sokiyna, M.; Alotaibi, Y.; Alsufyani, A.; Alghamdi, S. Web Attack Detection Using the Input Validation Method: DPDA Theory. Comput. Mater. Contin. 2021, 68, 3167–3184. [CrossRef]

[88] Suryanarayana, G.; Chandran, K.; Khalaf, O.I.; Alotaibi, Y.; Alsufyani, A.; Alghamdi, S.A. Accurate Magnetic Resonance Image Super-Resolution Using Deep Networks and Gaussian Filtering in the Stationary Wavelet Domain. IEEE Access 2021, 9, 71406–71417. [CrossRef]

[89] Lin, W.; Wang, H. Polarization reconfigurable circular patch antennae with multiple probes for biomedical applications. In IEEE International Symposium on Antennaes and Propagation (APSURSI); IEEE: Fajardo, PR, USA, 2016; ISSN 1947-1491.

[90] Nivethitha, T.; Palanisamy, S.K.; Prakash, K.M.; Jeevitha, K. Comparative study of ANN and fuzzy classifier for forecasting electrical activity of heart to diagnose Covid-19. Mater. Today Proc. 2021, 45, 2293–2305. [CrossRef]

[91] Subahi, A.F.; Alotaibi, Y.; Khalaf, O.I.; Ajesh, F. Packet Drop Battling Mechanism for Energy Aware Detection in Wireless Networks. Comput. Mater. Contin. 2021, 66, 2077–2086. [CrossRef]

[92] Prasad Jones Christydass, S.; Kusuma Kumari, E.; Sowjanya, A.; Satheesh Kumar, P.; Selvam, N.; Murali, K. Microstrip Metamaterial Bandpass Filter for 5G Application. Solid State Technol. 2020, 63. Available online: https://solidstatetechnology.us/ index.php/JSST/article/view/4370 (accessed on 15 September 2021).

[93] Karmakar, A. Fractal antennaes and arrays: A review and recent developments. Int. J. Microw. Wirel. Technol. 2021, 13, 173–197. [CrossRef]

[94] Prasad Jones Christydass, S.; Asha, S.; Mubeen, S.; Praveen Kitti, B.; Satheesh Kumar, P.; Karthik, V. Multiband Circular Monopole Metamaterial Antennae with Improved Gain. J. Comput. Theor. Nanosci. 2021, 18, 736–745.

[95] Krishna, C.; Prasad, D.; Orugu, R.; Varma, P.K.; Kumar, J. Design and Analysis of Tortoise Shaped Quadband Antennae for C & Ku–Band Applications. In Proceedings of the 2021 International Conference on Computer Communication and Informatics (ICCCI), Coimbatore, India, 27–29 January 2021; pp. 1–5.

[96] Anand, R.; Chawla, P. Optimization of inscribed hexagonal fractal slotted microstrip antennae using modified lightning attachment procedure optimization. Int. J. Microw. Wirel. Technol. 2020, 12, 519–530. [CrossRef]

[97] Kumar, S.; Dixit, A.S.; Malekar, R.R.; Raut, H.D.; Shevada, L.K. Fifth Generation Antennaes: A Comprehensive Review of Design and Concerts Enhancement Techniques. IEEE Access 2020, 8, 163568–163593. [CrossRef]

[98] Anand, R.; Chawla, P. A novel dual-wideband inscribed hexagonal fractal slotted microstrip antennae for C- and X-band applications. Int. J. RF Microw. Comput. Eng. 2020, 30, e22277. [CrossRef]

[99] Krzysztofik, W.J. Fractals in Antennaes and Metamaterials Applications. Fractal Anal. -Appl. Phys. Eng. Technol. 2017, 45–81. [CrossRef]

[100] Dhara, R.; Kundu, T. Dual-Band Dual-Mode Antennae with Polarization Diversity. Radioelectron. Commun. Syst. 2021, 64, 266–280. [CrossRef]

[101] Rasheda, H.M.; Shah, N.M.; Saif, A.; Abdullah, Q.; Ugurenver, A.; Mumin, A.R.O.; Sahar, N.B.M. An Optimization of Fractal Microstrip Patch Antennae with Partial Ground using Genetic Algorithm Method. In Proceedings of the 2021 International Congress of Advanced Technology and Engineering (ICOTEN), Taiz, Yemen, 4–5 July 2021; pp. 1–6. [CrossRef]

[102] Shinjo, S.; Nakatani, K.; Tsutsumi, K.; Nakamizo, H. Integrating the Front End: A

Highly Integrated RF Front End for High-SHF Wide-Band Massive MIMO in 5G. IEEE Microw. Mag. 2017, 18, 31–40. [CrossRef]

[103] Singhal, S.; Singh, A.K. CPW-fed hexagonal Sierpinski super wideband fractal antennae. IET Microw. Antennaes Propag. 2016, 10, 1701–1707. [CrossRef]

[104] Mondal, T.; Samanta, S.; Ghatak, R.; Chaudhuri, S.R.B. A Novel TRI-Band Hexagonal Microstrip Patch Antennae Using Modified Sierpinski Fractal for Vehicular Communication. Prog. Electromagn. Res. C 2015, 57, 25–34. [CrossRef]

[105] Bharti, G.; Sivia, J.S. A Design of Multiband Nested Square Shaped Ring Fractal Antennae with Circular Ring Elements for Wireless Applications. Prog. Electromagn. Res. C 2021, 108, 115–125. [CrossRef]

[106] Sharma, N.; Bhatia, S.S. Concerts enhancement of nested hexagonal ring-shaped compact multiband integrated wideband fractal antennaes for wireless applications. Int. J. RF Microw. Comput. Eng. 2019, 30, 22079. [CrossRef]

[107] Farsaei, A.A.; Mokhtari-Koushyar, F.; Seyed-Talebi, S.M.J.; Kavehvash, Z.; Shabany, M. Improved Two-Dimensional MillimeterWave Imaging for Concealed Weapon Detection through Partial Fourier Sampling. J. Infrared Millim. Terahertz Waves 2016, 37, 267–280. [CrossRef]

[108] Rahim, A.; Malik, P.K. Analysis and design of fractal antennae for efficient communication network in vehicular model. Sustain. Comput. Informatics Syst. 2021, 31, 100586. [CrossRef]

[109] Grubb, P.M.; Li, W.; Mokhtari-Koushyar, F.; Chen, R.T. All inkjet printed frequency steered phased array antennaes with multi angle receiving demonstrated via simulation. Laser 3D Manuf. V 2018, 10523, 105230T. [CrossRef]

[110] Grubb, P.M.; Bidoky, F.; Mahajan, A.; Subbaraman, H.; Li, W.; Frisbie, D.; Chen, R.T. X-band printed phased array antennaes using high-concerts CNT/ion gel/Ag transistors. In Laser 3D Manufacturing III; SPIE: Bellingham, WA, USA, 2016;

Volume 9738.

[111] Zhang, X.; Hosseini, A.; Subbaraman, H.; Wang, S.; Zhan, Q.; Luo, J.; Jen, A.; Chen, R.T. Integrated Photonic Electromagnetic Field Sensor Based on Broadband Bowtie Antennae Coupled Silicon Organic Hybrid Modulator. J. Light. Technol. 2014, 32, 3774–3784. [CrossRef]

[112] Gupta, M.; Mathur, V.; Kumar, A.; Saxena, V.; Bhatnagar, D. Microstrip Hexagonal Fractal Antennae for Military Applications. Freq. 2019, 73, 321–330. [CrossRef]

[113] Farswan, A.; Gautam, A.K.; Kanaujia, B.; Rambabu, K. Design of Koch Fractal Circularly Polarized Antennae for Handheld UHF RFID Reader Applications. IEEE Trans. Antennaes Propag. 2015, 64, 771–775. [CrossRef]

[114] Bhatia, S.S.; Sivia, J.S.; Sharma, N. An Optimal Design of Fractal Antennae with Modified Ground Structure for Wideband Applications. Wirel. Pers. Commun. 2018, 103, 1977–1991. [CrossRef]

[115] Singhal, S.; Jaiverdhan; Singh, A.K. Elliptical monopole based super wideband fractal antennae. Microw. Opt. Technol. Lett. 2019, 62, 1324–1328. [CrossRef]

[116] Dastranj, A.; Ranjbar, F.; Bornapour, M. A New Compact Circular Shape Fractal Antennae for Broadband Wireless Communication Applications. Prog. Electromagn. Res. C 2019, 93, 19–28. [CrossRef]

[117] Kaur, N.; Singh, J.; Kumar, M. Hexagonal Ring Shaped Dual Band Antennae Using Staircase Fractal Geometry for Wireless Applications. Wirel. Pers. Commun. 2020, 113, 2067–2078. [CrossRef]

[118] Khan, H.H.; Malik, M.N.; Zafar, R.; Goni, F.A.; Chofreh, A.G.; Klemeš, J.J.; Alotaibi, Y. Challenges for sustainable smart city development: A conceptual framework. Sustain. Dev. 2020, 28, 1507–1518. [CrossRef]

[119] Parchin, N.O.; Basherlou, H.J.; Alibakhshikenari, M.; Al-Yasir, Y.I.A.; Abd-Alhameed, R.A.; Limiti, E. Mobile-Phone Antennae Array with Diamond-Ring Slot Elements for 5G Massive MIMO Systems. Electronics 2019, 8, 521. [CrossRef]